ABSTRACT

Title of Document:	ASSESSMENT OF AN ELECTRICAL SHORTING AND METAL VAPOR ARCING POTENTIAL OF TIN WHISKERS
	Sungwon Han, Doctor of Philosophy (Ph.D.), 2012
Directed By:	Chair Professor and Director, Michael Pecht, Department of Mechanical Engineering

Tin whiskers are conductive crystal growths that form unpredictively from tin and tin alloy surfaces. The growth of tin whiskers presents a reliability concern in electronic equipment due to their potential to create electrical shorts and metal vapor arcs. Concern with tin whiskers is increasing due to the ever tightening conductor spacing in smaller electronic products and the increased use of pure tin and lead-free tin alloys.

While tin whiskers present a failure risk for electronics, a tin whisker mechanical bridging between two differently electrically biased conductors doesn't guaranteed electrical shorts due to surface films on tin whisker and conductors. The voltage must exceed a threshold level in order to produce the current flow through the tin whisker. However, the influence of contact force and presence of surface contaminations on breakdown voltage of tin whiskers has not been adequately

investigated. Furthermore, whisker-induced electrical shorts can initiate destructive metal vapor arcs. The potential for metal vapor arc formation is affected by several factors, including whisker geometry, bias voltage and pressure. Previous studies demonstrated metal vapor arc formation using gold- and tin-wires; however, material and geometry differences between these test articles and actual tin whiskers have not been examined. Further, a practical guide for assessing the potential for tin whisker–induced metal vapor arc formation has not been provided.

This dissertation provides characteristics and assessment of tin whisker-induced electrical shorts and metal vapor arcs. The breakdown voltage of tin whisker was measured using gold- and tin-coated probes to characterize the influence of two different contact materials on breakdown voltage. As a part of this effort, the effect of contact force on breakdown voltage and its current-voltage characteristics related with the failure mode and the possibility of electrical shorting by tin whiskers were also investigated. With regards to tin whisker-induced metal vapor arc formation, the effect of whisker geometry, bias voltage and pressure was investigated. Based on the experimental evidence, a metric defined as a function of bias voltage and resistance was proposed and the logistic regression model that can assess the likelihood of tin whisker-induced metal vapor arc formation was developed.

ASSESSMENT OF AN ELECTRICAL SHORTING AND METAL VAPOR ARCING POTENTIAL OF TIN WHISKERS

By

Sungwon Han

Dissertation submitted to the Faculty of the Graduate School of the
University of Maryland, College Park, in partial fulfillment
of the requirements for the degree of
Doctor of Philosophy
2012

Advisory Committee:
Professor Michael Pecht, Chair
Professor John Melngailis
Professor Bongtae Han
Professor Peter Sandborn
Associate Professor F. Patrick McCluskey
Senior Research Scientist Dr. Michael D. Osterman

© Copyright by
Sungwon Han
2012

Dedication

This thesis is dedicated to my parents, who always support and give me their endless love.

Acknowledgements

Foremost, I wish to genuinely acknowledge my advisor, Professor Michael Pecht for giving me the opportunity to work on this dissertation topic at CALCE Electronic Products and Systems Center and his enlightening guidance for this work as well as challenging me to set my benchmark higher.

I would like to especially thank Dr. Osterman for his insightful advices and stimulating discussions from time to time in this work. I also want to express my appreciation to Prof. Melngailis, Prof. Han, Prof, Sandborn, and Prof. McCluskey for serving on my dissertation committee and providing valuable advices in this thesis.

My many thanks extend to research faculty at CALCE, including Dr. Azarian, Dr. Das, Bhanu Sood, Swapnesh Patel, and Ahmed Amin for their helpful suggestions. I also with to thank all of my friends at CALCE including Anshul Shrivastava, Arvind Vasan, Bongmin Song, Daeil Kwon, Elviz George, Hyunseok Oh, Huan Ye, Lyudmyla Panashchenko, Moonhwan Chang, Preeti Chauhan, Sony Mathew, Thomas Fritzler and Xiaofei He, and all Korean graduate students at mechanical engineering department for their kind helps during my graduate experience.

Finally, I would like to thank my parent for their constant support and encouragement towards my endeavors.

Table of Contents

Dedication ii

Acknowledgements iii

Table of Contents iv

List of Tables vii

List of Figures viii

Chapter 1: Introduction 1

1. Growth mechanisms of tin whisker 3
2. Factors can contribute to whisker growth 4
3. Failures caused by tin whiskers 4
4. Mitigation strategies 7
5. Problem statement and objective 9

   2.1 Electrical shorting propensity of tin whiskers 9

   2.2 Metal vapor arcing propensity of tin whiskers 10

Chapter 2: Literature review 12

1. Electrical shorting propensity of tin whiskers 12
2. Metal vapor arcing of tin whiskers 13

Chapter 3: Electrical shorting propensity of tin whiskers 16

1. Experimental setup 16
2. Type of current-voltage (I-V) transitions in breakdown voltage 19
3. Effect of different probe materials on breakdown voltage 20
4. Breakdown voltage depending on type of voltage-current transitions 23
5. Probed surface depending on type of voltage-current transitions 24
6. The effect of contact force on breakdown voltage 28
7. Breakdown between the two whiskers 35
8. Oxide layer on whisker surface 39
9. Conclusion 42

Chapter 4: Metal vapor arcing propensity of tin whiskers 43

1. Experimental setup 44

1.1 Arc test specimen and test circuit ... 44
1.2 Verification of vapor arc by tin whisker ... 47
1.3 Conformal coated arc test specimen ... 48
2. Physical and electrical characteristics of arc test specimen ... 50
2.1 Physical characteristics ... 50
2.2 Electrical characteristics ... 52
3. Comparison between the specimens with arc initiated and no arc initiated ... 55
4. Two types of vapor arc behavior ... 57
4.1 Type I vapor arc event ... 58
4.2 Type II vapor arc event ... 59
5. Current and voltage transition during the vapor arc event ... 62
6. Contact erosion mechanism in vapor arc by tin whiskers ... 66
7. Effect of physical and electrical parameters on likelihood of vapor arc by tin whiskers ... 70
7.1 Physical parameters – Whisker geometries ... 70
7.2 Electrical parameter – Resistance of test specimen ... 72
7.3 Electrical parameter – Ramp time of power source ... 74
8. Arc Current Metric ... 75
9. Influence of Conformal Coating on Vapor Arc by Tin Whiskers ... 77
10. Conclusion ... 79
Chapter 5: Prediction Model for metal vapor arc by tin whiskers ... 80
1. Binary logistic regression ... 80
2. Statistical tests of individual predictor variables ... 82
3. Conclusion ... 93
Chapter 6: Melting current of tin whiskers ... 95
1. Experimental setup ... 95
2. Melting current of tin whiskers ... 95
3. Summary ... 103
Chapter 7: Contributions and Future work ... 104
1. Contribution ... 104
2. Future work ... 105

Appendices.. 107
References.. 109

List of Tables

Table 1 Kruskal-Wallis test on breakdown voltage depending on probe types.......... 22

Table 2 Kruskal-Wallis test on breakdown voltage depending on type of I-V transitions... 24

Table 3 Breakdown voltage between two whiskers... 38

Table 4 The measured resistance of arc test specimen 74

Table 5 Arc test result using conformal coated arc test specimens with 50 V at 30 torr 78

Table 6 Result of the first binary logistic regression analysis 84

Table 7 Result of the second binary logistic regression analysis................................ 85

Table 8 Classification table from the training data set (cutoff value = 0.5) 88

Table 9 Classification table from the validation data set (cutoff value = 0.5)............ 88

List of Figures

Figure 1 Tin whiskers on tin finish surface ... 1

Figure 2 Striations on the surface of tin whisker along the axis of the growth: (a) Tin whisker on tin plating and (b) Close-up of tin whisker surface in indicated figure 2(a) ... 2

Figure 3 The physically bridged conductors by tin whisker: (a) Grown whisker from adjacent tin plated surface, (b) Airborne whisker was settled on two conductors ... 5

Figure 4 Electrical failure diagram for bridged tin whiskers ... 6

Figure 5 Relay destroyed by suspected tin whisker induced metal vapor arc [32] ... 11

Figure 6 Whisker growths on 22 year-old tin-plated beryllium copper card rails ... 16

Figure 7 Schematic diagram of electric circuit for measuring breakdown voltage ... 17

Figure 8 Overview of test setup for measuring breakdown voltage ... 17

Figure 9 Whisker bent by contacted probe ... 18

Figure 10 The single transition for the current-voltage (I-V) characteristic ... 19

Figure 11 The multiple transitions for the current-voltage (I-V) characteristic ... 20

Figure 12 Probability density plot of breakdown voltage depending on probe material ... 21

Figure 13 Cumulative frequency plot in breakdown voltage of tin whiskers ... 22

Figure 14 Probability density plot of breakdown voltage depending on type of I-V transitions ... 23

Figure 15 (a) The probed point on the surface of tin whisker showed the single transition and (b) Its I-V transition ... 25

Figure 16 (a) The probed point on the surface of tin whisker showed the multiple transitions and (b) Its I-V transition ... 25

Figure 17 Probe contacted surfaces depending on type of current-voltage (I-V) transitions: (a), (b) Single transition, and (c), (d) Multiple transitions ... 26

Figure 18 Whisker deformation caused by probe contact: (a) Prior to contact by probe, (b) Close-up of root area of tin whisker indicated in figure 18(a), (c) After the test and (d) Close-up of root area of tin whisker indicated in figure 18(c) ... 27

Figure 19 Test specimen for contact force measurement ... 29

Figure 20 Image merged in which shows (a) Prior to contact and (b) After contacting by Au-coated probe 30
Figure 21 Plot of breakdown voltage versus contact force 31
Figure 22 Cumulative frequency plot of estimated contact force between airborne whisker and conductors 34
Figure 23 Cumulative frequency plot of estimated contact force between buckled whisker and conductor 34
Figure 24 Deflection of whisker by electrostatic force between probe and tin whisker 35
Figure 25 Current-voltage characteristic when deflected whisker touches the probe (the distance between probe and whisker: 294.1 μm) 36
Figure 26 Current-voltage characteristic depending on the distance between Au-coated probe and tin whisker 37
Figure 27 Tin whisker probe 37
Figure 28 Two whisker probes touched each other 38
Figure 29 A high resolution transmission electron microscopy (HRTEM) images of whisker body and whisker surface: (a) BF-STEM image of Whisker #1 surface (b) HR-TEM image of area indicated in figure 29(a) 39
Figure 30 The surface layer analysis using STEM-EDX: (a) HRTEM image of oxide layer on Whisker #2 surface, (b) STEM-EDX analysis of selected point in figure 30(a) 41
Figure 31 (a) Tin whisker arc test specimen and (b) Close-up of detached whisker on tin-plated electrodes 44
Figure 32 Schematic of the electric circuit for the metal vapor arc test by tin whiskers 45
Figure 33 Typical altitude of airplane and its altitude 47
Figure 34 (a) Light generation during the vapor arc by tin whisker and (b) Burn marks on the surface of the test specimen after the arc test 48
Figure 35 Conformal coated arc test specimen: (a) Test specimen in group 1, (b) Test specimen in group 2, and (c) Close-up of attached whisker indicated in figure 35(b) 49

Figure 36 Whisker length and conductor gap between tin-plated electrodes 50
Figure 37 Whisker length distribution depends on spacing between electrodes 51
Figure 38 Whisker diameter distribution depends on spacing between electrodes 52
Figure 39 (a) Thermally damaged test specimen due to biased current (higher than 10 μA) by mili-ohmmeter without the current limit and (b) Close-up of melted area at whisker 53
Figure 40 Distribution of the resistance of test specimen depends on spacing between electrodes (Conductor gap: 300 μm versus 600 μm) 54
Figure 41 The measured points for the resistance of test specimen 54
Figure 42 Specimen in which a vapor arc was not initiated: (a) Prior to and (b) After the arc test. (c) Close-up of the melted whisker indicated in figure 42(b)............ 56
Figure 43 Specimen in which vapor arc was initiated (a) Prior to and (b) After the arc test. (c) Close-up of the arc-damaged surface indicated in figure 43(b)................ 57
Figure 44 Vapor arc test at 50 V in atmospheric pressure (760 torr): Vapor arc initiated and extinguished 59
Figure 45 Vapor arc test at 50 V in vacuum (70 torr): Vapor arc sustained and propagated 61
Figure 46 Test specimen after the Type II vapor arc event 61
Figure 47 Current-voltage characteristic when the tin whisker was melted without initiation of vapor arcing (37.5 V at 75 torr).. 62
Figure 48 Current-voltage characteristic during the Type I arc event 63
Figure 49 (a) ~ (f) Light emission from the test specimen in Type II arc event by camera with 30 frames per second (FPS) and (g) Formation of metal bridge after the arc test 65
Figure 50 Current-voltage characteristic during the Type II arc event....................... 66
Figure 51 Formation of tin whisker-induced vapor arc and contact erosion 67
Figure 52 Contact erosion on anode and cathode electrode captured by SEM 68
Figure 53 Contact erosion on anode and cathode electrodes (top view and edge view) 69
Figure 54 Probability density plot of whisker length depending on the initiation of vapor arc by tin whiskers 71

Figure 55 Probability density plot of whisker diameter depending on the initiation of vapor arc by tin whiskers 72
Figure 56 Plot of probability density function in measured resistance of test specimen depending on the initiation of vapor arc by tin whiskers 73
Figure 57 Likelihood of vapor arc being caused by tin whisker depending on the resistance of the test specimen 73
Figure 58 (a) Rupture of melted whisker after the arc test using by power supply (20V/ 50A), and (b) Close-up of ruptured area of whisker in figure 58(a)............ 75
Figure 59 Effects of arc current metric on likelihood of vapor arc by tin whisker..... 76
Figure 60 Conformal coated arc test specimen (Arc current metric: 12.7 A): (a) Prior to and (b) After the arc test (50 V at 30 torr), and (c) Close-up of the area where the whisker was placed as indicated in figure 60(b) 78
Figure 61 Evaluation procedure of binary logistic regression model 81
Figure 62 Vapor arc event based on the arc current metric (129 test data) 84
Figure 63 (a) Vapor arc events depending on the arc current metric and (b) Estimated possibility depending on the arc current metric (Training data set)....................... 87
Figure 64 (a) Vapor arc events depending on the arc current metric and (b) Estimated possibility depending on the arc current metric (Validation data set).................... 89
Figure 65 Receiver operating characteristic (ROC) curve for vapor arcing prediction model.. 90
Figure 66 The sensitivity and specificity curves (Training data set) 92
Figure 67 Estimated possibility of vapor arcing based on the voltage and resistance of the test specimen 93
Figure 68 Melting test specimen: (a) Prior to, (b) After the test (b), (c) Close-up of disconnected whisker indicated in figure 68(b), and (d) Close-up of expunged part of whisker with oxide layer... 96
Figure 69 (a) Current-voltage plot in the melting test of tin whisker and (b) Current-resistance plot.. 97
Figure 70 Measured melting current of tin whisker depending on whisker diameter and whisker length (CALCE versus Dunn [11]).. 98

Figure 71 Measured melting current versus estimated melting current by Preece's and Onderdonk's equation 100
Figure 72 Remained melting tin with oxide layer after the melting current measurement 101
Figure 73 Measured melting current versus estimated melting current for tin whiskers 102

Chapter 1: Introduction

Over 50 years, tin and tin alloys have been widely used in the electronic industry for plating finishes because of their excellent solderability and electrical conductivity. Unfortunately, tin whiskers hair-like conductive structures grow spontaneously and unexpectedly from both the surface of pure tin and high tin content alloy finishes as a surface relief phenomenon of creep, as shown in figure 1. The growth of tin whisker is from the bottom by supplement of addition tin atoms from the plating layer [1-8].

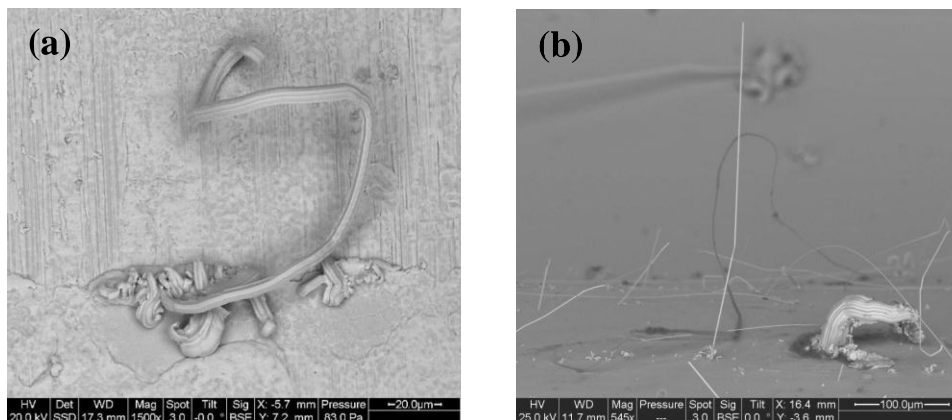

Figure 1 Tin whiskers on tin finish surface

In accordance with JEDEC standards, tin whisker have an aspect ratio (length/width) greater than two, with shorter growths referred to as nodules or odd-shaped eruptions (OSEs) [9].

Tin whisker can grew with various shapes, such as straight as needle-like filament, kinked, bent, forked and lumpy [6, 8, 9]. Whiskers may be solid or hollow

[10, 11] and striations along the axis of the growth are commonly observed as shown in figure 2. Typical diameter of whiskers are a few microns and the length of whisker is generally short but their length follow a lognormal distribution that allows for the possibility of very long whisker up to 20 mm [11-13]. The growth rate of tin whisker under ambient conditions was range around 0.01-0.1 Å /second in pure tin film and 2-6 Å /second in tin-manganese film [12, 14]. The growth rate is highly variable depending on various factors; (1) substrate material; (2) pre-plate chemical treatment of the substrate; (3) grain size; (4) crystallographic orientation of grains on plating layer; (5) plating solution; (6) post-plated thermal processing; (7) thickness of plating layer; (8) storage/operating conditions. It is still unknown that a quantitative relationship between these factors and the growth of tin whisker.

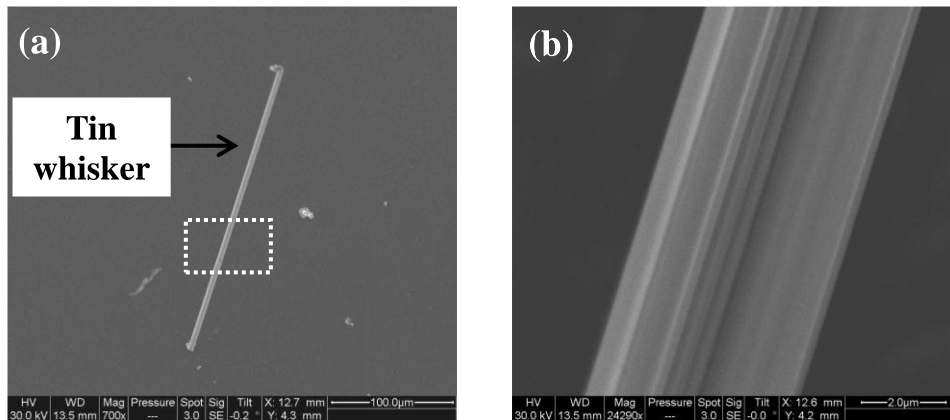

Figure 2 Striations on the surface of tin whisker along the axis of the growth: (a) Tin whisker on tin plating and (b) Close-up of tin whisker surface in indicated figure 2(a)

1. *Growth mechanisms of tin whisker*

Several models have been proposed to explain the growth of tin whiskers for many years, such as dislocation model, cracked oxide theory and recrystallization model. Although, it is widely documented in the literatures that stress gradients, which are generated in the plating layer is necessary factor to grow the tin whiskers.

– Dislocation model

Eshelby suggested that the negative surface energy drives to form the Frank-Read emission of dislocation loops and whiskers can grow by the gliding of these dislocation loops to the surface [15].

– Cracked oxide theory

In case of tin-plated copper substrates, the driving force for whisker growth is the compressive stress generated by the formation of Cu-Sn intermetallic compound (IMC), such as Cu_6Sn_5. The growth of whisker is the stress relief process and whisker can grow from the localized "weak" spots (fracture spots) of the oxide layer on tin plating surface. According to the cracked oxide theory, the absence of oxide layer on tin plating surface, tin whisker can't grow because the stress would be uniformly relieved in the plating surface [8, 16]. However, Moon et al [17] reported that the growth of tin whisker in the absence of an oxide layer on plating surface.

– Recrystallization model

According to Smetana [18], the key mechanism of tin whisker growth is the grain boundary sliding (creep) due to the oblique grain boundaries in tin plating layer. These oblique grain boundaries provide the path for diffusion to the base of the whisker grain. Due to the oblique grain boundaries, the compressive stresses in

plating layer induce the grain boundary sliding and it promotes the growth of tin whiskers.

2. *Factors can contribute to whisker growth*

– Internal stress [19-21]

The formation of intermetallic compound (i.e. Cu_6Sn_5) between the plating layer and substrate produces the compressive stresses in the plating layer. The mismatches in coefficient of thermal expansion (CET) between the plating material and substrate can generate the compressive stress as well.

– External stress [22-24]

Surface damages, such as scratches or nicks can introduce the stress in plating layer. The mechanical loading (bending or stretching) also generates the residual stress in plating layer. It is also reported that the pressure has been increase the whisker growth.

– Electroplating process [25, 26]

Residual stress can be caused by the electroplating process due to the additives (impurities) in plating solution, current density and plating bath temperature.

– Other factors [27-30]

The electrical field, corrosion, temperature, humidity and barometric pressure can also contribute the growth of tin whiskers.

3. *Failures caused by tin whiskers*

Tin whiskers present a mechanical and electrical reliability concerns due to their propensity to induce failures in electronic products and systems. For mechanical

failure, the broken whisker may interfere with optical surface or damage the microelectronic system (MEMs) devices [12]. The most common failure caused by tin whisker is electrical failure, such as electrical shorting and metal vapor arcing due unintended bridging by tin whisker. Tin whisker can grow enough to physically bridge two isolated conductors, and become airborne whiskers that can be transported into the electronic equipment as depicts in figure 3. It is also reported that the whisker can be attracted by electrostatic forces [31]. It represents that tin whisker can also bridge the differently biased conductor due to the electric field strength between conductor and whisker.

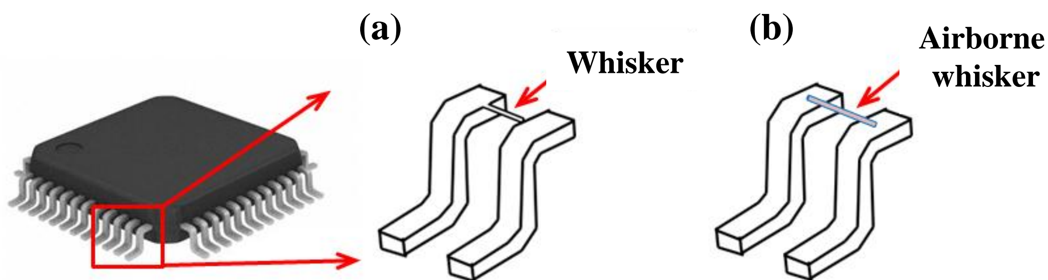

Figure 3 The physically bridged conductors by tin whisker: (a) Grown whisker from adjacent tin plated surface, (b) Airborne whisker was settled on two conductors

If the high enough current/voltage flows through the tin whisker, tin whisker can cause the vapor arcing that can result in the catastrophic failure. Tin whisker can be melted and vaporized due to the joule heating induced by high current density and simultaneously the bias voltage knocks off the loosed electrons from the atom that can produce the metal vapor arcing. If the current/voltage is not high enough to induce the vapor arcing, the electrical shorting can be occurred by tin whisker.

Depending on the bias current, tin whisker can be melted after the intermittent shorting failure established or whisker can cause the permanent shorting failure if the bias current is lower than the melting current of tin whisker. The electrical failure can be decided depending on the electrical characteristic of electronic products and systems, as describe in the electrical failure diagram for bridged whiskers in figure 4.

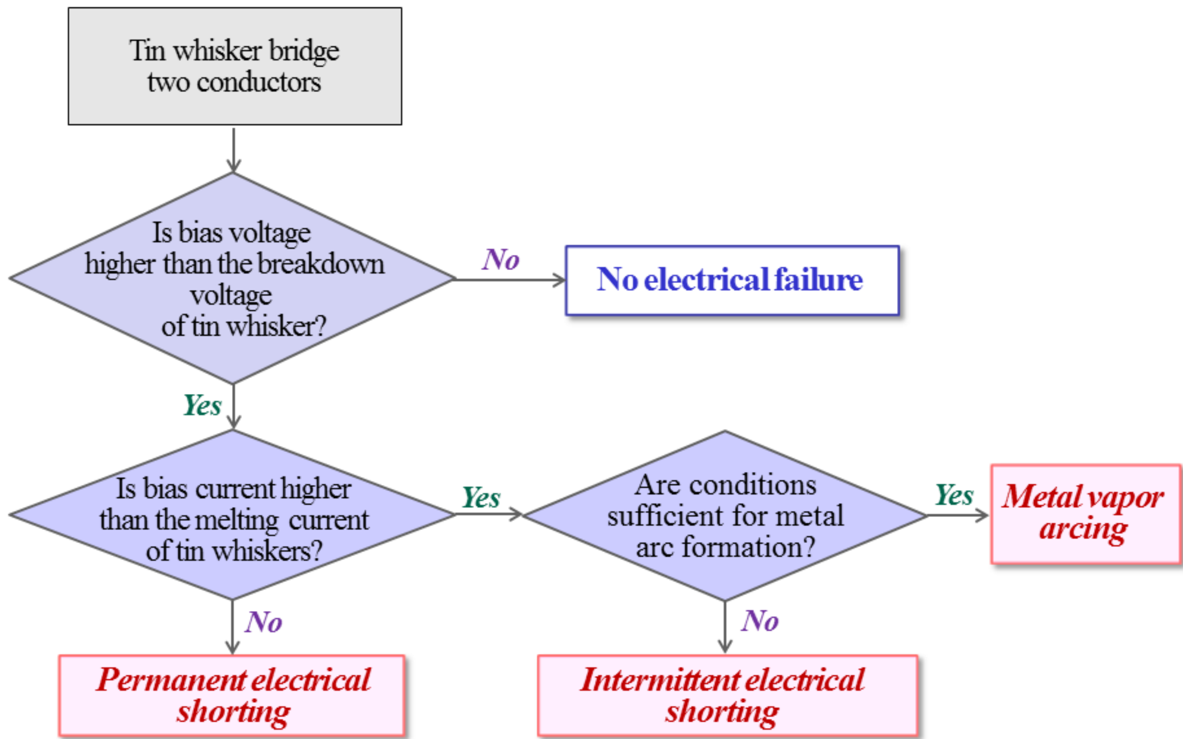

Figure 4 Electrical failure diagram for bridged tin whiskers

Several electrical failures caused by tin whiskers have been associated in satellite, power industry and other electronics. More commercial electronic components may have failed due to whiskers than has been reported by engineers because whiskers are difficult to observe even under a microscope and may melt or

vaporize after causing an electrical short circuit. Here are some of failure experience by tin whisker in power industry, military, satellite and other electronics [12, 25, 32].

- Power industry [33, 34]
  - An automatic reactor scram at the Duane Arnold Energy Center (1990)
  - A reactor pre-trip alarm occurred at South Texas Project (1999)
  - A nuclear reactor shutdown at the Millstone power plant (2005)
- Military [35]
  - Problems with Navy's Phoenix air-to air missile system (1989)
  - Failure of relays used on a military airplane (2002)
- Satellite [36, 37]
  - Complete losses of at least three commercial satellites due to the failure of their satellite control processors (1998, 1999, 2001)
- Medical [38]
  - Failure of the pacemaker due to the short circuit by tin whisker (1986)

4. Mitigation strategies

Unfortunately, there are no mitigation strategies which can perfectly prevent the growth of tin whiskers.

– Plating thickness [26, 39]

It is reported that growth of tin whisker could not grow on the plating layer with the thickness of 0.5 μm. The thinner plating thickness less than 0.5 μm or thicker thickness greater than 20 μm may reduce the growth of tin whisker.

– Heat treatment (Reflow and annealing) [40-42]

It has been reported that he reflow of plating surface may relieves the stress in the plating layer; however, some document claimed that the whisker can grow on reflowed plating surface.

Annealing at 150 C° for 1 hour within 24 hours after the plating process is also known as post-bake treatment. It has been reported that annealing relieved the residual stress in plating layer and promoted the formation of more uniform and even intermetallic compound layer between plating layer and substrate. This uniform and even intermetallic layer may act as a barrier against the grain boundary diffusion and slow down the growth of scallop shaped Cu_6Sn_5 intermetallic compound. Thus, it may reduce the amount of compressive stresses in plating layer.

– Ni barrier layer [43-45]

By means of a Ni barrier layer between the substrate and plating material, the formation of intermetallic compound between plating layer and substrate can be reduced. However, the Ni barrier layer may be cracked or damaged during the reflow process, if the thickness of Ni layer is too thin. Thus, the NEMI recommends the minimum thickness of Ni barrier as 1.27 μm.

– Conformal coating [46-48]

Conformal coatings are thin electrically nonconductive protective layers that are applied to printed circuit boards (PCBs) after assembly. It has been reported that the conformal coating may suppress the growth of tin whisker or increase the incubation of time for whisker formation. The use of conformal coating can reduce the probability of electrical failure by tin whisker. Conformal coating can act as the barrier layer on conductive surface preventing contact from an incoming whisker. In

addition, conformal coating can contain an emerging tin whisker and preventing it from extending out to contact an adjacent conductor. However, several documentations claimed that the whisker can be escaped from the conformal coating layer.

5. *Problem statement and objective*

Numerous filed failures have been attributed to the growth of tin whiskers since the 1940s. Despite of 70 years history in extensive studies of tin whiskers, most of researches were focused on the tin whisker growth mechanism and whisker mitigation strategies. Few publications have addressed the failure mechanism caused by tin whiskers to produce the electrical failures even though the potential for electrical failure by whisker is expected to increase with the development of ever smaller electronics.

2.1 Electrical shorting propensity of tin whiskers

Due to the conductive structure of tin whisker, it is known that the tin whisker can cause electrical failures, such as electrical short and metal vapor arc; however, when a tin whisker bridges differently biased conductors, an electrical short is not guaranteed. In many instances, the voltage must exceed a threshold level in order to produce the current flow through the whisker to bridged conductive surface, due to the weak physical contact and the presence of a non-conductive film, such as oxide layer [49-51]. It implies that the probability of a tin whisker inducing an electric short circuit is depending on the threshold level of voltage which can be determined by several contact parameters, such as contact force and presence of surface

contaminations. However, there is currently not enough data which can be used to assess the probability of electric short circuit by tin whiskers in an electronic product.

- **Objective**
  - **Investigate the effects of different contacted materials on the breakdown voltage of tin whiskers.**
  - **Examine the effects of contact force from probes on the breakdown voltage of tin whiskers.**

2.2 Metal vapor arcing propensity of tin whiskers

Metal vapor arcing by tin whisker may cause the catastrophic failure in an electronic product due to its higher conductivity. One of the failure experiences is the relay destroyed by suspected tin whisker induced metal vapor arc as shown in figure 5. It has been reported that the tin whisker can form a metal vapor arc both at ground conditions and in a vacuum [52-54]. A reduction in atmospheric pressure has been shown to reduce the required voltage to initiate a metal arc [55].

Previous studies [52, 56] which have been demonstrated the metal vapor arc failure by tin whisker using gold and tin wire which arouse an attention to metal vapor arc failures by tin whisker in avionic industries, because their applications were exposed in reduced pressure level which may increase the possibility of metal vapor arc. However, there has not yet been studied the effect of several factors such as available current, whisker geometry, and conductor gap on the possibility of establishing a vapor arc. In addition, there is currently no model to predict the

likelihood of vapor arc by tin whisker that can be used to as a guide line for circuit design in terms of minimizing the vapor arc by tin whisker. Further, previous studies used the gold and tin wires instead of real tin whiskers and it may also affect the vapor arc propensity by tin whisker due to the different metal ion source and larger diameter comparing to real tin whiskers.

- **Objective**
  - **Investigate the effects of several arc factors, such as whisker geometry, voltage, and pressure conditions on vapor arc possibility.**
  - **Identify the practical criteria for assessing the vapor arc formation by tin whiskers.**
  - **Develop a model that can predict vapor arc failures from tin whiskers.**

Figure 5 Relay destroyed by suspected tin whisker induced metal vapor arc [32]

Chapter 2: Literature review

1. *Electrical shorting propensity of tin whiskers*

Previous research has demonstrated the requirements of breakdown and measured the breakdown voltage to achieve the electrical conductivity in order to quantify the probability of electrical shorting due to whiskers.

Hilty et al [57] developed a Monte Carlo simulation for whisker risk assessment to predict the likelihood of electrical shorting between two adjacent leads. In their simulation, the whisker geometries (whisker length and diameter) was measured the tin whiskers on tin plating substrates which were exposed at the accelerated aging environment and the locations of the whiskers, the growth angle were randomly generated in the simulation. It was identified as an electrical shorting when the whiskers were long enough with the growth angle which allows the whiskers touch adjacent conductors. The simulation results provide a quantitative assessment of the effectiveness of plating process mitigation in reducing simulated failure rate by the tin whisker-caused electrical shorting.

The second whisker risk assessment using the Monte Carlo simulation was developed by Fang [58, 59]. In his simulation, the risk of electrical short from a tin whisker growth as well as the risk from free whiskers was predicted. Both Hilty's and Fang's simulation [57, 59], it is assumed that the physical contact between a whisker and conductive surface causes an electrical short; however, an electrical short is not guaranteed when the whisker physical bridged the conductors. Fang [59] reported that zinc whiskers bridging isolated conductors had nearly infinite electrical resistance and

suggested oxide, non-conductive surface films, and low contact force resulted in high contact resistance. Hilty et al [49] showed that at least 3V DC is required to achieve electrical continuity when a probe contacts a whisker's surface. Some of whiskers were occurred the electrical breakdown at 26 V. These results indicates that the voltage must exceed a threshold level in order to produce current flow in the presence of whisker bridges conductors due to weak physical contact and/or the presence of a non-conductive surface film. The voltage required to produce an electrical short is referred to as the breakdown voltage.

In order to evaluate the probability of the electrical shorting by whisker with considering the breakdown voltage, Courey et al [50, 51] developed an empirical probability model by measuring the breakdown voltage on a tin whisker and fitting their distributions. They reported that the Lognormal distribution was the best fitting distribution to describe the whisker breakdown voltage. In their studies, the probe was applied to the whisker on approximately the top 25 % of the whisker to minimize the effect of applied pressure; however the authors mentioned that it does not completely eliminate the difference. The contact force caused by the applied pressure from probe may affect the level of the breakdown voltage. In Hilty's paper [49], the predicted contact force generated by pre-bucked tin whiskers is about 1mN.

2. *Metal vapor arcing of tin whiskers*

In electric contacts, the arc is defined as "the ionized gas that 'burns' between parted contacts". The arc is also called as the plasma that a volume of gas with highly ionized with $N_{-} \approx N_{+}$ [60]. So, the plasma is a highly conductive state can carry hundreds of amperes.

When a sufficient electric current passes through a tin whisker at sufficiently reduced pressures, the high current density can vaporize the tin whisker due to joule heating and ionize into plasma. The metal vapor arc failure in relay during a thermal vacuum test at 10^{-3} to 10^{-5} torr conditions was reported by D. H Van Westerhuyzen et al [52]. It was reported that 10 A fuses inside a 30 V relay were blown out the case due to tin whiskers which had grown between the terminals and the case. In order to simulate the vapor arc failure, gold wires with diameters ranging from 18 ~ 25 μm instead of tin whiskers used to initiate the metal vapor arc. Initially, 30 A power supply and capacitor bank used to apply the current through gold wires; however, the metal vapor arc was not successfully initiated. The vapor arc failure could be reproduced by replacing the power supply with lead acid batteries. During the simulation, the vapor arc was established at pressures below 0.5 torr and arc existed for 12 to 14 milliseconds with flowing approximately 250 A of current [52].

J.H. Richardson et al [54] reported that the metal vapor arc can be initiated when the pressure is less than 150 torr in the circuit with low impedance and high current. In addition, it was mentioned that the metal vapor arc was observed at voltages greater than 13 V with available current of 15 A or more. Conformal coating was recommended as the effective material to prevent the metal vapor arc by mentioning that the thermal decomposition of the conformal coating in the metal vapor arc extinguishes the arc so effectively and quickly [54].

However, it was reported that a tin whisker vapor arc can be established in atmospheric pressure (760 torr) with 28 V by Mason et al [55]. In their study, the minimum voltage for sustaining a tin whisker vapor arc in a vacuum (0.2×10^{-6} ~

2×10^{-6} torr) is 4 V, for tin wires of 25 ~ 50 μm in diameter. It arouses an attention in avionic industries, because their applications were exposed in reduced pressure level which may increase the possibility of metal vapor arc by tin whisker.

Chapter 3: Electrical shorting propensity of tin whiskers

1. *Experimental setup*

Tin whiskers from 22-year-old tin-plated beryllium copper card rails (170 mm × 13 mm) were used to measure the breakdown voltage on tin whiskers. The card rails had variously shaped long whiskers as shown in figure 6, some whiskers were grown more than 20 mm in length. Among these whiskers, the breakdown voltages for long (> 50 μm) columnar or cylindrical filament whiskers were measured, since these whiskers are more likely to create electrical shorts in a real system.

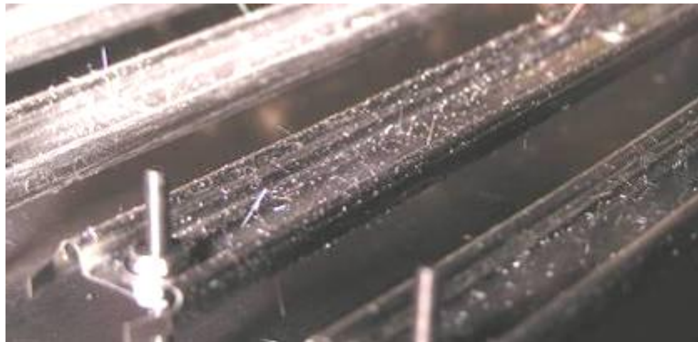

Figure 6 Whisker growths on 22 year-old tin-plated beryllium copper card rails

The breakdown voltage was measured using a semiconductor parameter analyzer (Agilent 4156C), which allows for monitoring current continuously while applying an increasing voltage potential. The voltage resolution and current measurement accuracy of a semiconductor parameter analyzer is 2 μV and 3 pA, respectively. The induced voltage ramp was between 0 V and 50 V, with 50 mV increments: a total of 1001 data units were collected as voltage increased. Because

tens of mA can fuse a whisker [11, 61], a 10 KΩ resistor was placed in the circuit to prevent the fusing of the whiskers after breakdown was achieved. The semiconductor parameter analyzer had a current limit function; however, it did not have a fast enough response to prevent fusing of the whiskers. The electrical circuit and the overall test setup for measuring the breakdown voltage of the whiskers are shown in figure 7 and 8.

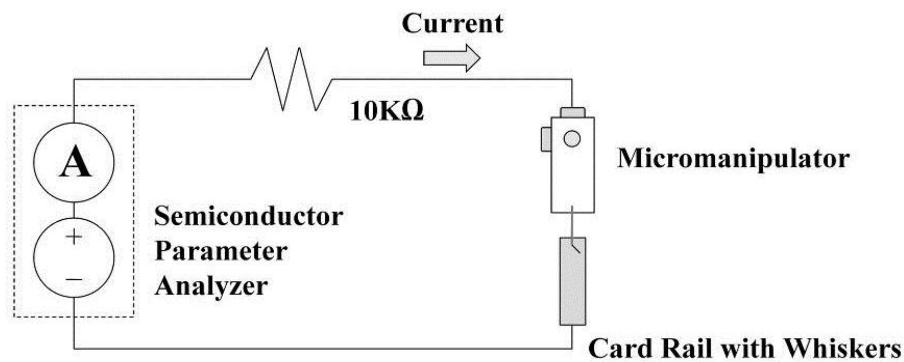

Figure 7 Schematic diagram of electric circuit for measuring breakdown voltage

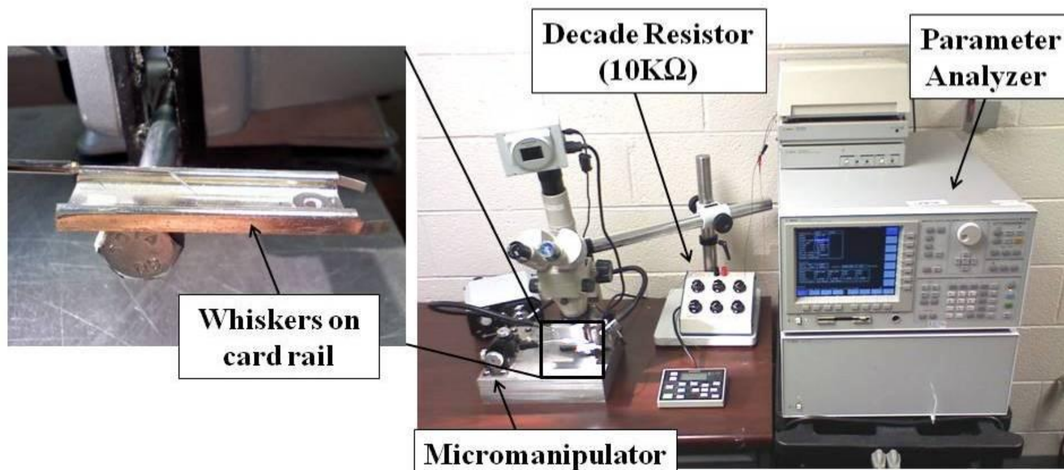

Figure 8 Overview of test setup for measuring breakdown voltage

The whiskers under test were probed using a micromanipulator, which allowed for precise control of position and displacement. Using the micromanipulator, the probe contacted the whisker under test and bent it slightly to verify mechanical contact, as shown in figure 9. The long whiskers tend to be quite flexible and have been observed to be easily moved by air flow. In order to reduce the effect of environmental noises, such as vibration and air flow, the micromanipulator and card rails were attached to a heavy aluminum block, and the whole experimental set-up was covered with a plastic cover during the measurement.

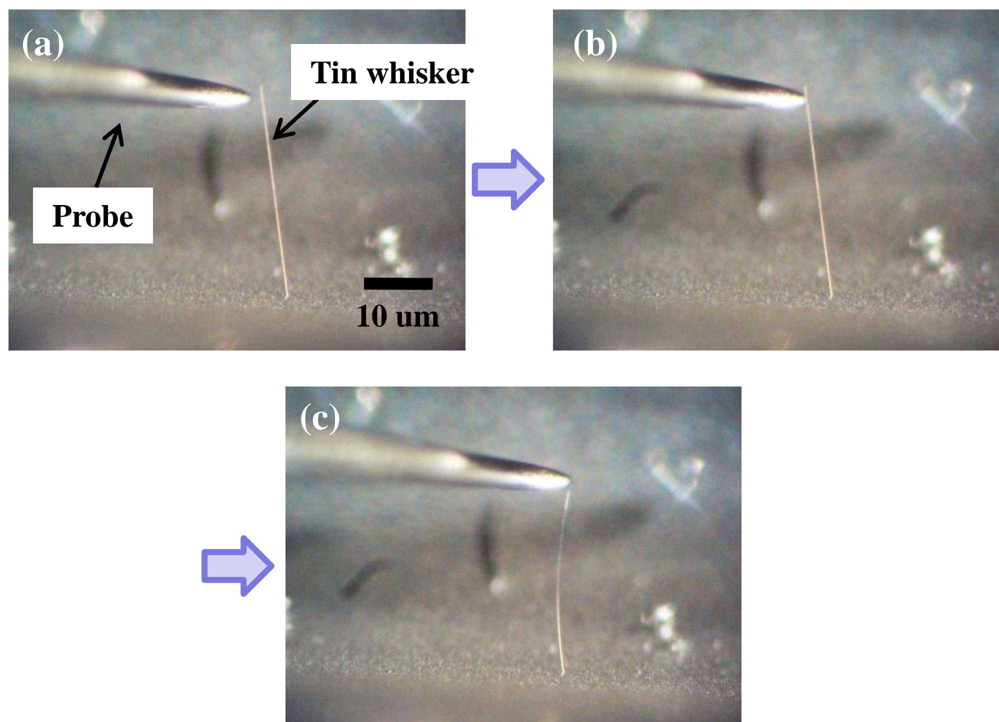

Figure 9 Whisker bent by contacted probe

The whiskers on the card rail were contacted with two kinds of plated tungsten probes. One probe was plated with Au, which has excellent oxidation resistance and good electrical contact performance. The Au probe can evaluate the breakdown

voltage between an oxide surface and an oxide-free surface. The other probe was plated with pure Sn over Cu-plated tungsten probe in order to characterize the breakdown voltage between oxide surfaces. Since both the Sn whisker and probe have native oxide layers on the surface, this condition may represent a more realistic field condition.

2. *Type of current-voltage (I-V) transitions in breakdown voltage*

The breakdown voltages were measured for 200 whiskers evenly split between Au-coated and Sn-coated probes. Both types of probes showed single and multiple transitions for the current-voltage (I-V) characteristic, as shown in figure 10 and 11. After breakdown, the current increased linearly with the increasing voltage. In multiple transitions, the voltage that caused the first transition was selected as the breakdown voltage of the tin whisker.

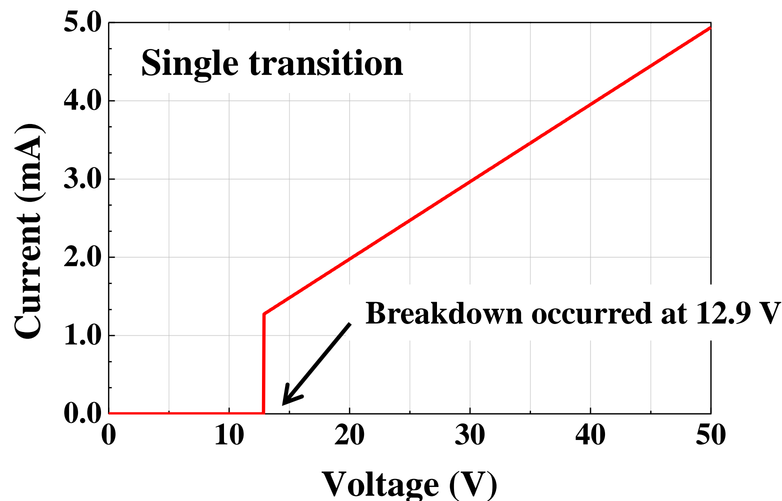

Figure 10 The single transition for the current-voltage (I-V) characteristic

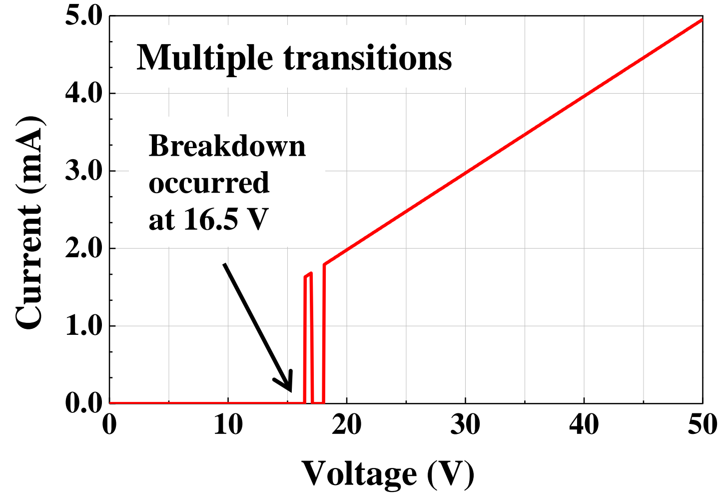

Figure 11 The multiple transitions for the current-voltage (I-V) characteristic

3. *Effect of different probe materials on breakdown voltage*

The probability density plot of measured breakdown voltage with Au-coated and Sn-coated probes is shown in figure 12. The range of measured breakdown voltage was 0 V to 43.85 V. The minimum breakdown voltage of 0 V means that the breakdown occurred at or less than 0.05 V, which was the minimum sensitivity for the experimental setup.

The optimal distribution for breakdown voltage was determined based on the probability plots and goodness of fit tests. According to the Anderson-Daring statistic (AD), which shows how well the data follow a particular distribution, the 3-parameter Gamma distribution with the smallest AD statistic was found to provide the best fit. The likelihood ratio test (LRTP) value of 0.048 for the Au probe and 0.022 for the Sn probe suggests that the 3-paremeter Gamma distribution improves the fit over the 2-parameter Gamma distribution.

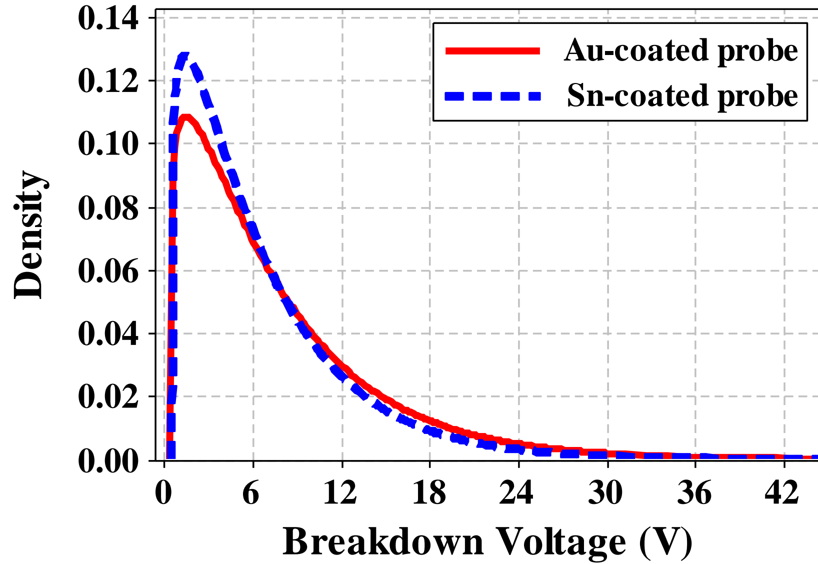

Figure 12 Probability density plot of breakdown voltage depending on probe material

Based on measurements, the mean breakdown voltage was 7.57 V (± 6.69) for the Au-coated probe and 6.60 V (± 5.70) for the Sn-coated probe. The average required voltage to break down the whisker for the Au-coated probe seemed slightly higher than that of the Sn-coated probe; however both breakdown voltage data had high standard deviation. In order to determine whether any statistical difference in breakdown voltage can be attributed to the probe plating material, the Kruskal-Wallis test was used. Kruskal-Wallis analysis is known as the non-parametric equivalent to ANOVA analysis in parametric methods. The hypotheses for this test are H_0: the population medians are all equal, H_1: the medians are not all equal [62]. The results of the Kruskal-Wallis test are shown in Table I. The sample medians for the breakdown voltage using the Au-coated and Sn-coated probes were calculated as 5.30 V and 4.78 V. The Z-value (Z-score) indicates that the mean rank for the Au-coated probe was higher than the mean rank for the Sn-coated probe. However, the test statistic (H) had

a p-value of 0.379 at both unadjusted and adjusted ties, which indicates that the null hypothesis cannot be rejected at levels below 0.379. Therefore, no statistical difference in measured whisker breakdown voltage can be assigned to the probe plating material. Figure 13 presents the cumulative frequency plot of breakdown voltage from 200 whiskers probed by both Sn- and Au-coated probe. This cumulative frequency plot may be used to estimate the probability of electrical shorting by tin whisker based on the voltage level of individual circuit.

Table 1 Kruskal-Wallis test on breakdown voltage depending on probe types

Types of probe	N	Median	Ave Rank	Z
Au-coated	100	5.300	104.1	0.88
Sn-coated	100	4.775	96.9	-0.88
H=0.77 DF=1 P=0.379				
H=0.77 DF=1 P=0.379 (adjusted for ties)				

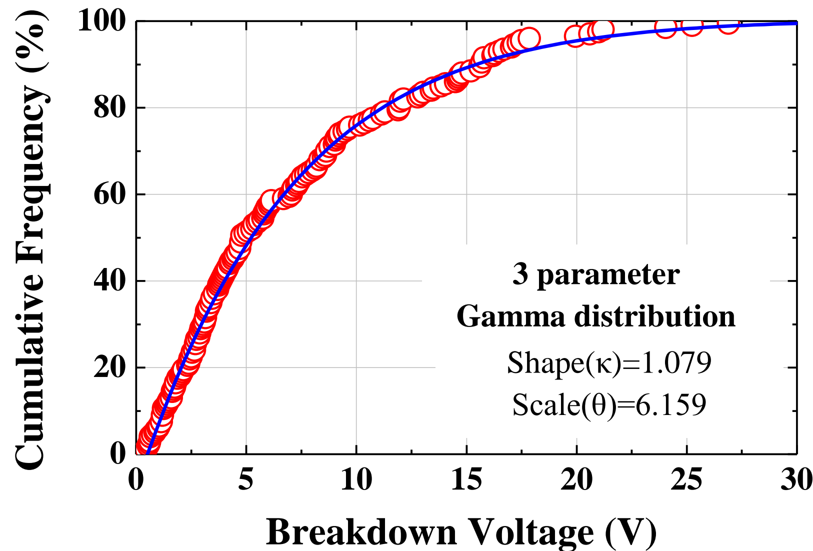

Figure 13 Cumulative frequency plot in breakdown voltage of tin whiskers

4. Breakdown voltage depending on type of voltage-current transitions

Among the 100 whiskers, 56 whiskers showed multiple transitions with the Au-coated probe. When the Sn-coated probe touched the whiskers, 65 out of 100 of the whiskers exhibited multiple transitions. A total 121 out of 200 whiskers showed multiple transitions, and the breakdown voltages measured on 200 whiskers were plotted depending on the type of I-V transitions in figure 14.

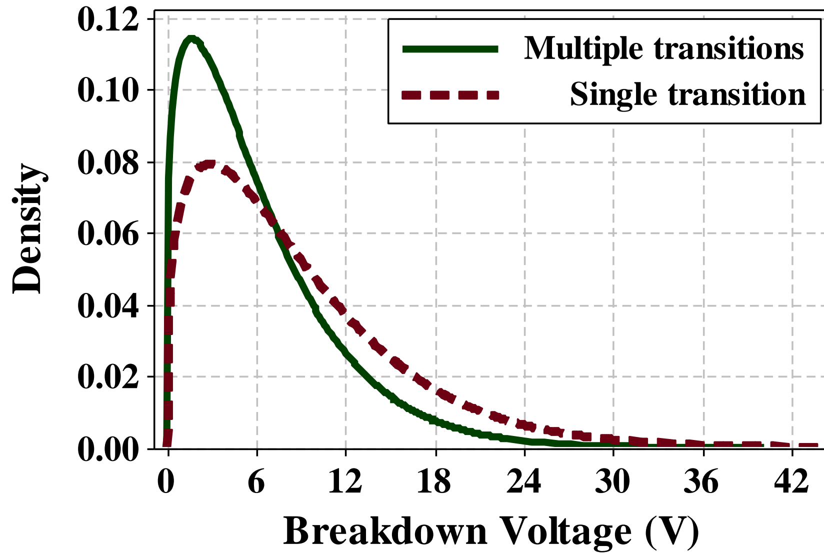

Figure 14 Probability density plot of breakdown voltage depending on type of I-V transitions

The AD statistic showed that the single transition followed the Weibull distribution and the Lognormal distribution was well-fitted for multiple transitions, respectively. Based on the fitted distributions, the average breakdown voltage for a single transition is 8.63 V and for multiple transitions is 6.25 V. The results of the Kruskal-Wallis analysis in Table 2 and it show that there is a statistical difference

between the average breakdown voltage for a single transition and for multiple transitions (p-value=0.003). This shows that multiple transitions have a smaller median breakdown voltage than single transitions.

Table 2 Kruskal-Wallis test on breakdown voltage depending on type of I-V transitions

Types of I-V transitions	N	Median	Ave Rank	Z
Single transition	79	8.000	115.7	3.01
Multiple transitions	121	4.000	90.5	-3.01
H=9.06 DF=1 P=0.003				
H=9.06 DF=1 P=0.003 (adjusted for ties)				

5. *Probed surface depending on type of voltage-current transitions*

Figure 15 and 16 present the probed surface of tin whisker depending on type of I-V transitions. In single transition occurred during the breakdown of tin whisker, the distinct probed point showed on the surface of tin whisker. The contacted point by probe was melted due to the joule heating caused by high current density between the probe and whisker surface after the breakdown occurs. As shown in figure 16, when the multiple transitions occurred, the probed point is larger than that of single transition. It might be caused by intermittent contact between the probe and whisker surface. Due to the intermittent contact, the probe point was slightly moved and it caused the multiple transitions in I-V transitions and larger damages on the surface of

tin whisker by contacted probe. Some more contacted surface by probe on tin whisker depending on the type of I-V transitions showed in figure 17.

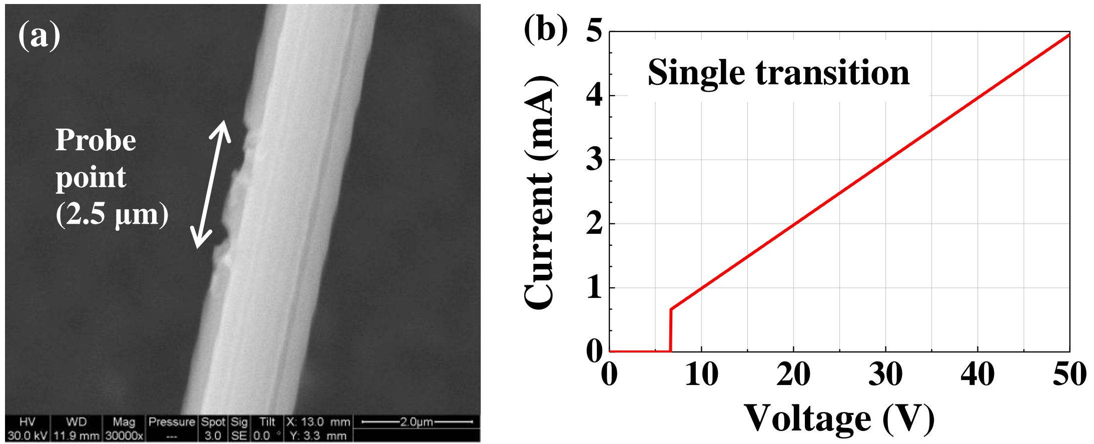

Figure 15 (a) The probed point on the surface of tin whisker showed the single transition and (b) Its I-V transition

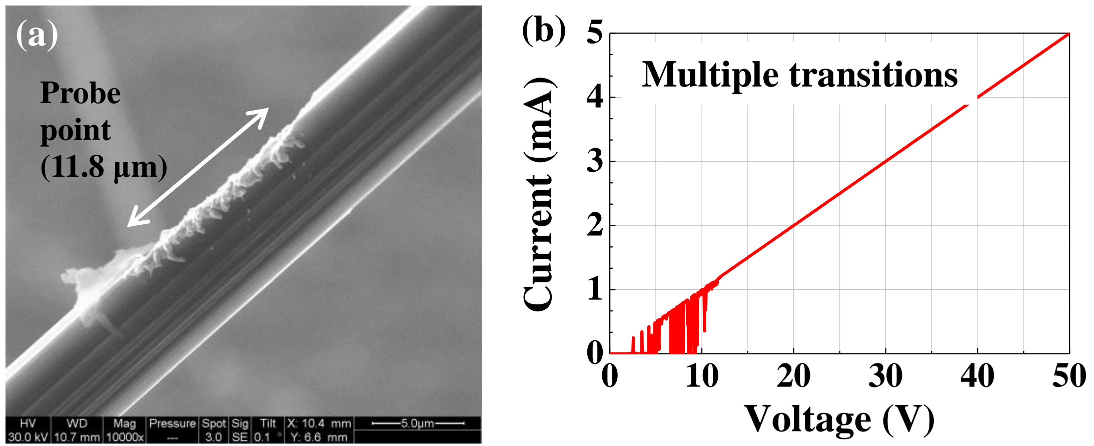

Figure 16 (a) The probed point on the surface of tin whisker showed the multiple transitions and (b) Its I-V transition

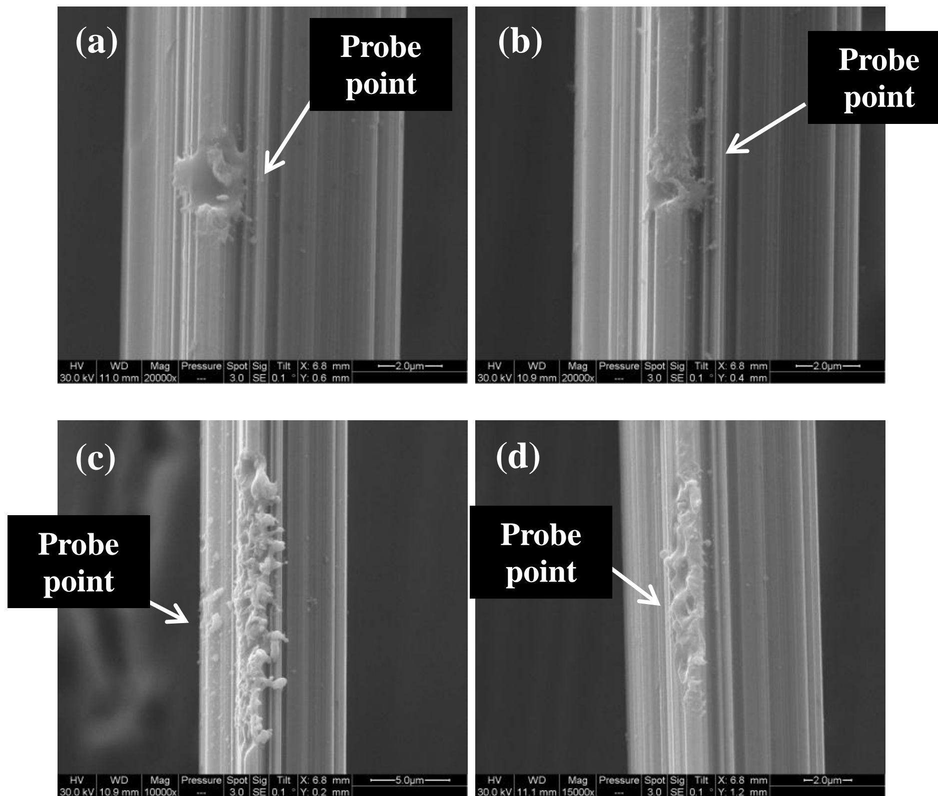

Figure 17 Probe contacted surfaces depending on type of current-voltage (I-V) transitions: (a), (b) Single transition, and (c), (d) Multiple transitions

After the breakdown voltage measurements, it was observed that 59 out of the 200 test whiskers did not return to their original positions after the probe was moved away. Among those 59 whiskers, 56 showed multiple transitions in their I-V characteristics. It was verified through physical examination that the root areas of the whiskers were permanently deformed or bent after contact. An example of the permanent deformation is depicted in figure 18. The permanent deformation of the root area in a whisker can be explained by a contact force sufficient to exceed the elastic limit of the tin whisker. The observed deformation may cause intermittent contact between the probes, producing multiple transitions during breakdown measurement. This result promoted an effort to quantify the contact force.

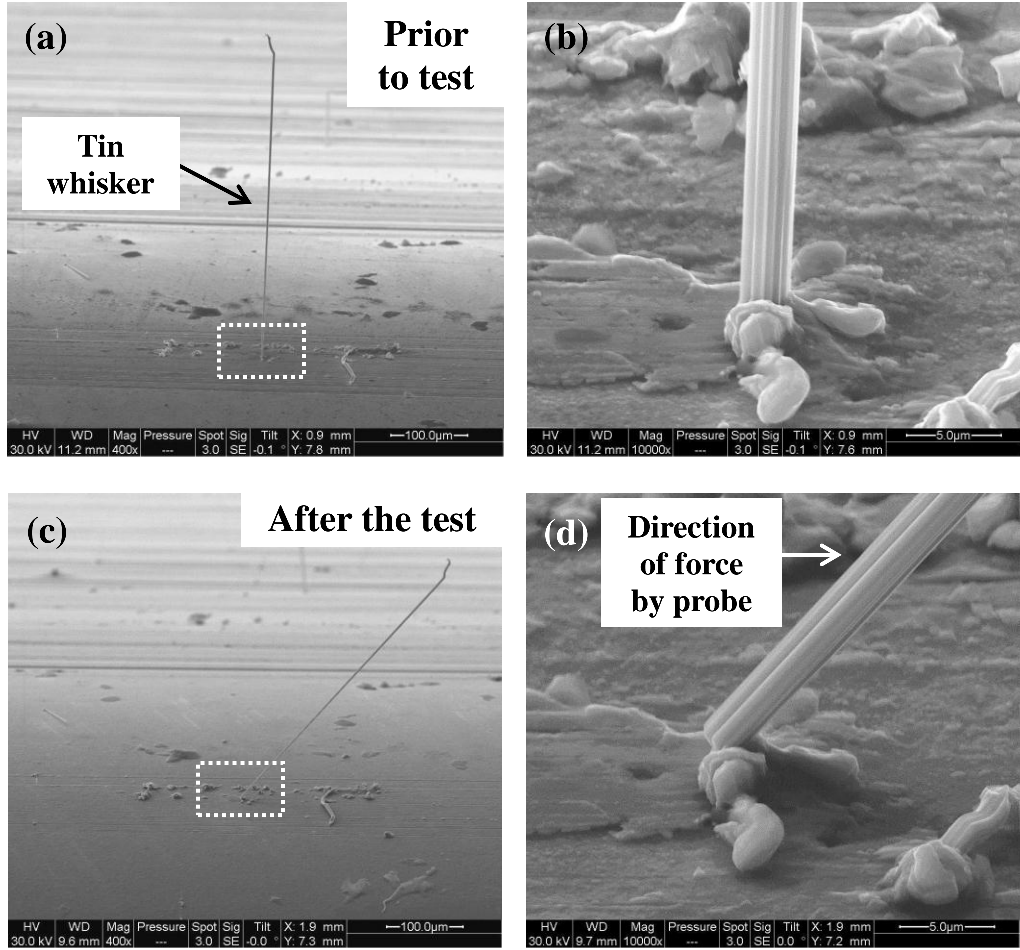

Figure 18 Whisker deformation caused by probe contact: (a) Prior to contact by probe, (b) Close-up of root area of tin whisker indicated in figure 18(a), (c) After the test and (d) Close-up of root area of tin whisker indicated in figure 18(c)

6. *The effect of contact force on breakdown voltage*

The presence of surface contaminants, surface hardness and contact force are the major factors that affect the fundamental properties of electrical contacts. In order to examine the role of contact force, a separate set of breakdown voltage tests were conducted. In these tests, the contact force was estimated by measuring the deflection of the whisker and applying a cantilever beam model. To facilitate contact force measurement, select whiskers were detached from the surface of the card rails and attached to a copper plate using a conductive silver paint as shown in figure 19. The silver paint holds the detached whiskers and provides an electrical path between the whisker and the copper plate. A scanning electron microscope (FEI Quanta 200F) was used to measure whisker diameter and the length of detached whiskers. Whisker diameter was measured at 3 different points on each whisker, from whisker root to whisker tip. Only whiskers with maximum diameters less than 10 % of their minimum diameters were selected for testing to minimize the effects of a non-uniform whisker diameter on contact force estimation using the cantilever beam model.

In order to correlate the contact force to the transition of I-V characteristics in breakdown voltages, the electrical breakdown was measured by bringing the Au-coated probe into contact with five different whiskers at 70 different points.

The estimated contact force due to contact between the probe and the whisker is given by (1), and the moment of inertia (I) is calculated using (2):

$$P = \frac{3EI\delta}{L^3} \qquad (1)$$

and

$$I = \frac{\pi r^4}{4} \qquad (2)$$

where P is the contact force of the contacted probe, E is the elastic modulus of tin (41.4 GPa), L is the distance from the base of the whisker, and δ is the deflection of the whisker. The deflection of the whisker was measured by merging an image of the whisker prior to probe contact with an image of the whisker under probe contact. Images were merged using imaging software, as shown in figure 20.

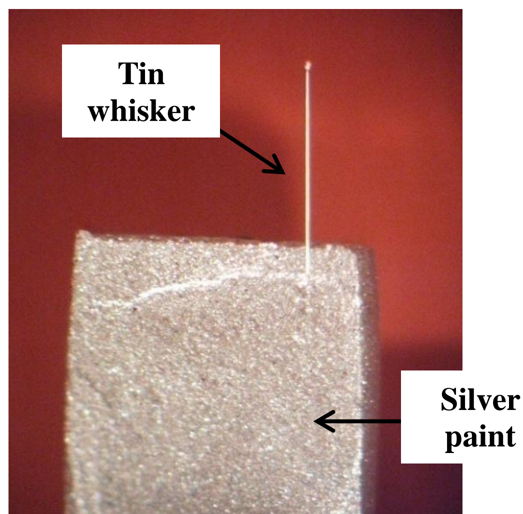

Figure 19 Test specimen for contact force measurement

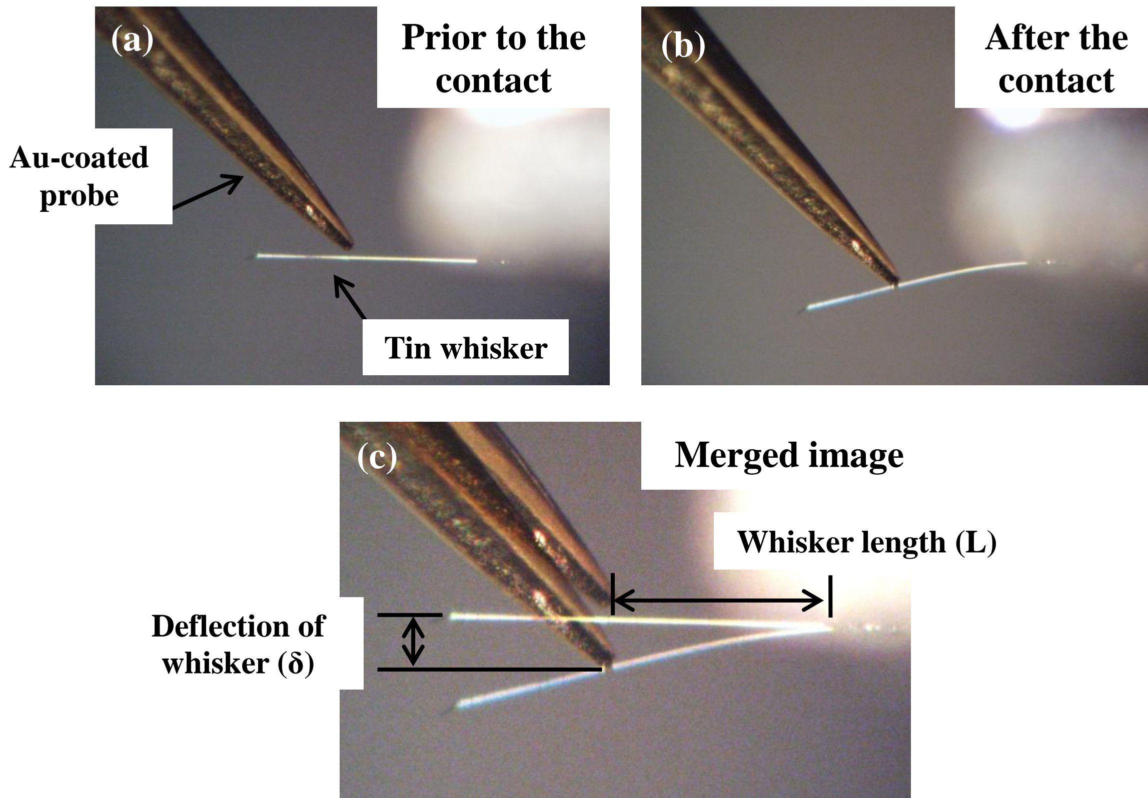

Figure 20 Image merged in which shows (a) Prior to contact and (b) After contacting by Au-coated probe

The breakdown voltage versus the estimated applied force for single and multiple transitions in I-V characteristics is shown in figure 21. A total of 10 out of 70 contact points exhibited multiple transitions, and 52 contact points showed a single transition. For 8 contact points, breakdown occurred at less than 0.05 V, which was the minimum sensitivity of the experimental setup. The correlation between contact force and breakdown voltage in multiple transitions is 0, which means that there is no linear relation between the two variables. However, the correlation of -0.298 in single transition indicates a negative relationship between breakdown voltage and contact force.

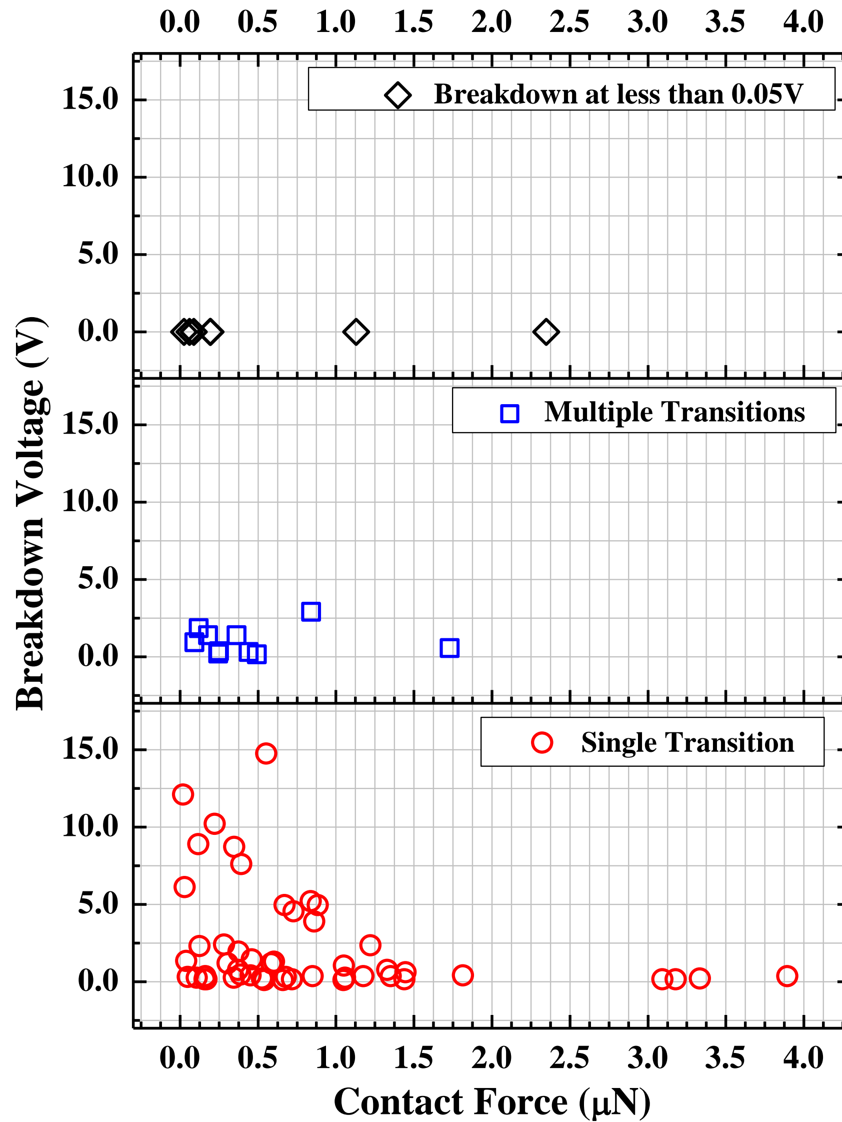

Figure 21 Plot of breakdown voltage versus contact force

Figure 21 also depicts that the multiple transitions have a much smaller than average breakdown voltage than that of the single transition, which is consistent with the result from the breakdown voltage measurement on 200 whiskers using Au- and Sn-coated probes. The average contact force for a single transition with 1.872 μN was higher than that of multiple transitions with 0.745 μN. This result can explain the

reason why permanently deformed whiskers are more likely to exhibit multiple transitions. When the probe deflected the whisker sufficiently to induce a permanent deformation, the contact force does not increase linearly with deflection. Therefore, the contact force is lower than similar whiskers that did not have permanent deformation. It is also observed that the level of the breakdown voltage is less than 1 V, when the contact force exceed than 1.5 μN.

Mechanical bridging by tin whisker between two isolated conductors can be established by either airborne whiskers or grown whiskers from the adjacent conductor (It was depicted in in figure 3). When the airborne whisker bridges the two isolated conductors, the force of gravity by tin whisker would be the contact force between the whisker and conductors. For mechanical bridging by grown whiskers, the whisker can be buckled after touching the adjacent conductor surface, thus the bucking force by tin whisker would be the contact force between the whisker and conductors. In order to investigate the range of contact force caused by airborne whiskers and buckled whiskers, the force of gravity and buckling force by tin whiskers were estimated.

The force of gravity by tin whisker can be estimated using following equations (3), (4) [63]:

$$F_{Gravity} = 9.8 \cdot V_{Whisker} \cdot \rho_{Sn} \qquad (3)$$

and

$$V_{Whisker} = L_{Whisker} \cdot \pi \cdot \left(R_{Whisker}\right)^2 \qquad (4)$$

where, $F_{Gravity}$ is the force of gravity by tin whisker, $V_{Whisker}$ is the volume of whisker, ρ_{Sn} is the density of tin (7310 kg/m^3), and $L_{Whisker}$ and $R_{Whisker}$ is the length and radius of whisker, respectively.

The buckling force by tin whisker can be estimated using following equation (5) [46]:

$$F_{Buckling} = \frac{\pi^3 E_{Sn} d^4}{32L^2} \qquad (5)$$

where, $F_{Buckling}$ is the buckling force by tin whiskers, E_{Sn} is the elastic modulus of tin (41.369 GPa), and L and d is the length and diameter of whisker.

Figure 22 and 23 presents the cumulative frequency plots of estimated contact force between the whisker and conductors. In this estimation, the whisker length and diameter information reported by Panashchenko [64] was used. Among 877 whiskers, the whisker length is longer than 50 μm were chosen to estimate the contact force, since 50 μm was the maximum allowable whisker length proposed by National Electronics Manufacturing Initiative (NEMI) [65].

The estimated contact force between airborne whisker and conductors is the range between 0.09 ~ 4.6 pN. While, it is the range between 0.01 ~ 88.7 mN from the estimated contact force between buckled whisker and conductor. Hilty et al [49] predicted the contact force generated by pre-buckled whisker and it was about 1 mN. The estimated contact force between airborne whisker and conductors represents that when airborne whisker physically bridges the two conductors' surfaces, either multiple or single transition in breakdown of tin whisker may occur since the contact force between whisker and conductors is much smaller than 1.5 μN as depicts in

figure 21. However, when the whisker contacts the conducts with buckled, only single transition in breakdown voltage of tin whisker might be established with lower breakdown voltage than 1 V as observed in figure 21 because the contact force is much higher than 1.5 μN.

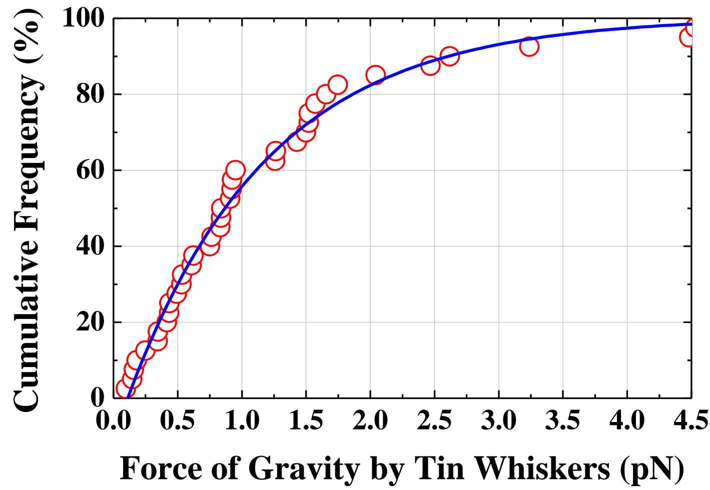

Figure 22 Cumulative frequency plot of estimated contact force between airborne whisker and conductors

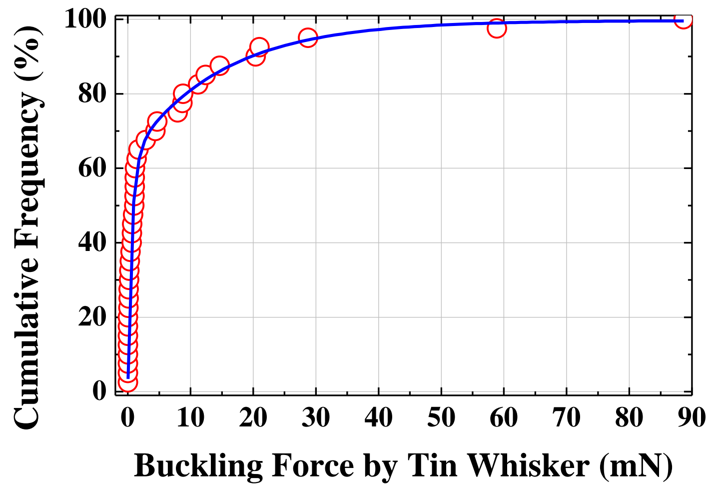

Figure 23 Cumulative frequency plot of estimated contact force between buckled whisker and conductor

7. *Breakdown between the two whiskers*

It is reported that the tin whisker can be attracted by electrostatic force [31] and it implies that the electrical failure can be caused by touching the whiskers grew from two different biased conductors even two whiskers did not physical bridged.

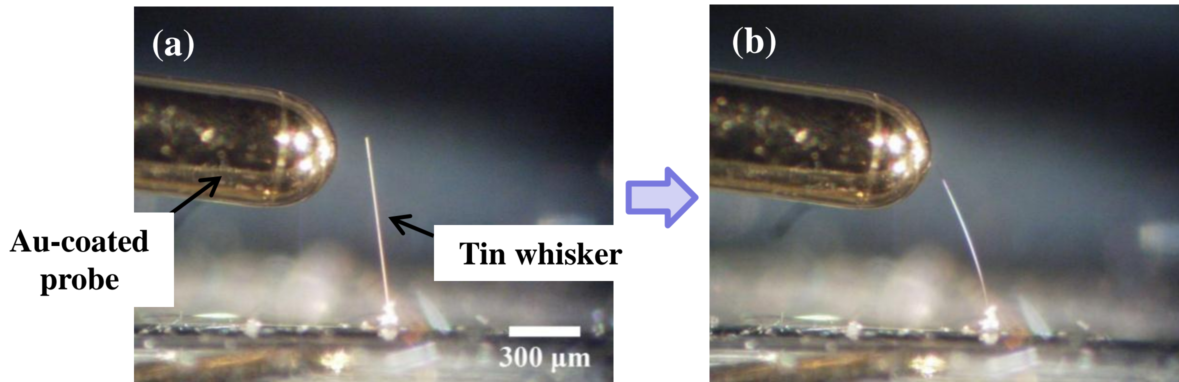

Figure 24 Deflection of whisker by electrostatic force between probe and tin whisker

Figure 24 depicts the deflection of whisker by electrostatic force between the tin whisker and voltage biased Au-coated probe. The distance between Au-coated probe and whisker was 294.1 µm and the voltage was applied from 0 V to 50 V using the parameter analyzer. As shown in figure 25, when the voltage increased to 25 V, the current flow through the whisker, which represents that the whisker deflected and touched the probe surface by the attraction due to the electrostatic force between the Au-coated probe and whisker. After the voltage cut off, the connection between whisker and probe disconnected and the whisker was deflected back to its original position. It is also observed that the required voltage can establish the connection between the probe and whisker was decreased when the distance between the probe

and whisker decreases as depicted in figure 26 It is because the magnitude of the electrostatic force between two point electric charges is directly proportional to the magnitudes of each charge and inversely proportional to the square of the distance between the charges. When whisker attracted by electrostatic force and touched the Au-coated probe, only single transition in current-voltage characteristic were observed.

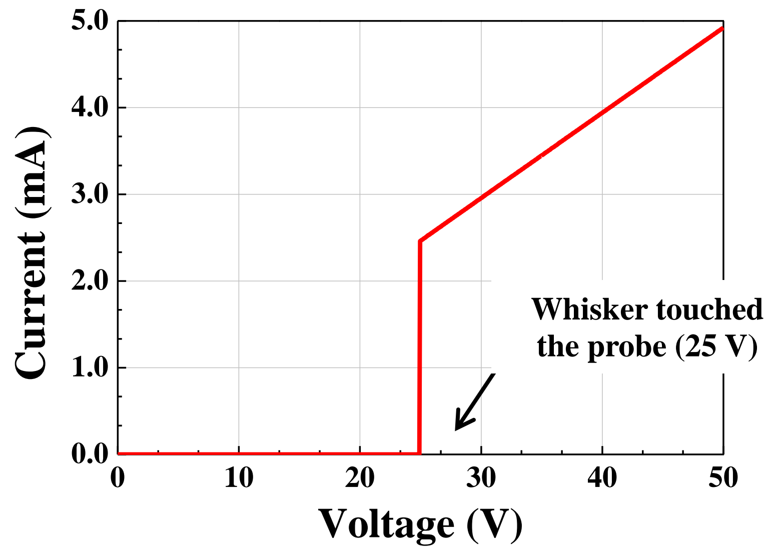

Figure 25 Current-voltage characteristic when deflected whisker touches the probe (the distance between probe and whisker: 294.1 μm)

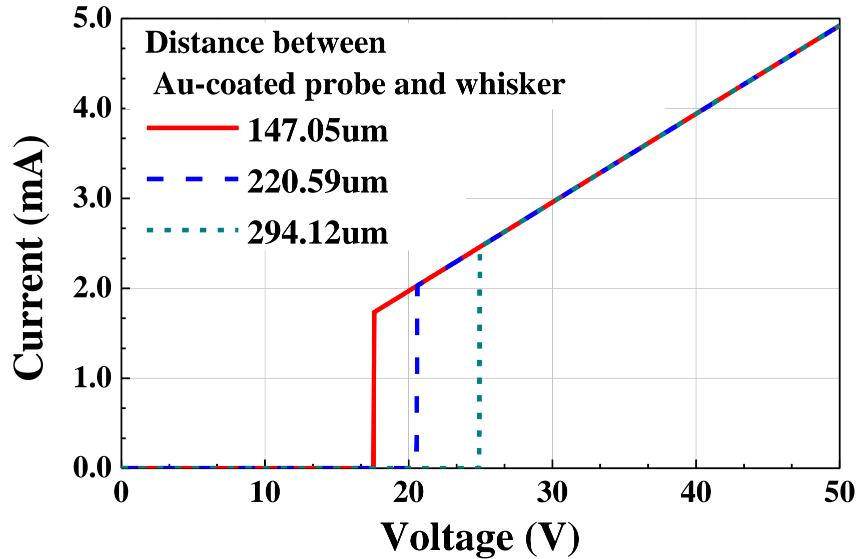

Figure 26 Current-voltage characteristic depending on the distance between Au-coated probe and tin whisker

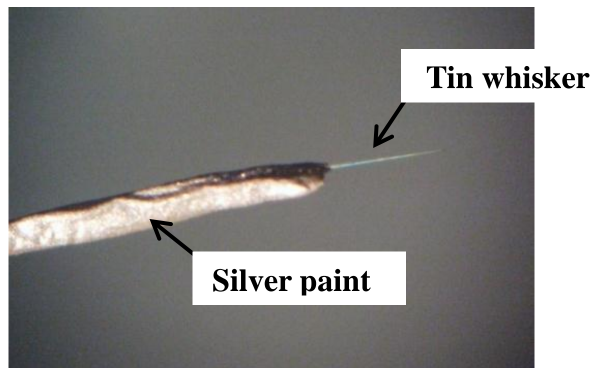

Figure 27 Tin whisker probe

The whiskers grown from the card-rail surface were harvested and attached on the copper wire (diameter 500 μm) using the silver paint as shown in figure 27. In order to evaluate the breakdown between two tin whiskers, two whisker probes touched each other as depicted in figure 28 and measured the breakdown voltage. The breakdown voltages were measured 5 times using the whisker probes. The measured

breakdown voltage presents in Table 3. The average measured breakdown voltage between two whiskers was lower (1.08 V) than the average measured breakdown voltage from the Au- and Sn-coated probes (7.08 V). In addition, the breakdown between two tin whiskers only showed the single transition in current-voltage characteristic.

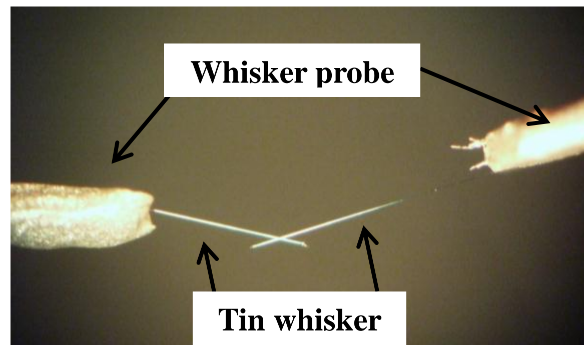

Figure 28 Two whisker probes touched each other

Table 3 Breakdown voltage between two whiskers

Measurement #	Breakdown voltage (V)
1	0.2
2	0.2
3	0.15
4	4.6
5	0.25

8. *Oxide layer on whisker surface*

The presence of a non-conductive surface layer and its thickness may be another major factor in determining the whisker breakdown voltage level. In order to verify the presence of a non-conductive surface film on the whisker, the cross-sectional transmission electron microscopy (TEM) specimens of select tin whiskers were prepared using a focused ion beam (FIB) with a gallium (Ga) ion source at an acceleration of 30 keV. Select whiskers on the card rail were coated by carbon (C) and platinum (Pt) to protect the surface from ion-beam induced damage and unwanted milling during the FIB process. The prepared cross-sectional specimens were observed using FE-TEM (JEM-2100F, JEOL) and FE-STEM (HD-2300A, Hitachi) at an acceleration voltage of 200 keV. The chemical composition of the non-conductive surface film on the whisker surface was determined using scanning TEM-energy dispersive X-ray microanalysis (STEM-EDX).

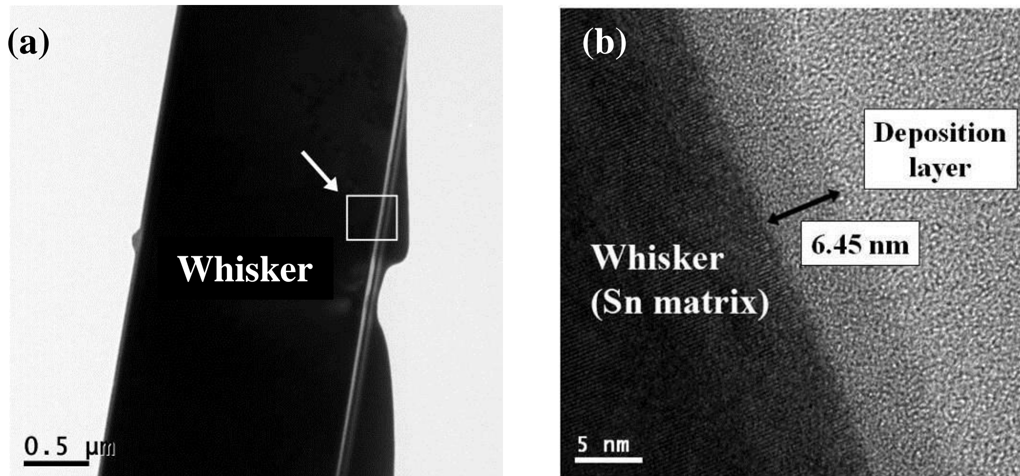

Figure 29 A high resolution transmission electron microscopy (HRTEM) images of whisker body and whisker surface: (a) BF-STEM image of Whisker #1 surface (b) HR-TEM image of area indicated in figure 29(a)

Figure 29(a) and (b) show a bright field (BF) image of a part of the whisker body and a high resolution transmission electron microscopy (HRTEM) image obtained from the area indicated by a white box with an arrow in figure 29 (a). The HRTEM image showed the presence of a surface layer with a thickness of approximately 6.45 nm between the whisker (Sn matrix) and the deposition layer. The surface layer was identified from the analysis of STEM-EDX as the composition of Sn and O, or Sn oxide, as shown in figure 30(a) and (b). The surface Sn oxide layer on whisker #2 with 3.75 nm thickness had a smaller thickness than the oxide layer on whisker #1, and both Sn oxide layers had amorphous structures.

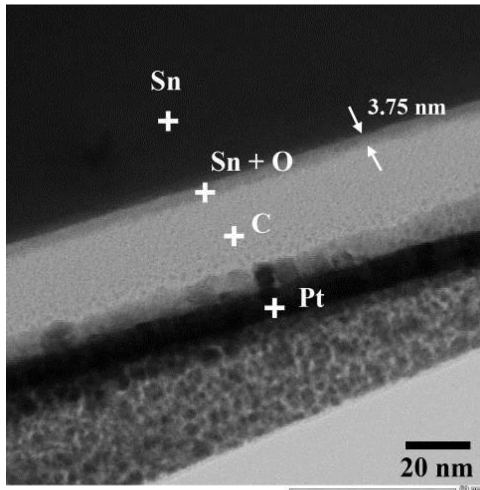

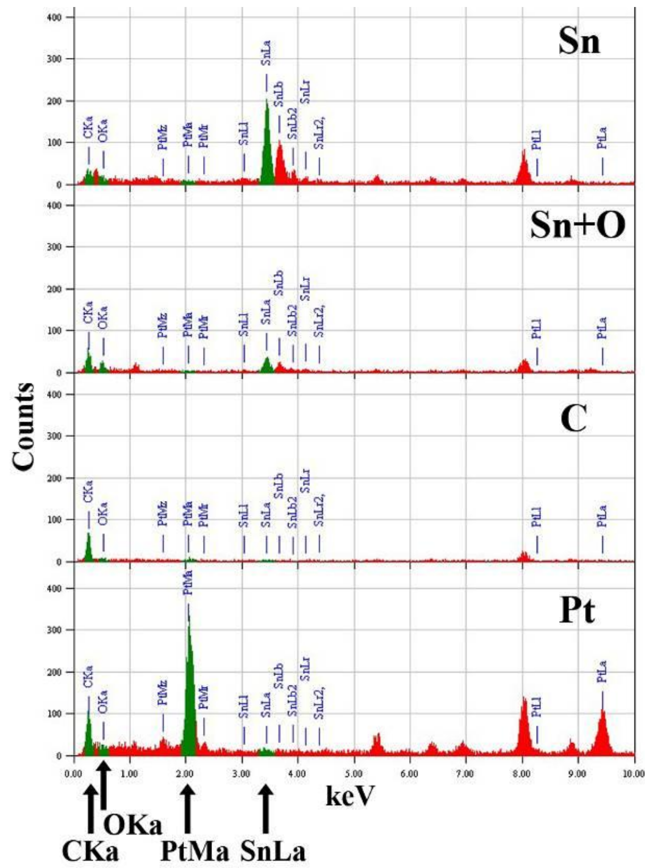

Figure 30 The surface layer analysis using STEM-EDX: (a) HRTEM image of oxide layer on Whisker #2 surface, (b) STEM-EDX analysis of selected point in figure 30(a)

9. Conclusion

The average breakdown voltage for tin whiskers was 7.57 V with the Au-coated probe and 6.60 V with the Sn-coated probe. Statistically, there is no significant difference in the mean breakdown voltage that can be assigned to the probe finish. The contact forces between the probe and the whisker induced by whisker deflection was estimated using a cantilever beam model. Multiple transitions in the current-voltage (I-V) characteristics were found to have a lower than average breakdown voltage and contact force than the single transition breakdown voltage. In a single transition breakdown voltage, the relationship between breakdown voltage and contact force had a negative correlation of -0.298. Thus, it is verified that contact force is an important factor in determining the types of I-V transition and breakdown voltage.

In addition to the correlation between breakdown voltage and contact force, the presence of 6.45 nm thickness Sn oxide layer on the surface of test tin whiskers was verified using TEM. The results indicate that the contact force should be considered along with the voltage potential in determining if an electrical short will occur.

Chapter 4: Metal vapor arcing propensity of tin whiskers

Whiskers also present a safety concern, since whisker-induced electrical shorts can initiate metal vapor arcs, which are capable of melting the metal and incinerating the plastics used in electronic products. The potential for this catastrophic failure is affected by several factors, including whisker geometry, bias voltage and ambient pressure. Previous studies have demonstrated metal vapor arc formation using gold and tin wires and reported that the minimum voltage for sustaining a metal vapor arc in both vacuum and atmospheric pressures [54, 55]. However, material and geometry differences between gold and tin wire (25 to 50 μm) and tin whiskers (0.5 to 10 μm) may influence metal vapor arc formation. Further, the combined effects of several factors - such as whisker geometry, voltage, and pressure conditions - have not yet been studied and a practical guide for assessing the potential for tin whisker–induced metal arc formation has not been provided.

In this chapter, the metal vapor arc failure by tin whiskers will be assessed using test specimens with harvested tin whiskers. Tests will be conducted at various voltages and pressures in order to characterize the conditions required for metal vapor arc formation and, if feasible, identify practical criteria for tin whisker–induced metal vapor arc formation. In addition, a logistic regression model that can assess the likelihood of vapor arc formation by tin whisker will be discussed. The effectiveness of conformal coating on vapor arcing by tin whisker will be also evaluated using the conformal coated arc test specimens.

1. *Experimental setup*

1.1 Arc test specimen and test circuit

Tin whiskers were harvested from an inventory of whisker-bearing structures and attached between two tin-plated copper electrodes using conductive silver paint, to simulate when a tin whisker from tin plating layer bridges the adjacent tin plating conductor surfaces. Figure 31 shows an individual test specimens using tin whisker; a close-up of a detached whisker on tin-plated copper electrodes is shown in figure 31 (b). The gap spacing between the edges of the tin-plated electrodes was fixed at approximately 300 μm and 600 μm. After the harvested tin whisker attached on the tin-plated electrodes, the electrical continuity of the each test specimen was verified using an electrical multimeter.

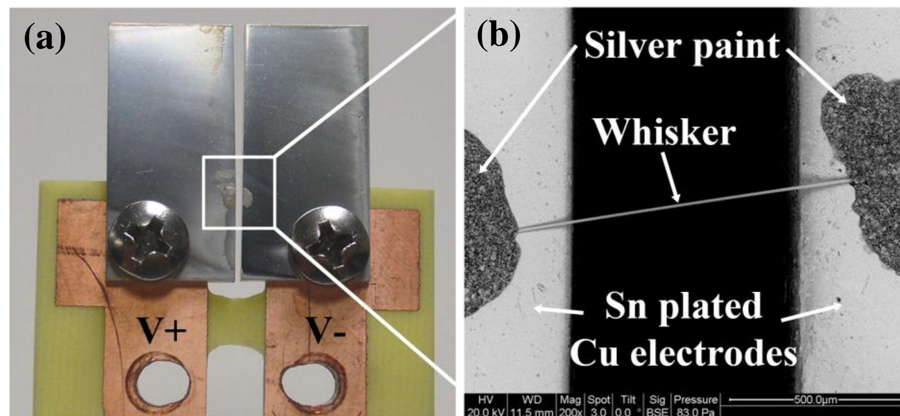

Figure 31 (a) Tin whisker arc test specimen and (b) Close-up of detached whisker on tin-plated electrodes

Individual test specimens were placed under a vacuum jar capable of a minimum pressure of 25 torr in order to control pressure conditions. Pressure was

measured using a digital vacuum gauge. As shown in the schematic of the electric circuit in figure 32, the test specimen was connected with lead-acid batteries in order to supply the voltage and current. In the test circuit, one side of each tin-plated electrode was set to a positive voltage potential (+V), while the other side was set to a negative voltage potential (–V). The positive voltage potential was supplied by up to three lead-acid batteries ranging from 0 to 37.5 V in 12.5 V steps. The negative voltage potential was provided by a single lead-acid battery between 0 and 12.5 V in steps of 2.5 V using a voltage divider. The setup allowed for fixed voltage levels up to 50 V to be supplied to the test specimen. With the batteries as the power source, the rise time of the current was nearly instantaneous.

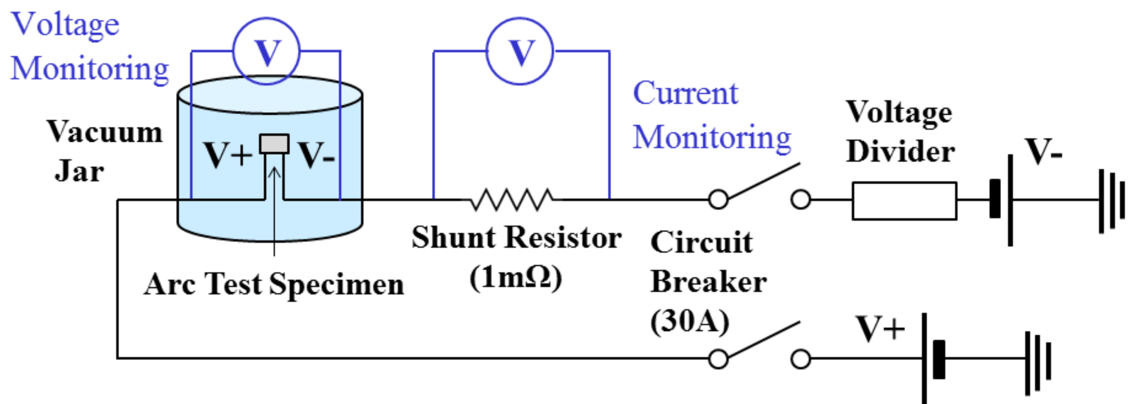

Figure 32 Schematic of the electric circuit for the metal vapor arc test by tin whiskers

The instantaneous current and voltage characteristic during the metal vapor arc were collected using an oscilloscope capable of maximum sampling rate of 2 GSa/s. The current transition during the metal vapor arc was monitored using the

instantaneous voltage across the shunt resistor (1 mΩ) due to the large amount of current flow during the vapor arc by tin whisker. A 30 A circuit breaker was placed in the arc test circuit to interrupt the current flow and minimize anomalous conditions resulting from the arc test.

Arc tests were conducted at four pressures: 760 torr (sea level), 400 torr (approximately 15,000 feet above sea level), 178 torr (approximately 35,000 feet above sea level), 75 torr (approximately 52,000 feet above sea level) and 30 torr (approximately 66,000 feet above sea level). The test pressure conditions were intended to represent conditions that may be experienced by avionic applications as shown in figure 33.

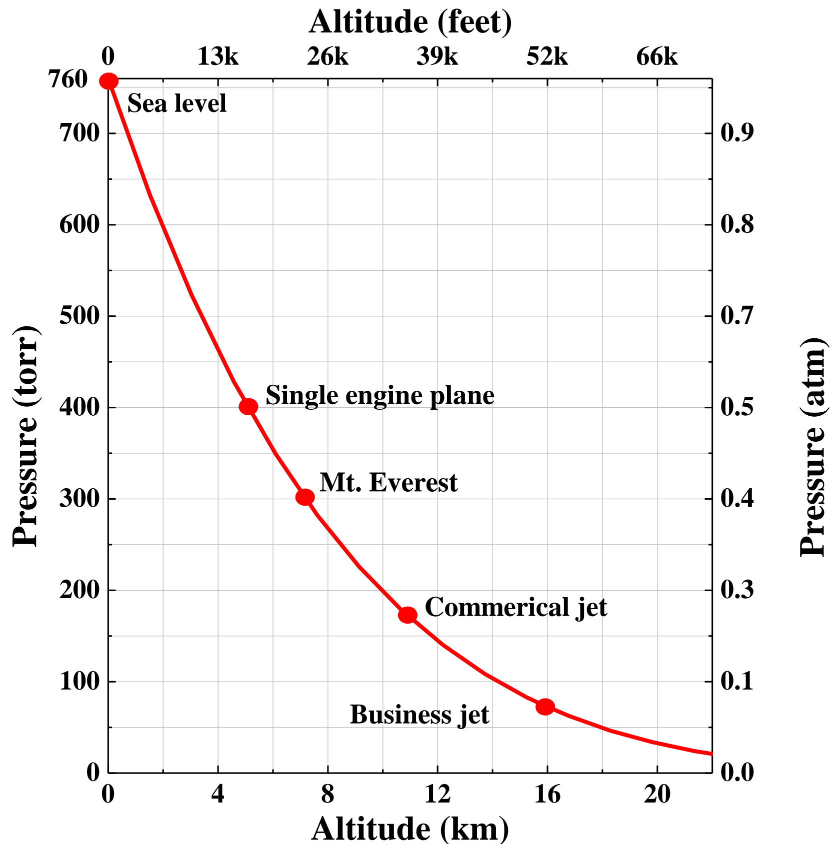

Figure 33 Typical altitude of airplane and its altitude

1.2 Verification of vapor arc by tin whisker

Metal vapor arcs were identified by light emissions during the test and post-test observations of surface damage on the tin-plated copper coupons, such as burn marks or craters which indicates the cathode spot formation after the test using both optical microscope and SEM. Figure 34 shows the light generation during the vapor arc by tin whisker and observation of burn marks on the surface of Sn-plated Cu electrodes after the arc test. In addition to post-arc observation, the arc formation process was documented using a high-speed camera (180 kHz frame rate), because the vapor arc event is usually restricted to a few milliseconds.

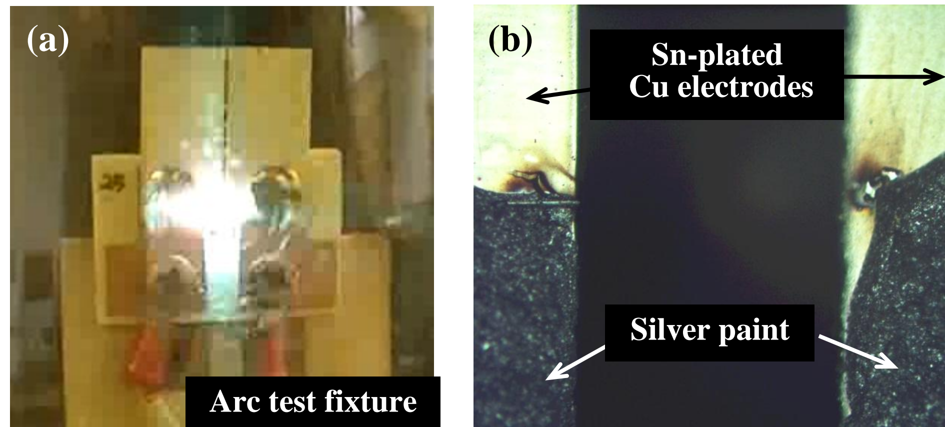

Figure 34 (a) Light generation during the vapor arc by tin whisker and (b) Burn marks on the surface of the test specimen after the arc test

1.3 Conformal coated arc test specimen

The possibility of whisker induced electrical failures can be minimized by means of application of a conformal coating on exposed electrical conductive surfaces [46-48]. In order to evaluate the effectiveness of application of a conformal coating on vapor arc failure by tin whisker, the arc test specimens were coated using Acrylic (AR) coating by spray method.

Two groups of conformal coated test specimens were created; Test specimens in group 1 was applied the conformal coating after the tin whisker was attached on the tin-plated copper electrodes. As shown in figure 35(a), both tin whisker and electrodes are covered by conformal coating. It may represent the situation that the whisker has been bridged the adjacent conductors before the conformal coating is applied. It is known that the whiskers can escape from the conformal coated surface [46-48] and these escaped whiskers may establish the physical connection to the conductor surface. To simulate this situation, test specimen in group 2, the surfaces of

electrodes are coated by conformal coating except the areas for whisker attachment and metal fasteners, as shown in figure 35(b) and 35(c). Thus, the whisker is free from the conformal coating but the gap spacing the electrodes are also covered by conformal coating. Four test specimens in each group were prepared and conducted the arc test with 50 V at 30 torr condition.

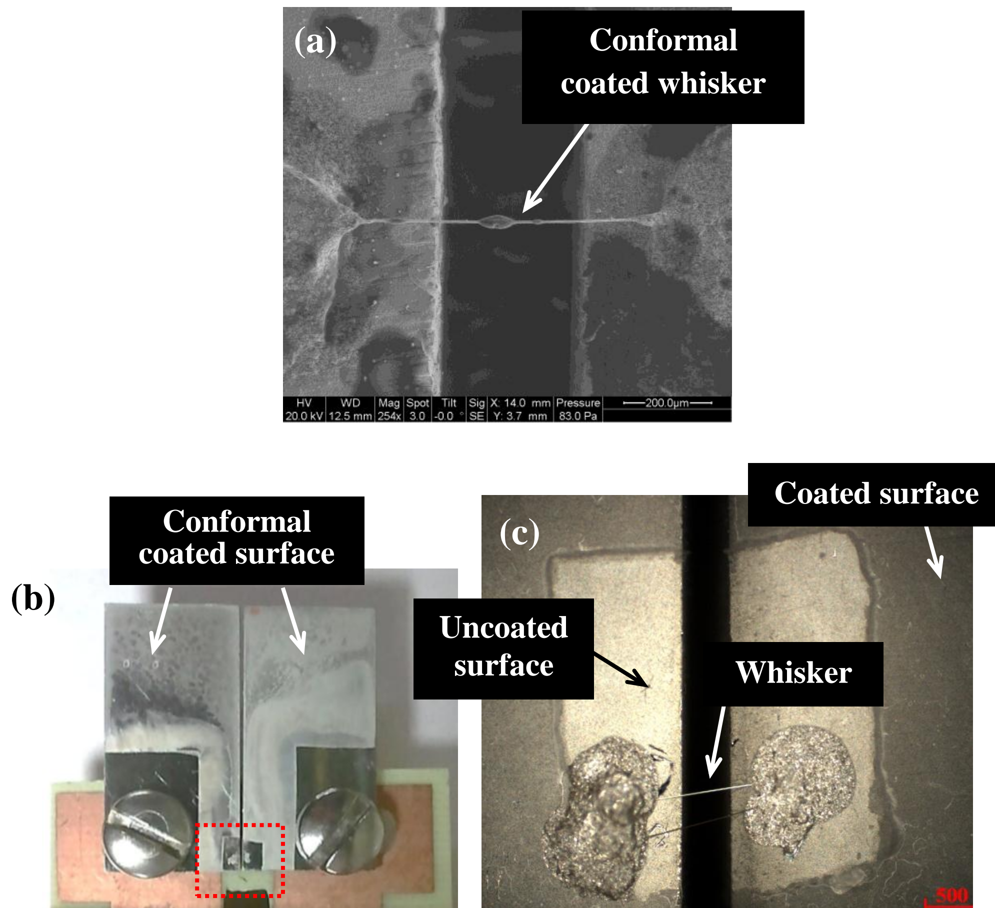

Figure 35 Conformal coated arc test specimen: (a) Test specimen in group 1, (b) Test specimen in group 2, and (c) Close-up of attached whisker indicated in figure 35(b)

2. *Physical and electrical characteristics of arc test specimen*

2.1 Physical characteristics

Due to the natural variation in harvested tin whiskers, the whisker geometry including the length and diameter of whiskers and conductor gap which defined as the spacing between the edges of the tin-plated copper electrodes were documented by a scanning electron microscope (SEM) prior to each test. The measured whisker lengths and diameters were identified as the physical parameters for a metal vapor arc caused by a tin whisker. For the purposes of these tests, the documented whisker length was defined as the measured distance between the points where the both ends of whisker made contact with the conductive silver paint as shown in figure 36.

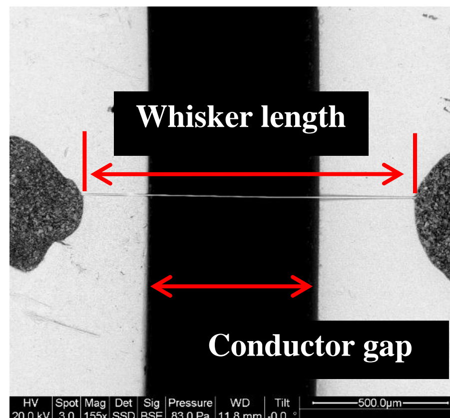

Figure 36 Whisker length and conductor gap between tin-plated electrodes

The probability density distribution of whisker length and whisker diameter in test specimens depends on the conductor gap depicted in figure 37 and 38. According to the Anderson-Daring statistic (AD), both distributions of whisker length and whisker diameter followed the 3 parameter Weibull distribution.

For whisker length, as decreasing the gap spacing between electrodes, the mean of whisker length was decrease and there is significant statistical difference between the groups of specimens with 300 μm conductor gap and 600 μm conductor gap (p-value < 0.001 from Kruskal-Wallis test). The median length of whisker was 746 μm for 300 μm gap spacing and 1209 μm for 600 μm gap spacing, respectively.

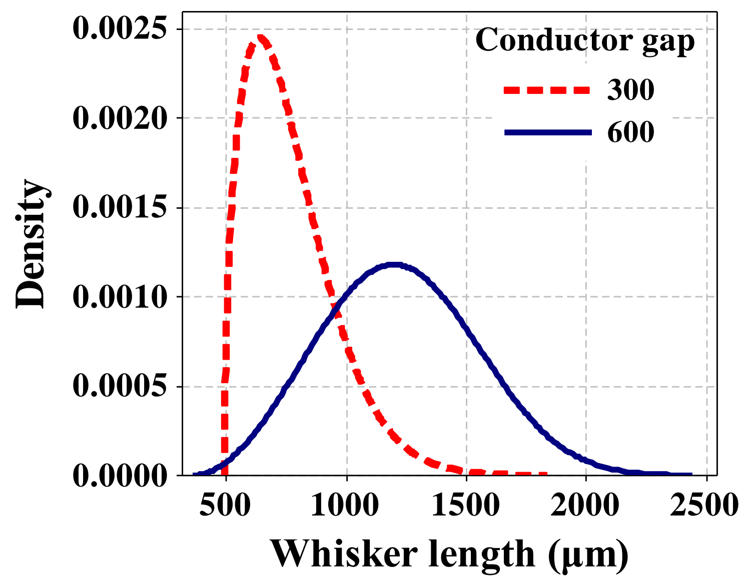

Figure 37 Whisker length distribution depends on spacing between electrodes (Conductor gap: 300 μm versus 600 μm)

While, there is no statistical difference in terms of diameter of whisker depending on the gap spacing between 300 μm and 600 μm (p-value=0.96). The median diameter of whiskers in both groups of samples is 5.52 μm. Thus, the increment of conductor gap between electrodes only increases the whisker length but the whisker diameter was not affected by gap spacing. The median diameter of whiskers (5.52 μm) in arc test specimens is similar compared to the median diameter

of 877 whiskers (4.38 μm) on tin-plated brass that grew over 11 years of ambient storage conditions [64].

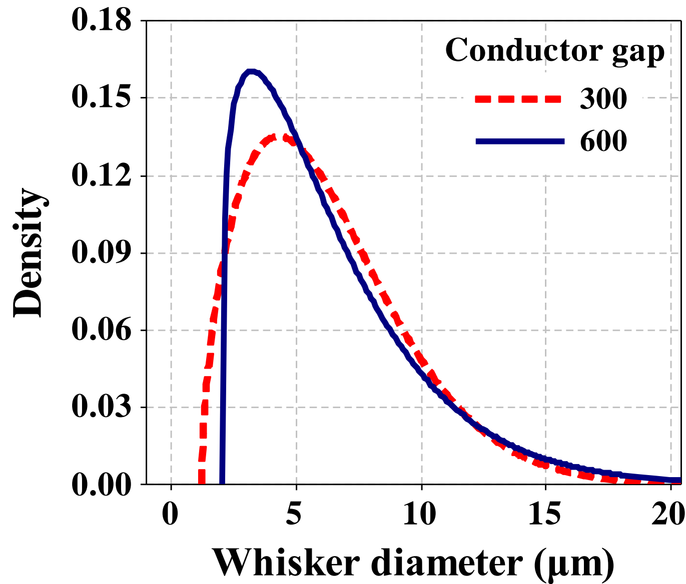

Figure 38 Whisker diameter distribution depends on spacing between electrodes (Conductor gap: 300 μm versus 600 μm)

2.2 Electrical characteristics

As an electrical parameter for arcing test by tin whisker, the resistance of test specimen was measured using the milliohm-meter by four probe method. The resistance of test specimen was the average value from 196 measurements by milliohm-meter. The detection current supplied by the milliohm-meter was limited to 10 μA. This limit was set after partially melted whiskers were observed when current flow was higher than 10 μA, as depicted in figure 39.

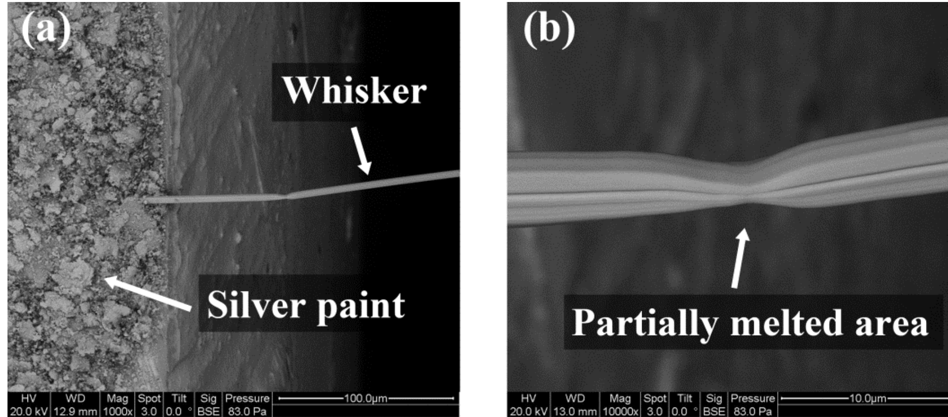

Figure 39 (a) Thermally damaged test specimen due to biased current (higher than 10 μA) by mili-ohmmeter without the current limit and (b) Close-up of melted area at whisker

Figure 40 shows the distribution of measured resistance of test specimen. Due to the structure of arc test specimen as shown in figure 41, the measured resistance of test specimen can be defined as following series of resistances (6):

$$R_{\text{Test specimen}} = R_{\text{Whisker}} + R_{\text{etc}}\,(R_{\text{Silver paint}} + R_{\text{Electrodes}} + R_{\text{Metal fasteners}}) \quad (6)$$

where, R_{etc} includes the resistance of silver paint, electrodes and metal fasteners which depend on test specimen, and $R_{Whisker}$ is the resistance of whisker. However, the resistance of R_{etc} was quite small (less than 0.8 Ω) comparing to the measured $R_{Test\ specimen}$. It indicates that the measured $R_{Test\ specimen}$ was mainly influenced by the $R_{Whisker}$.

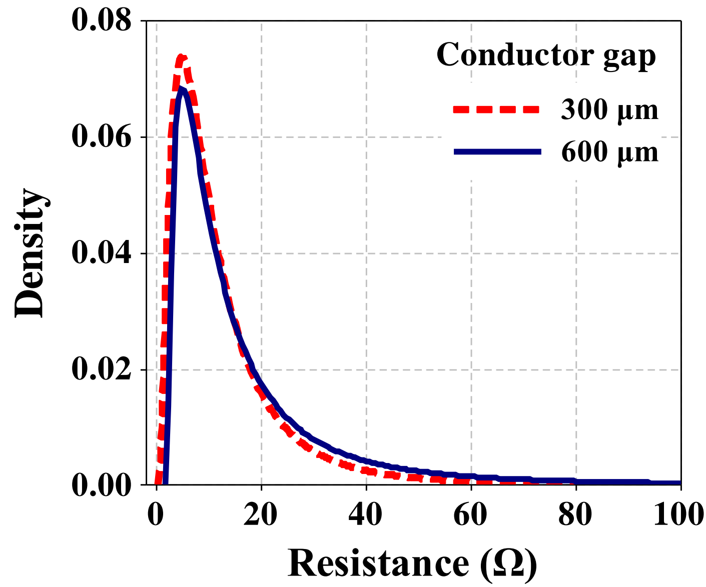

Figure 40 Distribution of the resistance of test specimen depends on spacing between electrodes (Conductor gap: 300 µm versus 600 µm)

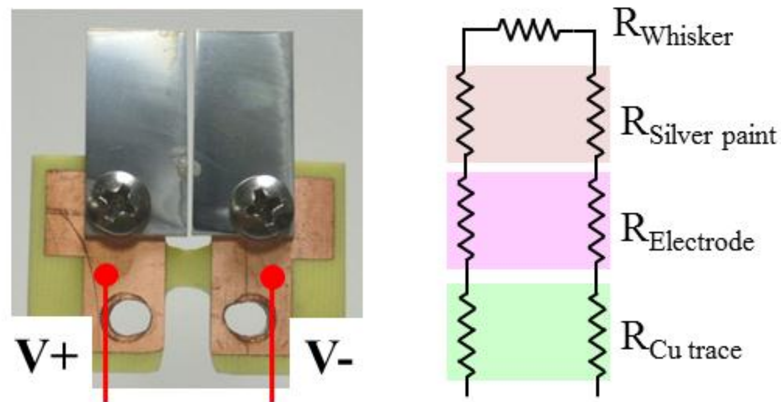

Figure 41 The measured points for the resistance of test specimen

The distribution of the measured resistance of test specimen which depicts in figure 40 presents that there is no statistical difference between 300 µm and 600 µm conductor gap (p-value=0.22 from Kruskal-Wallis test). Even the whisker length was decreased by decreasing the gap spacing; there is no significant difference in terms of

the measured resistance of test specimen, due to the no significant changes in the whisker diameters.

3. *Comparison between the specimens with arc initiated and no arc initiated*

When the tin whisker bridges, the two differential current potential will flow through the tin whisker and the current density through tin whisker is high enough for the joule heating to melt the whisker. The amount of energy for melting and vaporizing the tin whisker depends on the whisker geometry and surrounding pressure. The molten metal globule or bridge can be formed between the surfaces of conductors. The shape of molten bridged whisker will be determined by surface tension and gravity [66]. At the same time, the resistance of molten bridged whisker will increase and the temperature will be increased. When the molten bridged whisker finally breaks the maximum temperature may reach up to the boiling temperature of tin whisker (2875 K). The hottest point of tin whisker during the current flows may be the midst of the molten bridged whisker where the whisker hanged between two conductors, due to the conduction of heat. It indicates that the closed circuit by molten bridged tin whisker can be opened unless the entire tin whisker did not melted and vaporized before the gravity pull down the liquid bridge of tin whiskers.

Figure 42 depict a test specimen in which a metal vapor arc was not initiated. Two tin-plated copper electrodes were bridged by tin whisker as depicted in figure 42 (a) prior to apply the voltage. After the arc test, remnants of whiskers, such as strings of tin beads on the electrodes due to the disconnection of molten bridged whiskers influenced by gravity and surface tension, indicating a melting rather than arcing event, were observed as shown in figure 42(b) and 42(c).

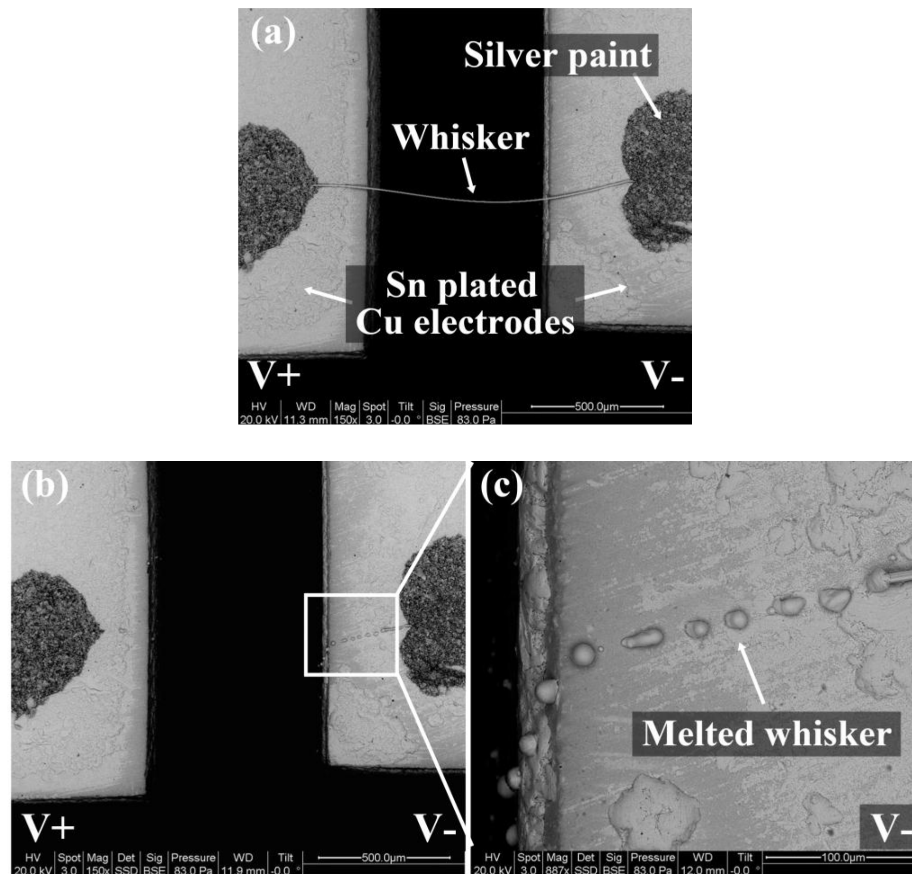

Figure 42 Specimen in which a vapor arc was not initiated: (a) Prior to and (b) After the arc test. (c) Close-up of the melted whisker indicated in figure 42(b)

When a metal vapor arc initiates, the vaporized tin atoms are ionized and the ions move toward the cathode while electrons move toward the anode. The ion bombardment on the cathode creates cathode spots, or hot spots. Thus, specimens that initiated a metal vapor arc showed multiple spot eruptions on the surfaces of the electrodes and metal flow, as shown in figure 43. Surface damage by ion bombardment during the vapor arc event was depicted in figure 43(c).

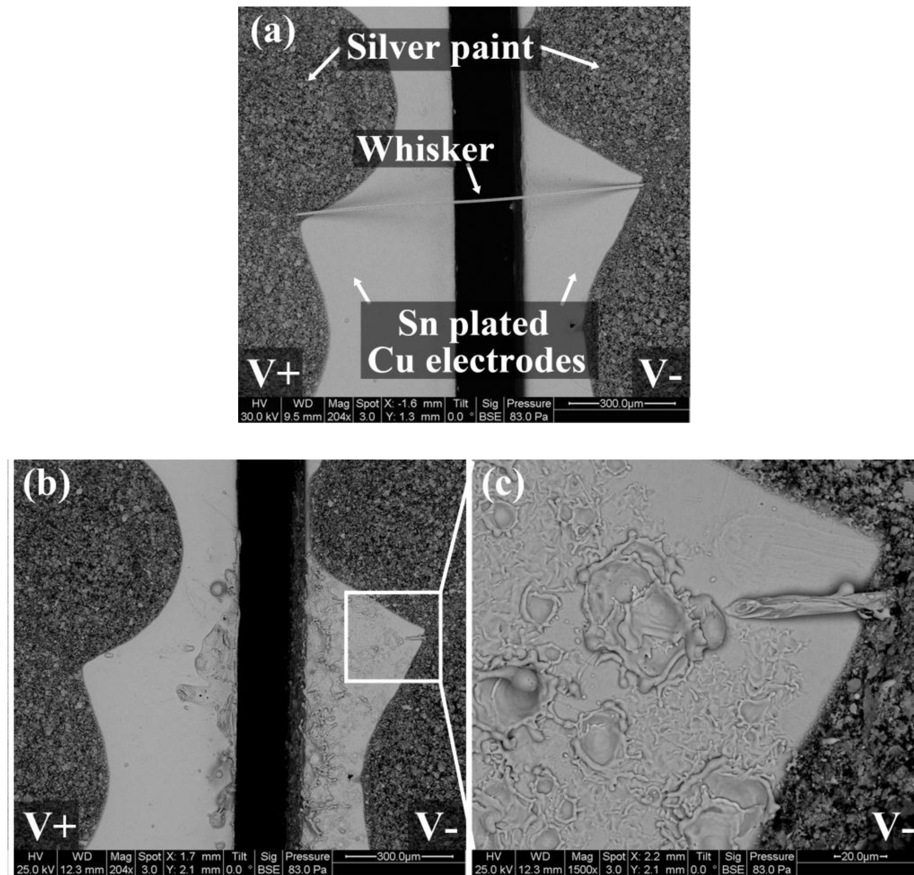

Figure 43 Specimen in which vapor arc was initiated (a) Prior to and (b) After the arc test. (c) Close-up of the arc-damaged surface indicated in figure 43(b)

4. *Two types of vapor arc behavior*

The metal vapor arc events caused by tin whiskers were categorized as Type I and Type II. Type I is a metal vapor arc that initiated and extinguished in less than a few microseconds. Type II represents a metal vapor arc initiated and propagated along the gap between tin-plated electrodes with arc duration of more than a few milliseconds. Most of the vapor arc by tin whiskers in arc test showed the Type I vapor arc event throughout all pressure conditions; however some of the test

specimens showed the Type II vapor arc event when the pressure is low and their resistance of test specimen is less than 10 Ω.

4.1 Type I vapor arc event

Figure 44 shows light emission captured via a high-speed camera, lasting 294 μs for a Type I vapor arc event at 760 torr under 50 V bias. For this particular event, the 30 A circuit breaker was not tripped and little to no participation of the tin-plated copper electrodes was observed. For the Type I metal vapor arc, the air is suspected of quenching the propagation of the arc. When a metal vapor arc forms, the surrounding gas molecules, such as air, will start to intermingle with the metal vapor in the arc. The intermingled gas molecules absorb the heat of the arc, and the arc is quickly quenched. In order to sustain the arc, these intermingled molecules must be ionized; however, most of the gases found in air have a significantly higher ionization potential (14 eV) than tin (7.3 eV) [60]. If voltage sufficient to ionize the quenching additives is not available, the current will gradually decrease to less than the minimum arcing current, and therefore the arc will die out [67]. In order to sustain the arc, a higher voltage is needed to overcome the effects of the surrounding quenching gases and/or a greater initial volume of ionized gas.

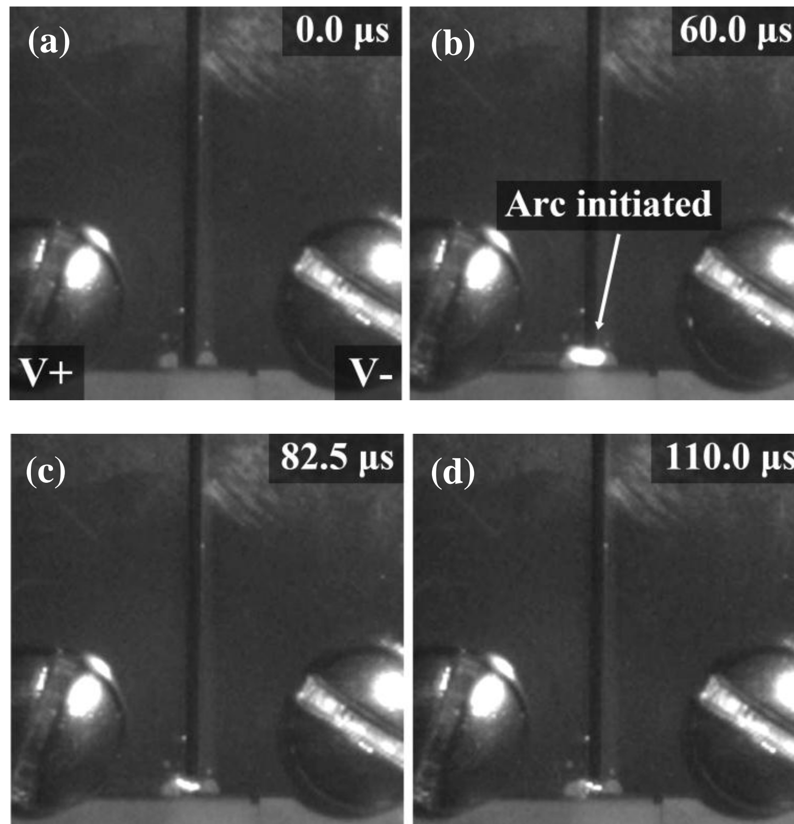

Figure 44 Vapor arc test at 50 V in atmospheric pressure (760 torr): Vapor arc initiated and extinguished

4.2 Type II vapor arc event

Under low pressure conditions (70 torr) with 50 V, some of arc test specimen showed a Type II metal vapor arc event as shown in figure 45. In this case, the arc was initiated from the bridged tin whisker and propagated with a number of arc re-ignitions caused by the supply of additional metal ions from the tin-plated copper coupons. Melting of tin-plated copper electrodes was also observed after the Type II metal vapor arc event. In this case, the arc lasted for 440 ms. A Type II metal vapor arc event occurred because the amount of surrounding gases that could absorb the energy of the arc was significantly decreased due to the low pressure conditions. In

addition to the decrease of energy losses to the surrounding gases, the energy required to melt and vaporize the tin whiskers and surrounding metals (tin-plated copper electrodes) was also decreased by the lower melting and boiling temperatures at 70 torr (compared to 760 torr). During the sustained arc event, the elevated temperature caused by the ion and electron bombardment vaporized the surrounding tin and copper from the electrode surfaces; in turn, the increased supply of these metal ions with tin and copper promoted the continued re-ignition of arcs. Once the surrounding tin from the plating layer was dispersed, the underlying copper substrate could also be ionized, which indicates that the local temperatures during the metal vapor arc event were much greater than 2530 K (the boiling point of copper at 70 torr). The temperature of a copper arc in air has been reported at 5100 K [68]. The sustained arc was finally extinguished when the molten copper from the cathode and anode sides joined due to the flow of molten copper under gravity to form a low resistance metal path between the originally separated electrodes, as shown in figure 46.

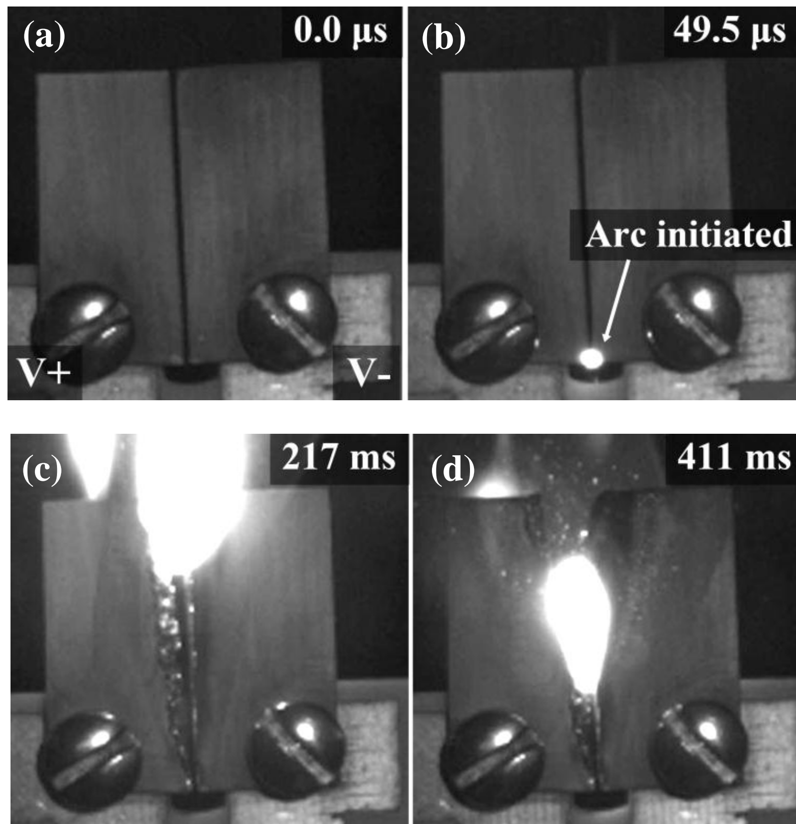

Figure 45 Vapor arc test at 50 V in vacuum (70 torr): Vapor arc sustained and propagated

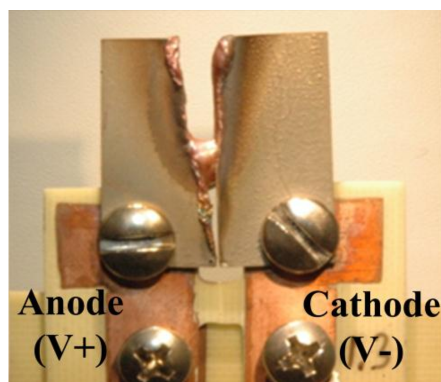

Figure 46 Test specimen after the Type II vapor arc event

5. *Current and voltage transition during the vapor arc event*

Figure 47 depicts the current and voltage characteristic, when tin whisker on arc test specimen melted without initiation of vapor arc. The maximum current of 90 A was flowed through the tin whisker in the arc test specimen but the whisker was melted less than 1 μs.

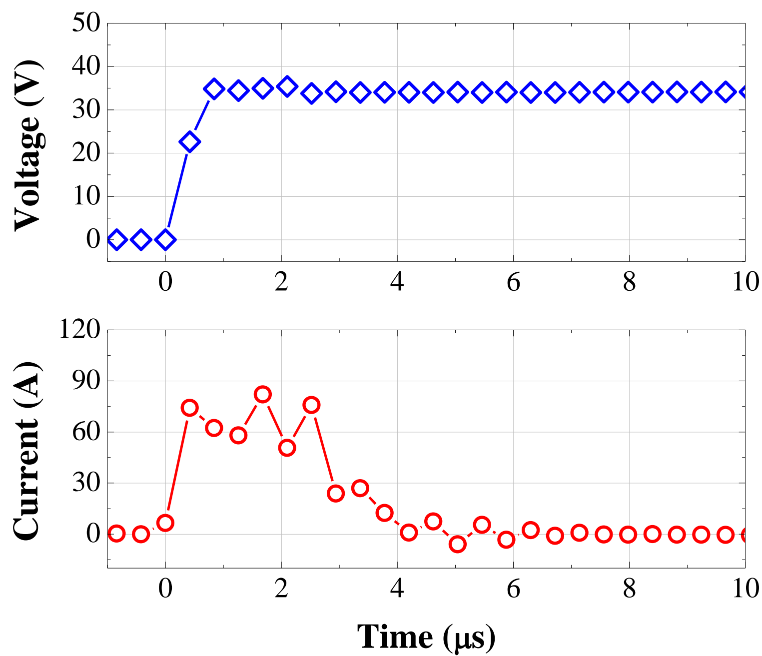

Figure 47 Current-voltage characteristic when the tin whisker was melted without initiation of vapor arcing (37.5 V at 75 torr)

The instantaneous current and voltage characteristic during the vapor arc event caused by tin whisker were presented in figure 44 (Type I arc event) and 45 (Type II arc event). The arc duration for Type I arc event was 210 μs and the maximum current of 130 A was carried by metal vapor arc as depicted in figure 48.

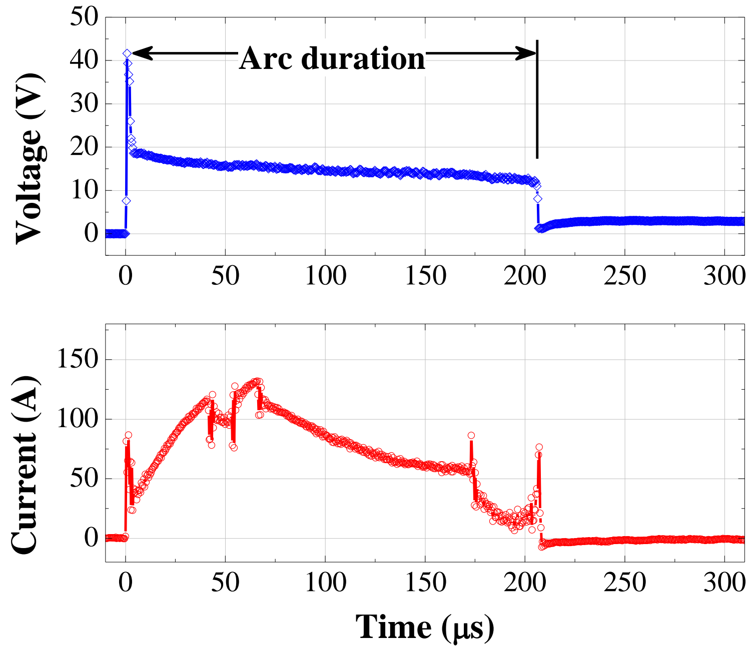

Figure 48 Current-voltage characteristic during the Type I arc event

For the Type II arc event (37.5 V at 75 torr), initially vapor arc was initiated by tin whisker and the vapor arc can be propagated due to the additional supplement of tin and copper metal vapors. Figure 49(a) ~ 49(f) depicts that Type II arc event captured by camera with 30 frames per second (FPS). The current/voltage was applied between the frame #1 and the frame #2, and vapor arc sustained until the vapor arc was extinguished after the frame #7. The arc duration is approximately 0.231 ms.

As shown in figure 49(g), the vapor arc was extinguished because the flow of molten copper electrode formed the metal bridge between the anode and cathode sides of electrodes under gravity. According to the current and voltage characteristic during the Type II arc event, the vapor arc was sustained for about 1.8 ms (figure 50). After the metal path formed due to the molten copper, the maximum current of 220 A

flowed through the metal path between two electrodes. Comparing to Type I arc even, the Type II arc event flowed the higher level of the current than Type I arc event. The measured resistance of test specimens for Type I arc event is 14.9 Ω, while the test specimen showed the Type II arc event is 5.3 Ω. It is observed that the likelihood of Type II arc event may increase when the test specimens have lower resistance than 10 Ω and the arc test conduces at lower pressure than 400 torr.

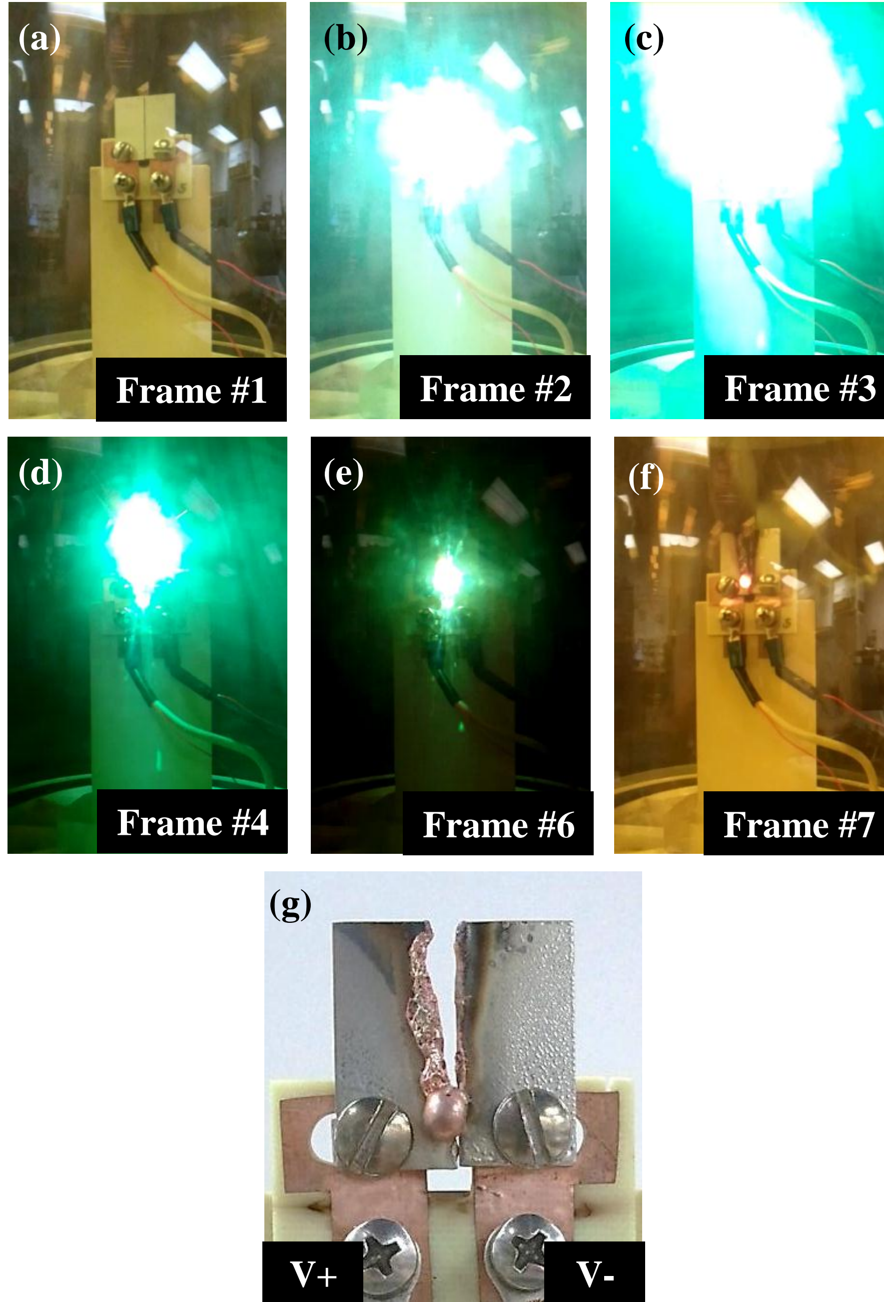

Figure 49 (a) ~ (f) Light emission from the test specimen in Type II arc event by camera with 30 frames per second (FPS) and (g) Formation of metal bridge after the arc test

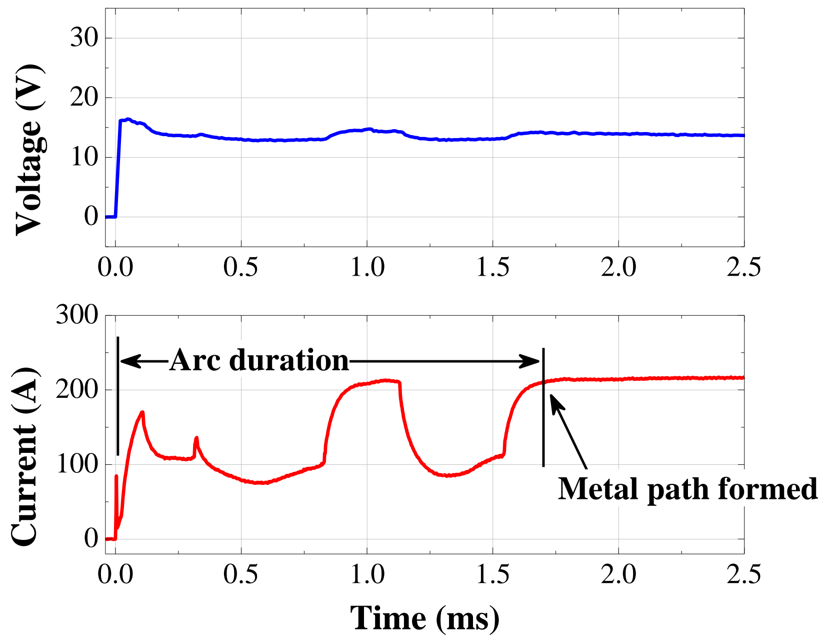

Figure 50 Current-voltage characteristic during the Type II arc event

6. *Contact erosion mechanism in vapor arc by tin whiskers*

When high current passes through a tin whisker, if the transferred heat energy is less than the heat of vaporization of tin (295.80 kJ mol^{-1}), the tin whisker merely melts. If the amount of energy exceeds the ionization energy of tin (first ionization energy: 708.6 kJ mol^{-1}), the vaporized tin atoms will start to lose the outermost electrons, which means the gaseous condition of tin atoms will be ionized [60, 69]. The atoms which lose the electrons become positively charged (positive ions) and, with the lost electrons, form an ionic cloud which is known as plasma, as depicted in figure 51. Because of the electric field strength between the anode and cathode electrodes, the positively charged metal ions move rapidly towards the cathode side of the electrode, and the lost electrons from the tin atoms move rapidly to the anode

side [60, 69, 70]. The electric field will accelerate the electron move to the anode side. Once the electrons impact on the anode surface, their energy is converted to heat; thus, the temperature of the anode side will be increased, and it will locally evaporate the anode material.

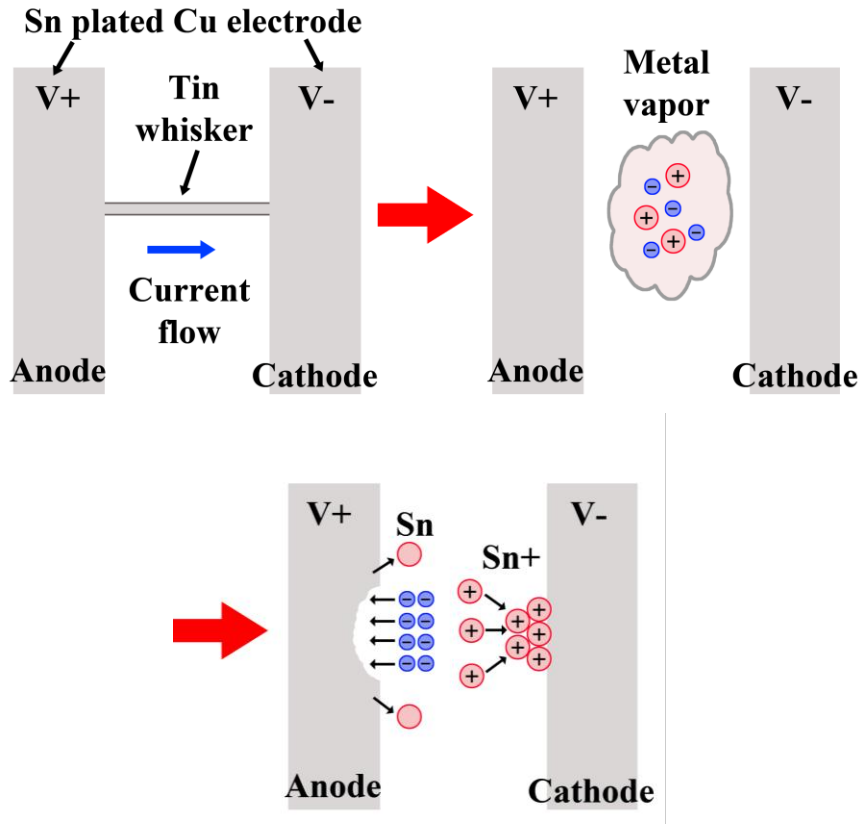

Figure 51 Formation of tin whisker-induced vapor arc and contact erosion

As shown in figure 52, the anode side of the tin-plated copper electrode was deformed due to electron bombardment while there was deposition of ionized tin metals on cathode side. When positive metal ions impacted on the cathode side, the cathode surface also heated up, while the deposited tin ions locally eroded the

surface. The contact erosion on both the cathode and anode sides is clearer on the edge of the tin-plated copper electrodes, as shown in figure 53.

Due to electron bombardment, the anode electrode revealed the underlying copper, which indicates that additional tin metals may have come out from the anode surface and those evaporated tin metals were attached on the edge of the cathode electrode. It also explains why the deposited area on the edge of the cathode is quite large compared to the volume of the whisker which bridged the two electrodes.

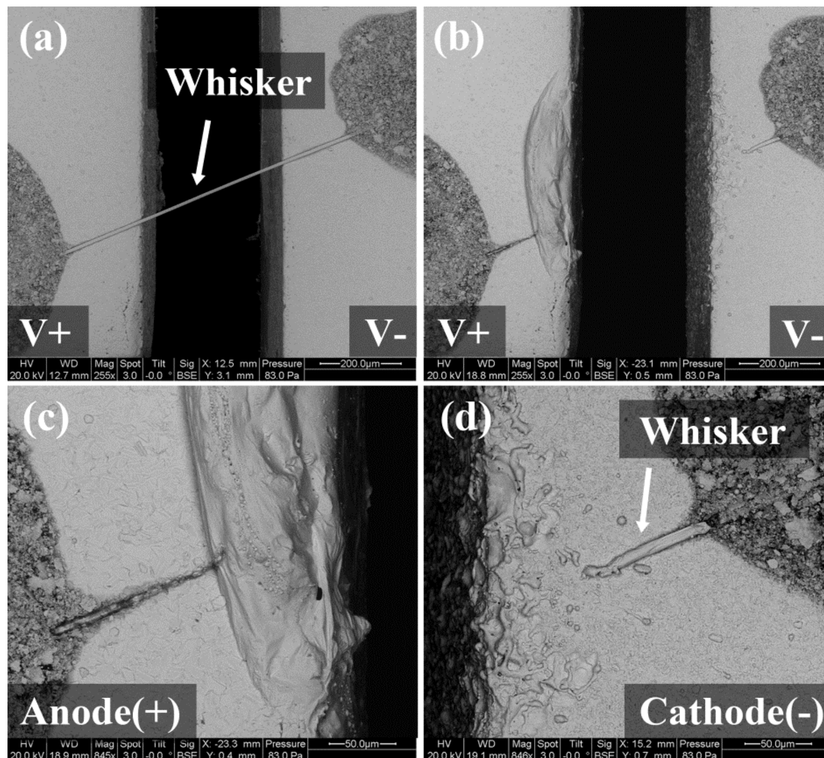

Figure 52 Contact erosion on anode and cathode electrode captured by SEM

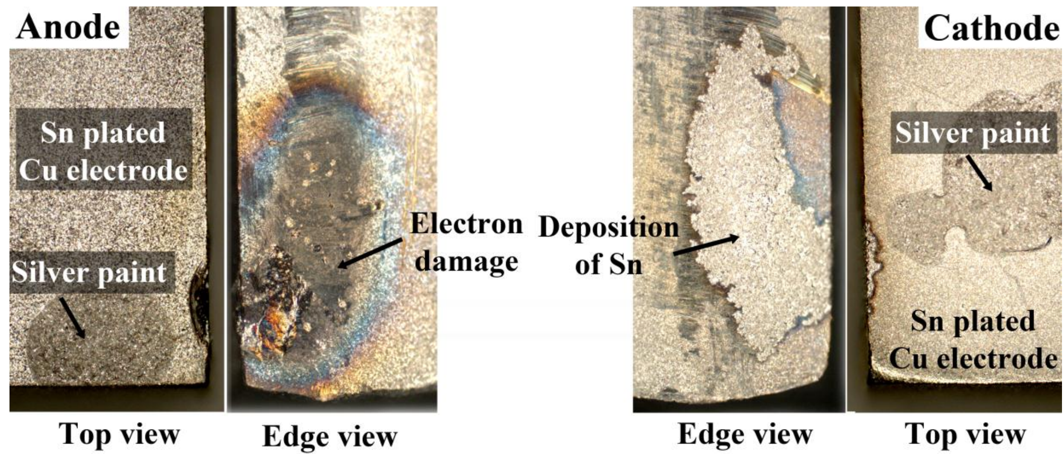

Figure 53 Contact erosion on anode and cathode electrodes (top view and edge view)

Depending on the surface erosion during the arc, there are two types of arc: an anode arc, which erodes the anode material, and a cathode arc, which erodes the cathode surface [60, 66, 71].

An anode arc occurs when the contact gap space is small; this is also known as a metallic phase arc because the metal vapor is dominant. If the gap space is increased, surrounding gases, such as O_2 or N_2, can become involved in the metal vapor, so the arc transfers from a metallic phase arc to a gaseous phase arc, forming a cathode arc. In the case of an anode arc, materials transfer from the anode to the cathode, whereas the direction of material transfer is opposite for a cathode arc [71].

In tin whisker-induced vapor arcing, once the arc is initiated, the metallic vapor is dominant due to the vaporized whiskers, thus resulting in a dominant anode arc. The evidence of a tin whisker-induced anode arc is electron damage on the anode side and tin deposition on the cathode side after short arcing by the tin whisker, as depicted in figure 52 and 53. In a Type II metal vapor arc event, additional tin and

copper materials including the surrounding gases involved in the arc. This type of arc is the cathode arc because the contact gap space increased due to the vaporization of bridged whisker. However, in the arc test specimen after a Type II metal vapor arc event, as shown in figure 46 and 49(g), the anode electrode was consumed more than the cathode electrode was consumed, because, even for an anode arc, copper tends to transfer material from the anode to the cathode [60].

7. *Effect of physical and electrical parameters on likelihood of vapor arc by tin whiskers*

In the metal vapor arc test, both the physical electrical parameters, including whisker geometry, electrical resistance of the test specimen, bias voltage, and pressure, were considered to affect the likelihood of vapor arc formation.

In order to analysis the effect of individual parameters on likelihood of vapor arc formation, the test specimens were divided into two groups with “Arc” and “No arc” after the arc test. “Arc” group includes both Type I and Type II vapor arc events.

7.1 Physical parameters – Whisker geometries

Figure 54 and 55 shows the probability density plots of whisker length and whisker diameter depends on the arc initiation. The probability density plots indicate that whether there is a difference between “Arc” and “No arc” group, in terms of whisker length and whisker diameter. With regard to the whisker length, there is no difference between the specimens formed the vapor arc (“Arc” group) and the specimens failed to initiate the vapor arc (“No arc” group). The p-value of 0.94 calculated by Kruskal-Wallis test also supports that there is no statistical difference

between “Arc” and “No arc” groups in terms of whisker length in their test specimen. For the whisker diameter, as shown in figure 55, there is a significant statistical difference between “Arc” and “No arc” groups (Kruskal-Wallis test: p-value < 0.001). The specimens showed the vapor arc (“Arc” group) had larger median diameter (7.27 μm) than the specimens did not initiate the vapor arc (“No arc” group: 4.08 μm). This result indicates that the whisker diameter appear to be a strong parameter for determining the vapor arc formation than whisker length, in terms of whisker geometries.

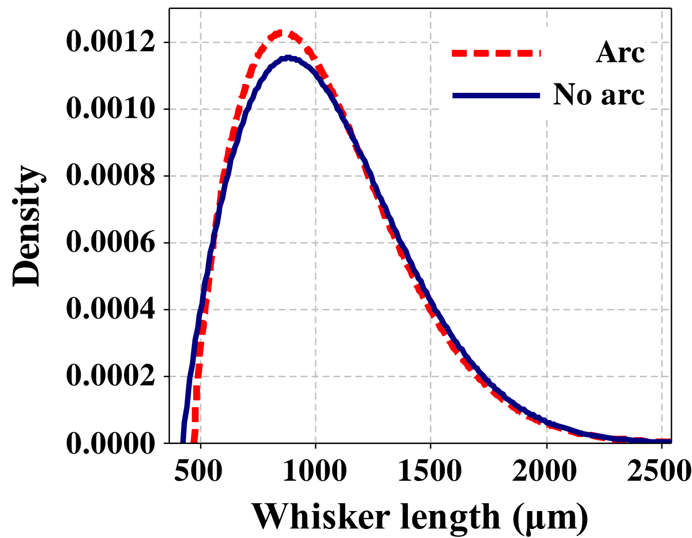

Figure 54 Probability density plot of whisker length depending on the initiation of vapor arc by tin whiskers

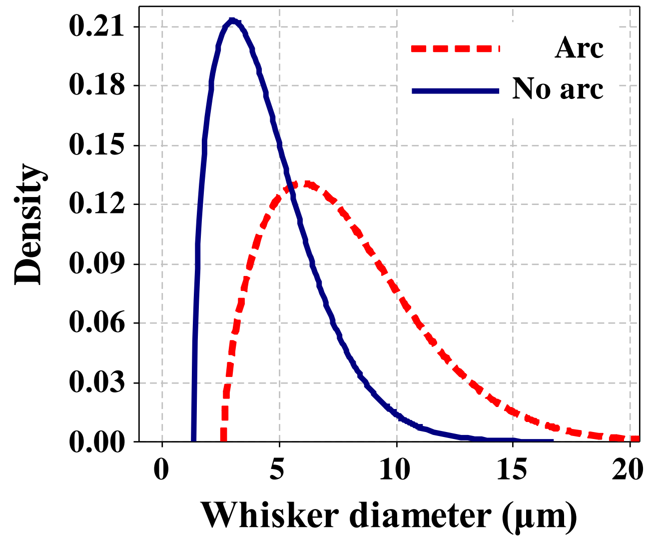

Figure 55 Probability density plot of whisker diameter depending on the initiation of vapor arc by tin whiskers

7.2 Electrical parameter – Resistance of test specimen

The probability density plot of resistance of test specimen showed in figure 56. The resistance of test specimen also showed a significant statistical difference between "Arc" and "No arc" groups (Kruskal-Wallis test: p-value < 0.001). In terms of median resistance of test specimen, "No arc" group showed three times larger resistance (18.93 Ω) than "Arc" group (6.92 Ω).

Figure 57 depicts the effects of the electrical resistance of the test specimen on the likelihood of a metal vapor arc. While a dependence on pressure was observed, no arcs were initiated when the electrical resistance of the test specimens was higher than 25.8 Ω, regardless of the pressure level and applied voltage.

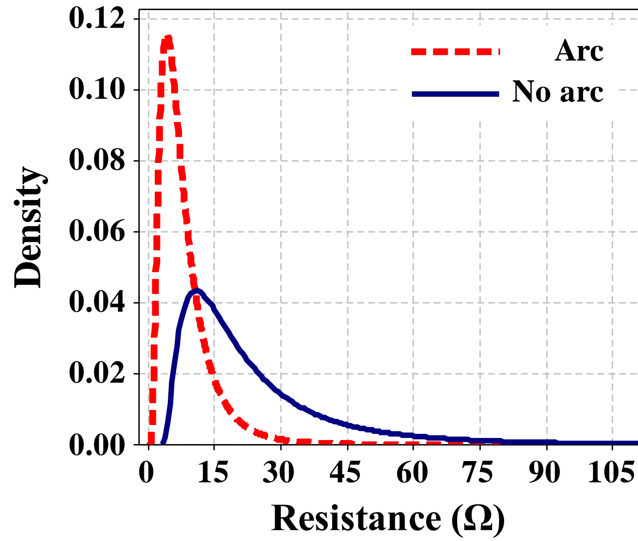

Figure 56 Plot of probability density function in measured resistance of test specimen depending on the initiation of vapor arc by tin whiskers

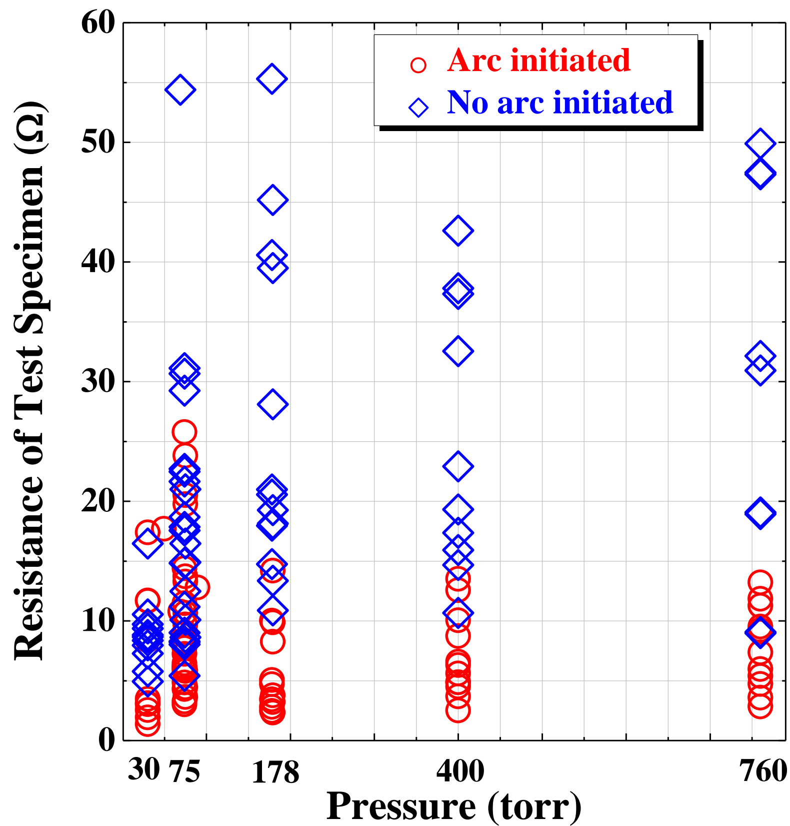

Figure 57 Likelihood of vapor arc being caused by tin whisker depending on the resistance of the test specimen

7.3 Electrical parameter – Ramp time of power source

In vapor arc test, lead-acid batteries were used to bias the maximum current and voltage instantaneously when the switch is on. If the ramping of current was slow to take whisker from solid to liquid to vapor state, the melted bridged whisker can be disconnected due to the pull down by gravity. In addition, the maximum capable current/voltage in power source could not be applied to the test specimen.

The vapor arc test conducted using the power supply in order to evaluate the effect of ramp time of power source. The maximum output voltage and current of each power supply is 20 V and 50 A. The measured resistance of arc test specimen is low enough to produce the vapor arc when the current and voltage applied using lead-acid batteries as shown in Table 4. However, all four test specimens did not initiate the vapor arc, when the power supply used to bias the current and voltage as shown in figure 58. Because the ramp time of power supply is not enough to melt the entire tin whisker, thus it shows the rupture at the middle of the tin whisker.

Table 4 The measured resistance of arc test specimen

Specimen #	Resistance of specimen (Ω)
#1	6.9
#2	7.8
#3	5.4
#4	7.5

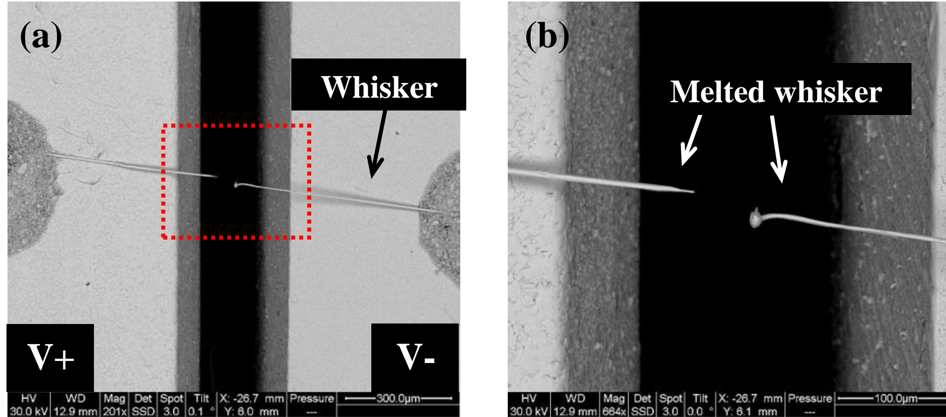

Figure 58 (a) Rupture of melted whisker after the arc test using by power supply (20V/ 50A), and (b) Close-up of ruptured area of whisker in figure 58(a)

8. *Arc Current Metric*

While the resistance of the test specimen and diameter of the whisker appear to be good metrics for determining metal vapor arc formation, they do not completely explain the observations. In particular, the applied voltage must also be considered. Therefore, some combination of test parameters may be required to determine the likelihood of metal vapor arc formation. To simultaneously consider multiple parameters, the "arc current metric" is proposed. This arc current metric represents the theoretical current that would flow, if the whisker was able to carry the load. The arc current metric is defined as (7):

$$Arc\ current\ metric = \frac{V_{Applied}}{R_{Specimen} + R_{Test_circuit}} \quad (7)$$

where $V_{Applied}$ is the bias voltage, and $R_{Specimen}$ and $R_{Test_circuit}$ are the measured electrical resistances of the test specimen and the test circuit, respectively. For the tests reported here, the measured resistance of the test circuit was 82.83 mΩ.

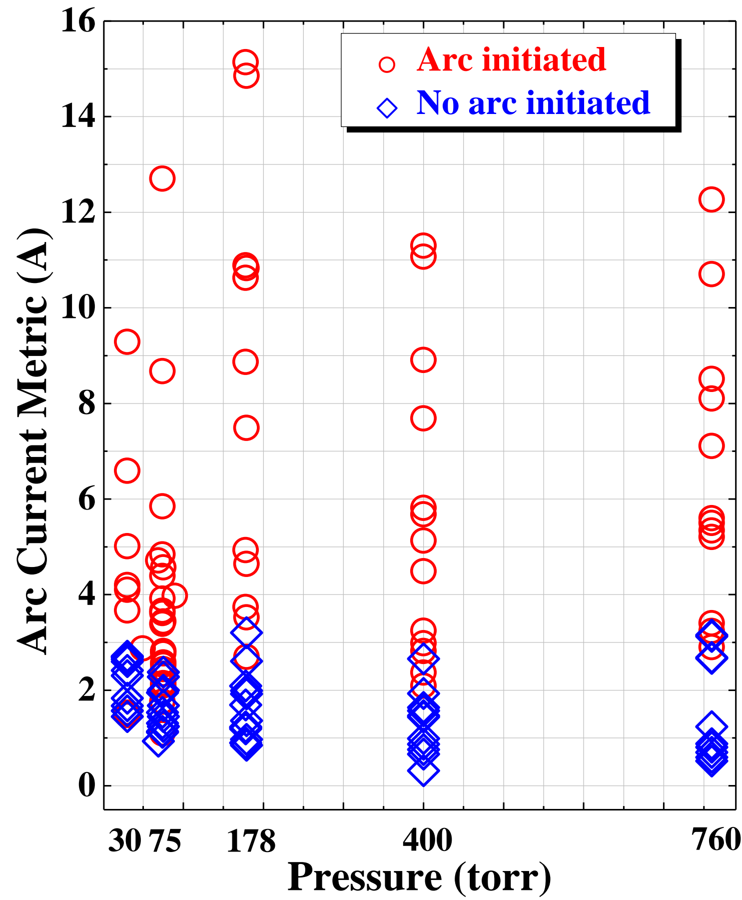

Figure 59 Effects of arc current metric on likelihood of vapor arc by tin whisker

By examining the test data of metal vapor arc formation and the arc current metric, it was determined that a threshold value for arc formation appears to exist. The possibility of a vapor arc based on the arc current metric is shown in figure 59. At 760 torr, the tin whiskers initiated vapor arcs when the arc current metric was higher than 3 A; vapor arcs can be initiated when the arc current metric is greater than 3.2 A at 75 torr. Further, the likelihood of an arc occurring for arc current metric values below these stated numbers appears to be quite low.

9. *Influence of Conformal Coating on Vapor Arc by Tin Whiskers*

In order to evaluate the influence of conformal coating on vapor arc by tin whiskers, the conformal coated arc test specimen applied the 50 V at 30 torr condition to increase the probability of vapor arc by tin whisker.

Figure 60 shows the conformal coated test specimens in group 1 prior to and after the vapor arc test. The conformal coated test specimens did not initiated the vapor arc caused by tin whisker while there is a coating damage on anode electrode side as shown in figure 60(b). When the bridged whisker coated by conformal coating, the conformal coating may mitigate the formation of vapor arc by tin whisker because the conformal coated whisker can be easily disconnected due to the pull down by gravity. During the test, it also showed that the broken conformal coated whisker on test specimens due to the decreased flexibility.

For test specimens in group 2, all four test specimens were initiated the vapor arc and two out of four specimens showed the Type II vapor arc event even though the surfaces of electrodes were coated by conformal coating. During Type II vapor arc event, the coated conformal coating and tin-plated copper electrodes were burn out altogether due to the propagation of vapor arc. It indicates that the conformal coating could not extinguish the vapor arc if once the vapor arc formed by tin whisker was sustained. Table 5 depicts the resistance of test specimen and their arc current metric value.

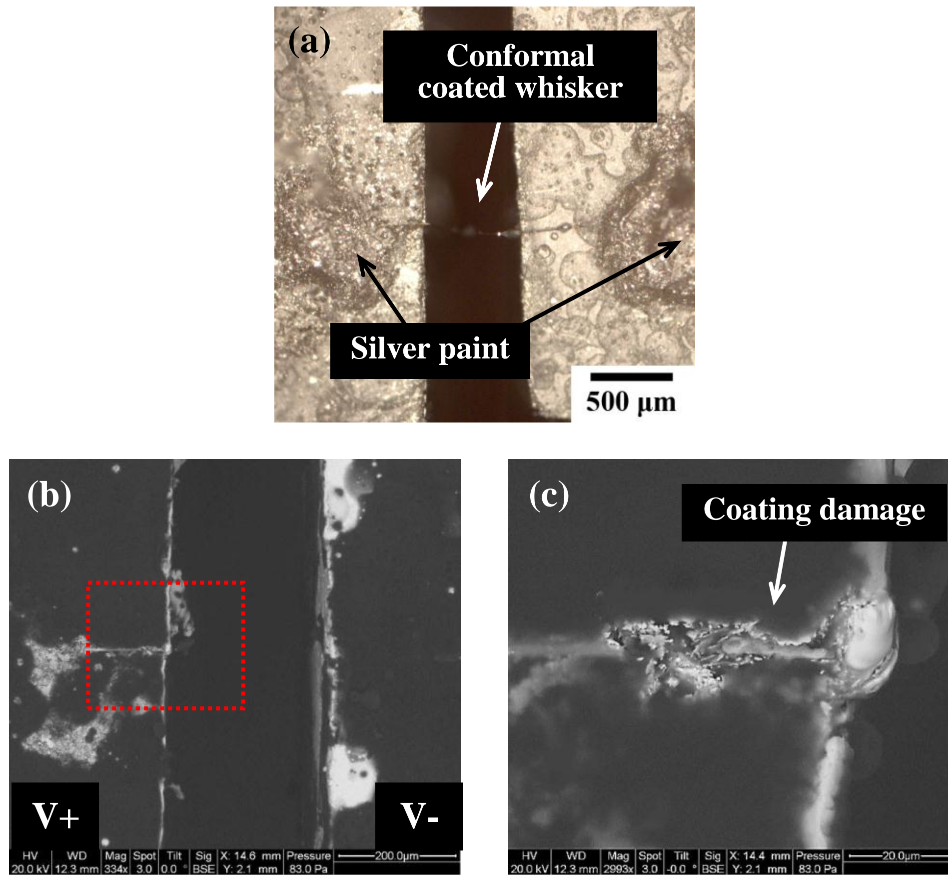

Figure 60 Conformal coated arc test specimen (Arc current metric: 12.7 A): (a) Prior to and (b) After the arc test (50 V at 30 torr), and (c) Close-up of the area where the whisker was placed as indicated in figure 60(b)

Table 5 Arc test result using conformal coated arc test specimens with 50 V at 30 torr

Specimen	Resistance of specimen (Ω)	Arc current metric (A)	Arc event
#1	5.90	8.48	Type I
#2	4.57	10.94	Type II
#3	4.79	10.44	Type I
#4	2.52	19.84	Type II

10. Conclusion

Tin whisker–induced metal vapor arc behavior was observed in five different pressure conditions (30, 75, 148, 400 and 760 torr) using actual tin whiskers. Under low pressure, metal vapor arcs were initiated from tin whiskers and propagated along the gap between the tin-plated copper electrodes by supplying additional metal ions of tin and copper. Under the test conditions, the initiated metal vapor arc extinguished quickly at atmosphere pressure (760 torr) with relatively little damage to the tin-plated electrodes. This result was due to limited initial metal ions and insufficient circuit conditions required to ionize the surrounding gases. Among several parameters that can affect metal vapor arc formation, the electrical resistance of the test specimen appears to be the strongest factor. However, this neglects the voltage potential from which the energy to vaporize and ionize the tin whisker is derived. In order to consider the voltage, an arc current metric as a function of bias voltage and resistance was proposed. Using the arc current metric, there appears to be a threshold value above which an arc event is likely to occur and below which an arc event is unlikely to occur. This arc current metric may be used as a guideline for circuit design in terms of minimizing the vapor arc propensity via tin whiskers. For conformal coating as tin whisker vapor arcing mitigation strategy, conformal coating could not extinguish the vapor arc if once the arc was sustained.

Chapter 5: Prediction Model for metal vapor arc by tin whiskers

In chapter 4, an "arc current metric" was proposed to assess the potential of tin whisker-induced metal vapor arc formation. The arc current metric was defined as (7):

$$Arc\ current\ metric = \frac{V_{Applied}}{R_{Specimen} + R_{Test_circuit}} \quad (7)$$

where $V_{Applied}$ is the bias voltage, and $R_{Specimen}$ and $R_{Test_circuit}$ are the measured electrical resistances of the test specimen and the test circuit with wires, respectively.

Tin whisker-induced metal vapor arcs have a high probability of occurring when the arc current metric is above a certain value. This value appears to be weakly tied to pressure. Therefore, in order to predict the possibility of tin whisker-induced vapor arcing, binary logistic regression analysis, a statistical technique, was used.

1. *Binary logistic regression*

Logistic regression is a statistical method which can find a relationship among an outcome variable and other descriptive variables. Especially, when the outcome variable is the binary categorical outcome (preferably in the form of 0 and 1), binary logistic regression is well suited for studying the relation between an outcome variable and one or more descriptive variables (predictor variables) [72]. In the simplest case of one predictor X and one binary outcome variable Y, the logistic model predicts the logit of Y from X [68].

The simple logistic model has the form (8) [68]:

$$\ln\left(\frac{\pi}{1-\pi}\right) = \text{logit} = \beta_0 + \beta_1 X \qquad (8)$$

Hence, the estimated probability of event of interest can be (9):

$$E(Y/X) = \pi = \frac{e^{(\beta_0+\beta_1 X)}}{1+e^{(\beta_0+\beta_1 X)}} \qquad (9)$$

where π is the estimated probability the event of interest , β is parameter for the variable X.

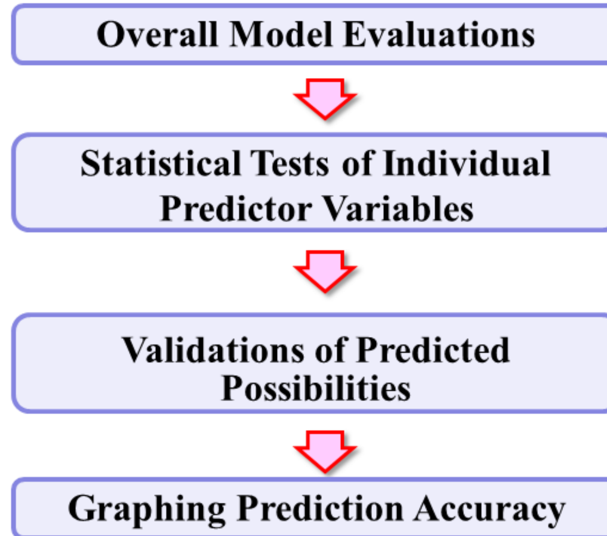

Figure 61 Evaluation procedure of binary logistic regression model

The logistic model for the vapor arc test was evaluated based on the procedure shown in figure 61. Initially, by means of binary logistic regression, the individual predictor variables will be evaluated their statistical significance on outcome variable.

Based on the result of binary logistic regression, the logistic model for assess the probability of vapor arc by tin whisker will be optimized using training data. The optimized logistic model will be evaluated using validation data and the prediction accuracy will be evaluated using the receiver operating characteristic (ROC) curve.

2. *Statistical tests of individual predictor variables*

For binary logistic regression analysis, the arc current metric and pressure were chosen as predictor variables for the binary response ("Arc" or "No arc") from the vapor arc tests. The arc event from the test was defined as Y=1 when the arc initiated ("Arc") and Y=0 when the arc did not initiate ("No arc").

The objective of binary logistic regression is to predict the probability of Y=1 ("Arc") from the variable (arc current metric and pressure). The following model was used for the binary logistic regression analysis (10) [68]:

$$E\left(Y\ /\ X_i\right)=\pi_i=\frac{e^{(\beta_0+\beta_1 X_i)}}{1+e^{(\beta_0+\beta_1 X_i)}} \qquad (10)$$

where π is the estimated possibility of the event of interest (Y=1; "Arc"), and β_0 and β_1 are the parameters for the variable X_i (arc current metric and pressure).

Seventy percent of the test data (90 out of 129 test data points from arc tests) was used to optimize the logistic regression model as the training data set and the other thirty percent (39 test data points) was used to validate the optimized logistic regression model. The 90 training data points and 39 validation data points were arbitrary selected from the 129 data.

The result of the first binary logistic regression conducted using Minitab is shown in Table 6. The effect of predictor variables (arc current metric and pressure) on the response (vapor arc test) can be evaluated based on the statistical significance. In terms of the statistical significance of each predictor variable, only the arc current metric has a statistically significant relationship (p-value < 0.001; In Minitab if p-value is less than 0.001, it reports as p-value=0.000) with the response (vapor arc test). For pressure, the p-value is higher than 0.05, which indicates that the effect of pressure (range of 30 ~ 760 torr; low vacuum conditions) on the arc event is not statistically significant, which means the coefficient value of β can be considered as 0. Whether the model describes the data well or not can be assessed based on the deviance test. The deviance p-value in our data is 0.995, which can't reject the null hypothesis (H_0: model does fit the data). It indicates that there is statistically significant evidence that the model fits the data and that there is a relationship between the response (vapor arc test) and the predictor variable (arc current metric).

The vapor arc test results using the arc current metric are plotted in figure 62 because the effect of pressure for the range of test data can be neglected based on the result of statistical significance (p-value was less than 0.05). When the arc current metric is greater than 3.1 A, only the "Arc" events were observed, while the "Arc" and "No arc" events mixed when the range of the arc current metric was between 1.1 ~3.1 A.

Table 6 Result of the first binary logistic regression analysis

Predictor	Coef	SE Coef	z	p	Odds Ratio	95% CI	
						Lower	Upper
Constant	-4.74	1.16	-4.07	0.000			
Arc current metric	2.06	0.51	4.06	0.000	7.87	2.90	21.34
Pressure	-0.0002	0.0002	-1.38	0.169	1.00	0.99	1.00

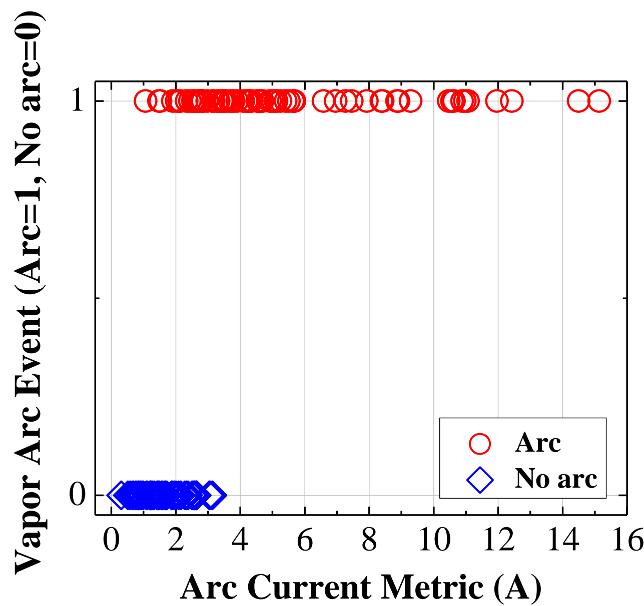

Figure 62 Vapor arc event based on the arc current metric (129 test data)

According to the first binary logistic regression, between predictor variables (arc current metric and pressure), the arc current metric has a statistically significant effect on the response (varc test). Therefore, in order to simplify the logistic regression model, which can be used for the prediction model of tin whisker-induced vapor arcing, only the arc current metric was considered as the predictor variable for the second binary logistic regression analysis. Table 7 shows the result of the second binary logistic regression analysis. The second binary logistic regression result also

shows that the arc current metric has a statistically significant effect on the arc event (p-value < 0.001). The coefficient (β_1) presents that the positive and negative effect on the response. In order words, as the arc current metric increases, the response is more likely to be 1, which means that a tin whisker-induced metal vapor arc is more likely to form. This is consistent with the arc test result. The odds ratio for the arc current metric is 6.63, which indicates that with a 1 A increase in the arc current metric, the response is 6.63 times more likely to be a 1 than a 0. Additionally, the deviance p-value is 0.996, which means that our logistic regression model describes the arc test result quite well.

Table 7 Result of the second binary logistic regression analysis

Predictor	Coef	SE Coef	z	p	Odds Ratio	95% CI	
						Lower	Upper
Constant	-4.75	1.09	-4.37	0.000			
Arc current metric	1.89	0.45	4.25	0.000	6.63	2.77	15.86

Based on the result of the second binary logistic regression analysis, the optimized logistic regression model that can be used as a prediction model for tin whisker-induced metal vapor arc formation can be expressed as follows (11):

$$\pi = \frac{e^{(-4.75+1.89\times\text{Arc current metric})}}{1+e^{(-4.75+1.89\times\text{Arc current metric})}} \tag{11}$$

The estimated possibility of tin whisker-induced vapor arcing (π) can be calculated based on the arc current metric, and the "Arc" can be predicted when the estimated possibility is larger than the cutoff value of 0.5. Thus, if the estimated possibility is larger than 0.5, an "Arc" event is predicted.

Figure 63 shows the training data set (90 data points) prior to and after the transformation by the optimized logistic regression model. Using the cutoff value of 0.5, the "Arc" and "No arc" event mixed region where the range of the arc current metric was between 1.1 ~3.1 A can be assessed as "Arc" and "No arc" events. Table 8 shows the accuracy of the optimized logistic regression model from the 90 training data points. Only 8 out of the 50 actual "Arc" events were predicted as "No arc," so the accuracy for predicting the "Arc" event is 84 %. The accuracy for predicting the "Arc" event is slightly higher than the accuracy for the "No arc" event (82.5 %), because the binary logistic regression was targeted to predict the "Arc" event, not the "No arc" event. The sensitivity (true positive rate) can be defined as the proportion of "Arc" event observations predicted as "Arc," while the specificity (true negative rate) can be defined as the proportion of "No arc" event observations predicted as "No arc" [68]. Thus, the cutoff value is 0.5, the sensitivity (true positive rate) is 0.84, and the specificity (true negative rate) is 0.83.

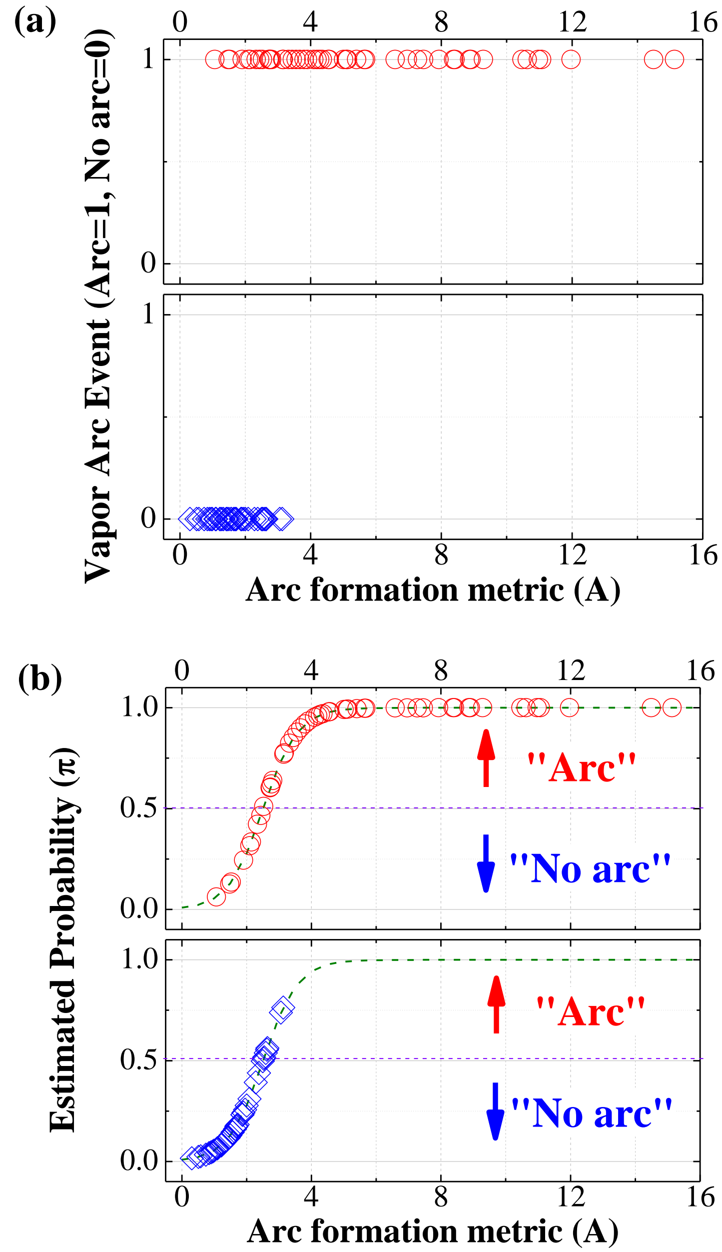

Figure 63 (a) Vapor arc events depending on the arc current metric and (b) Estimated possibility depending on the arc current metric (Training data set)

Table 8 Classification table from the training data set (cutoff value = 0.5)

Observed	Predicted		
	"Arc"	**"No arc"**	**Percentage Correct**
"Arc"	42	8	84.0
"No arc"	7	33	82.5
Overall Percentage			83.3

The prediction model was validated using the 39 validation data points. The validation data set (39 data points) prior to and after the transformation by the optimized logistic regression model is shown in figure 64, and the accuracy of the prediction from the validation data is shown in Table 9. The validation result using 39 validation data shows that the accuracy of prediction of "Arc" event is quite high (95.5%) when the cutoff value of 0.5 applied, while the accuracy of "No arc" event prediction is decreased down to 76.5% comparing to the accuracy from training data.

Table 9 Classification table from the validation data set (cutoff value = 0.5)

Observed	Predicted		
	"Arc"	**"No arc"**	**Percentage Correct**
"Arc"	21	1	95.5
"No arc"	4	13	76.5
Overall Percentage			87.2

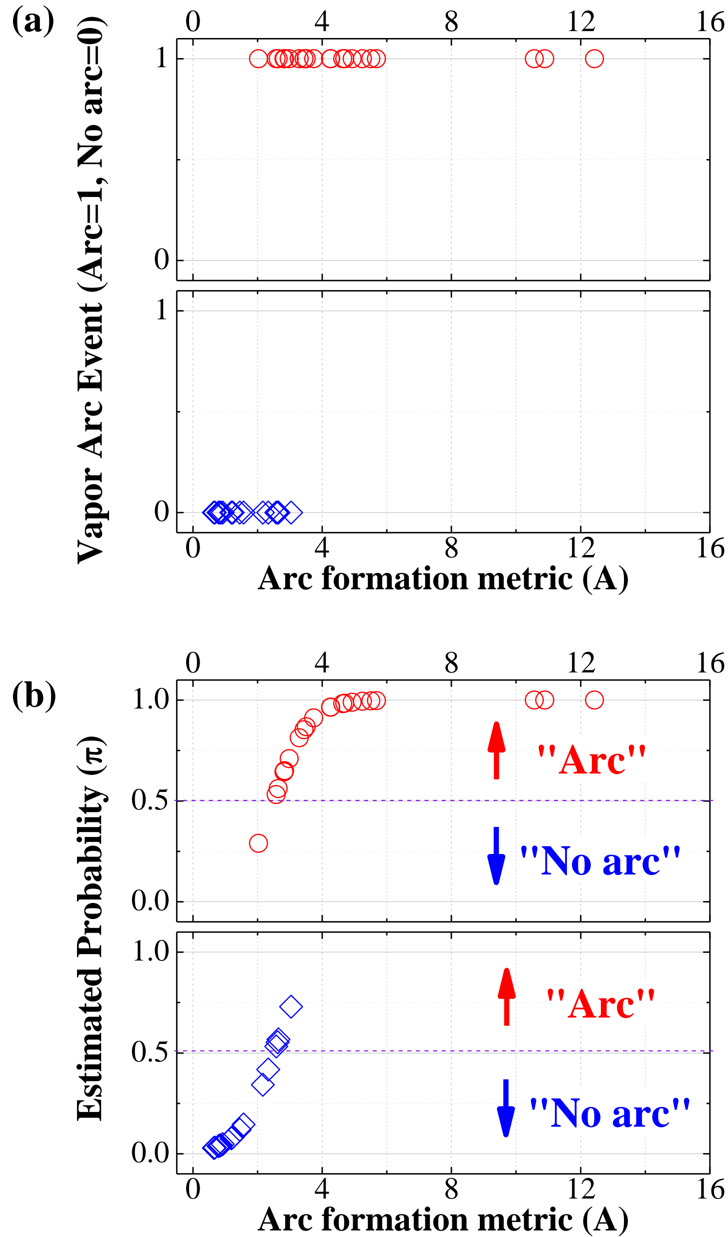

Figure 64 (a) Vapor arc events depending on the arc current metric and (b) Estimated possibility depending on the arc current metric (Validation data set)

Initially, the cutoff value of 0.5 was used to predict the "Arc" event based on the estimated possibility; however, the sensitivity (true positive rate) and specificity (true negative rate) vary depending on the cutoff value. The receiver operating

characteristic (ROC) curve was used to evaluate the performance of the prediction model across the entire range of cutoff values. The ROC curve has been extended for use in visualizing the performance of classification in machine learning and medical decision making [73, 74].

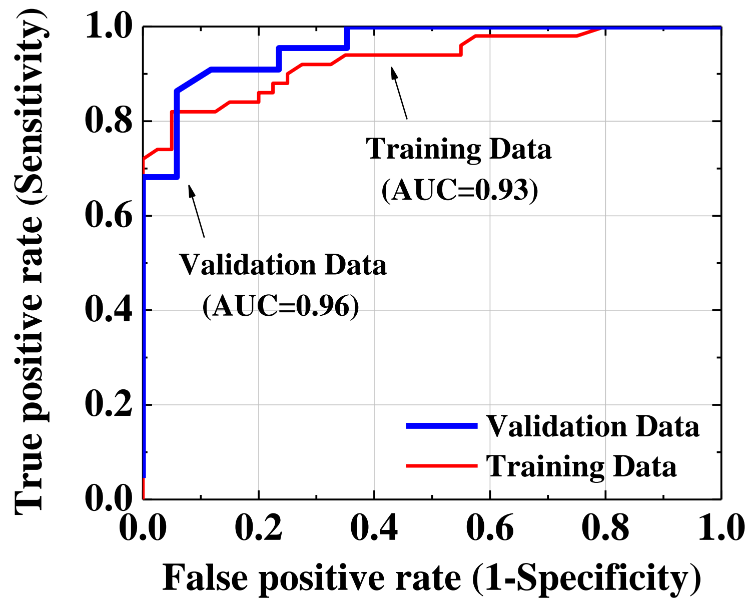

Figure 65 Receiver operating characteristic (ROC) curve for vapor arcing prediction model

The ROC curve is the plot of the true positive rate (sensitivity) versus the false positive rate (1-specificity) as depicted in figure 65. It represents that the 95% of “Arc” events were correctly predicted as “Arc” events, while it has the misprediction of about 35% of “No arc” events were incorrectly predicted as “Arc” events in the training data set. Researchers evaluate the accuracy of prediction based on the area under the ROC curve (AUC) [73-74]. The AUC can vary from 0.5 when there is no discrimination to 1.0 for perfect discrimination, which means that the true positive

rate is 1.0 and the false positive rate is 0. The AUC from both the training data (0.93) and the validation data (0.96) are greater than 0.9, indicating that our prediction model has a high degree of both precision and accuracy.

The optimal cutoff value depends on the relative costs of false positive and false negative errors. One of the ways to decide the optimal cutoff value is to choose the point of intersection between the specificity and sensitivity curves, where the sensitivity is equal to specificity. By choosing the point of intersection of both the sensitivity and specificity correspond the greatest both sensitivity and specificity. In other words, the intersection point indicates the greatest true positive rate and lowest false positive rate. However, the cost of false prediction of vapor arcing by tin whisker may not be identical for all applications. For example, for life critical applications, a metal vapor arc failure will be catastrophic; thus, the cost of false prediction is quite expensive. Therefore, the cutoff value should be flexible depending on the cost of false prediction in individual industries. In order to help to decide the cutoff value, the sensitivity and specificity changes based on cutoff value are shown in figure 66.

In our analysis, the initial cutoff value of 0.5 was used, which was the intersection point of the sensitivity and specificity curve. By using a cutoff value of 0.5, a sensitivity of 84 % and specificity of 83 % can be obtained. If the cost of false prediction is high, the sensitivity of our prediction model can be increased by decreasing the cutoff value. If the cutoff value is moved to 0.2, the sensitivity is 90%; however, the specificity will be decreased to 70% at the same time.

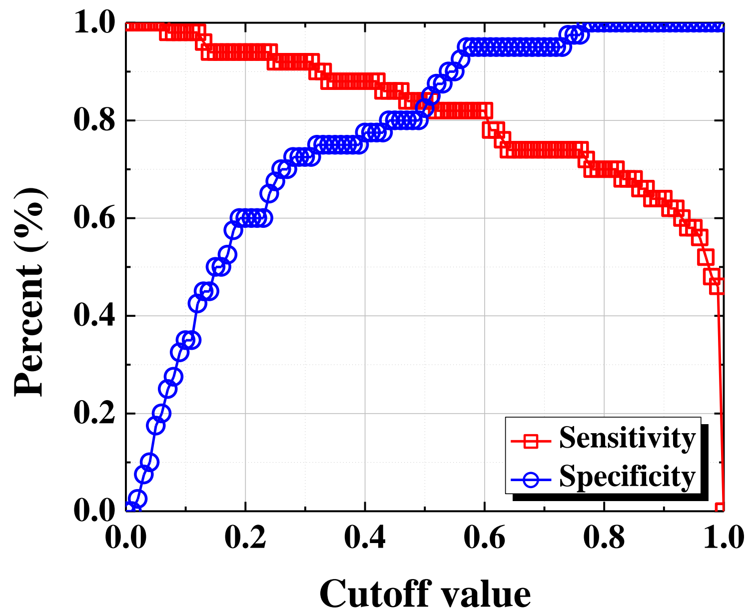

Figure 66 The sensitivity and specificity curves (Training data set)

Since the arc current metric has been shown to be a good indicator of tin whisker-induced metal vapor arc formation, a plot of arc formation probability against voltage for constant resistances, as depicted in figure 67. For example, if the resistance of the test specimen is 20 Ω, a tin whisker-induced arc has only a 17% probability at 30 V. If the resistance of the test specimen is 5 Ω, then the estimated possibility is larger than the cutoff value of 0.5 when the bias voltage is higher than 13 V. It indicates that tin whisker-induced vapor arcing may have occurred. Thus, it may be required to consider the mitigation strategy for tin whisker-induced vapor arcing failures, such as applying the conformal coating.

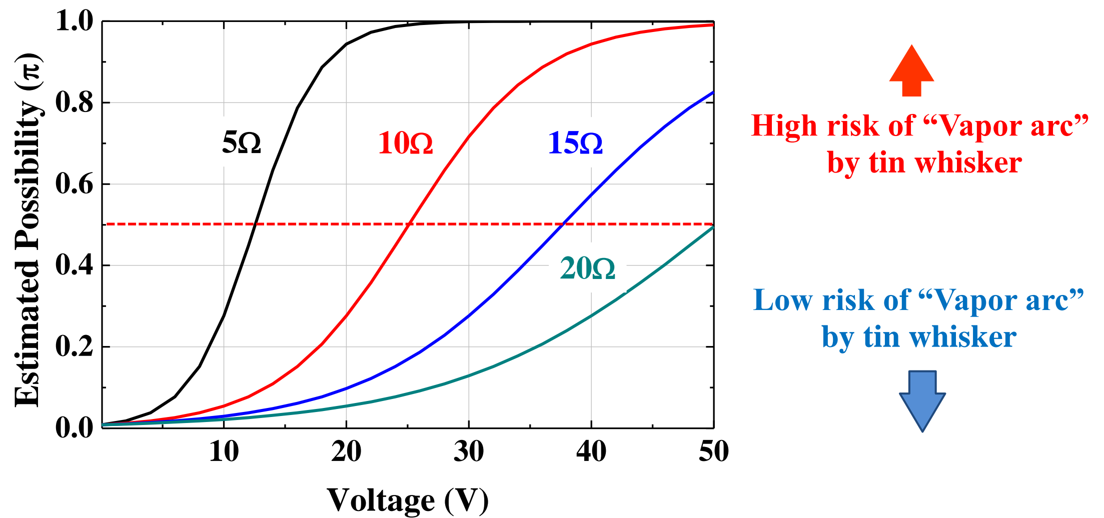

Figure 67 Estimated possibility of vapor arcing based on the voltage and resistance of the test specimen

3. *Conclusion*

The binary logistic regression model was developed in order to assess the probability of vapor arcing by tin whiskers. Statistically, the effect of arc current metric is significant on the probability of vapor arcing by tin whisker, while the pressure is not a significant parameter which can decide the vapor arc formation by tin whiskers when the pressure range is between 30 and 760 torr (low vacuum conditions).

The prediction accuracy in binary logistic regression model is higher than 80 %. In addition, the performance of the prediction model was evaluated by the area under the receiver operating characteristic (ROC) curve (AUC) shows that the developed prediction model has outstanding discrimination of tin whisker-induced vapor arcing. Finally, the optimal cut off value is suggested using the sensitivity and

specificity curves. The proposed prediction model may be used as a guideline for circuit design in order to avoid tin whisker-induced vapor arcing failures.

Chapter 6: Melting current of tin whiskers

1. *Experimental setup*

Tin whiskers were harvested from whisker growth specimens and attached the vapor arcing specimen using a conductive silver paint. The length and diameter of whiskers were documented by SEM and the resistance of test specimen was measured by a milliohm-meter. The length of whisker was defined as the distance between the points where the both ends of whisker made contact with the conductive silver paint. Individual test specimen was applied the current level from 0 to 100 mA with 100 μA increments (50 ms duration time) using a semiconductor parameter analyzer. The maximum voltage was limited by 5 V using a semiconductor parameter analyzer. Simultaneously, the voltage was monitored to decide the melting current of whiskers. All measurements were conducted in ambient condition (760 torr).

2. *Melting current of tin whiskers*

For measuring the melting current of tin whiskers, total 19 test specimens were prepared. Figure 68(a) presents the whisker on test specimen prior to apply the current and the melted whisker after the test showed in figure 68(b). The whisker was melted due to the joule heating by current flow and the midst of tin whisker where the hottest point was disconnected as shown in figure 68(c). Figure 68(d) presents that the part of melted tin and presence of remained oxide layer from tin whisker. The test specimen in figure 68, the whisker length and diameter is 1143 μm and 3.6 μm, respectively, and the measured resistance of test specimen is 32.41 Ω.

When the current applied to the test specimen, the current increased until the hottest point of whisker was disconnected when the current was 14.6 mV as shown in figure 69. As shown in figure 69(c), the resistance of test specimen was increased as current increased due to the temperature increment in tin whisker by joule heating.

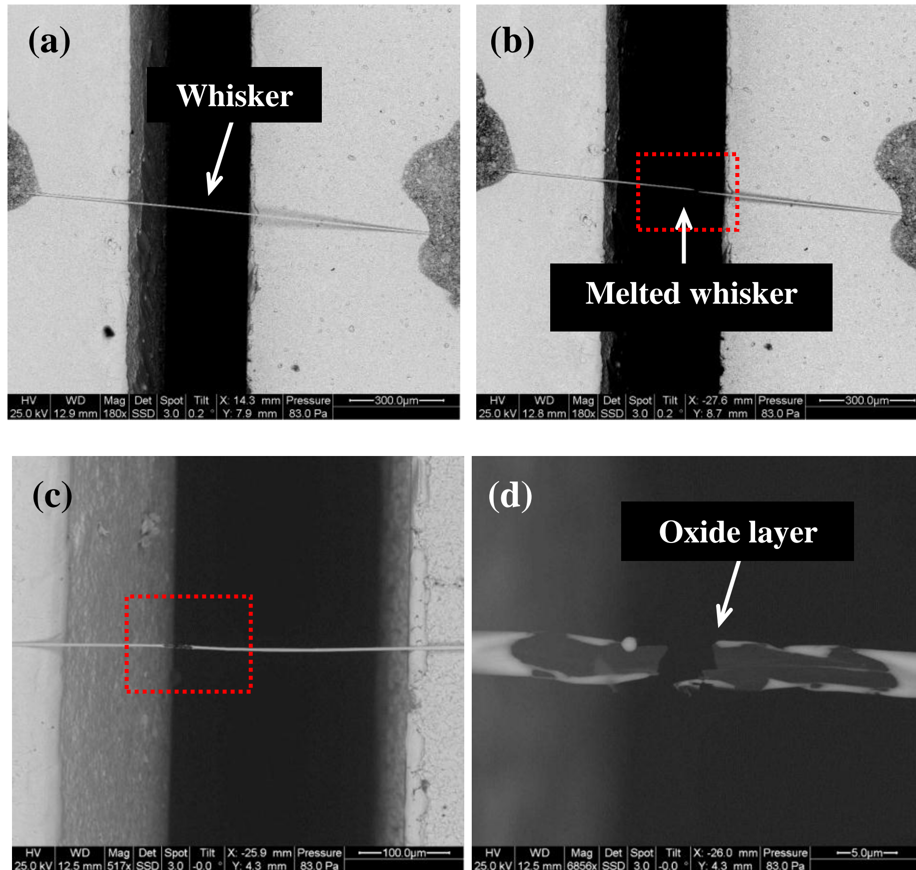

Figure 68 Melting test specimen: (a) Prior to, (b) After the test (b), (c) Close-up of disconnected whisker indicated in figure 68(b), and (d) Close-up of expunged part of whisker with oxide layer

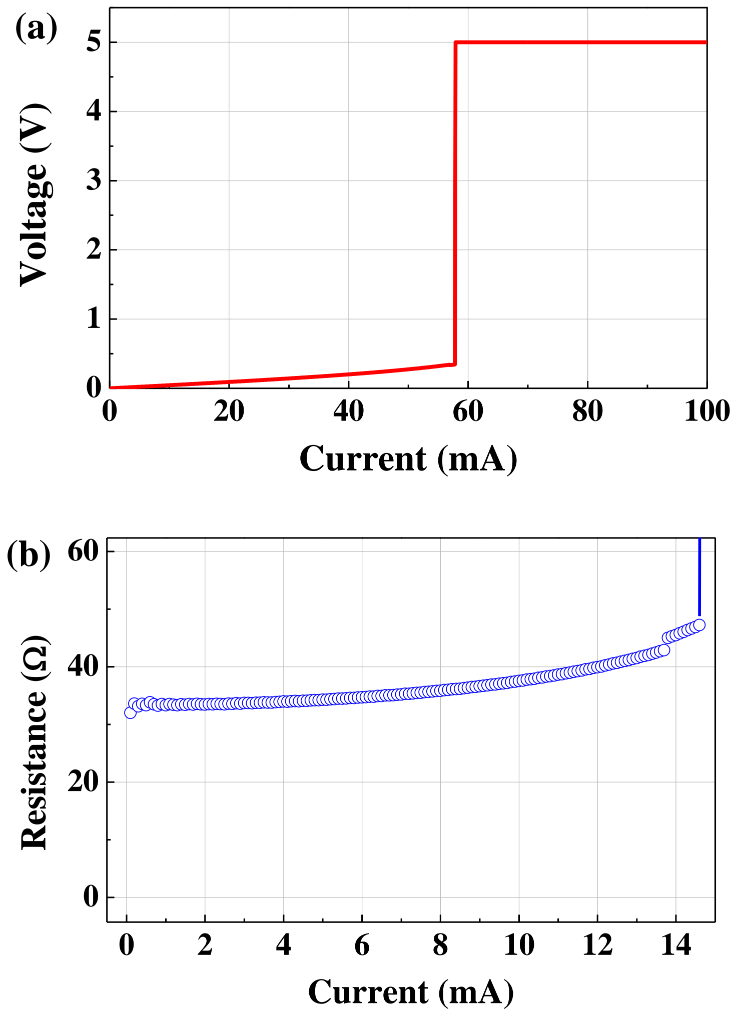

Figure 69 (a) Current-voltage plot in the melting test of tin whisker and (b) Current-resistance plot

The measured melting current from 19 whiskers presents in figure 70 with melting current of 4 whiskers reported by Dunn [11]. The melting current of whisker increases as whisker diameter increases and the measured melting current of tin whiskers is the range between 10 ~ 60 mA. There is a positive linear relation (Pearson correlation = 0.839, p-value < 0.001) between the whisker diameter and measured

melting current of whiskers, while there is no statistical correlation between the whisker length and melting current of whiskers.

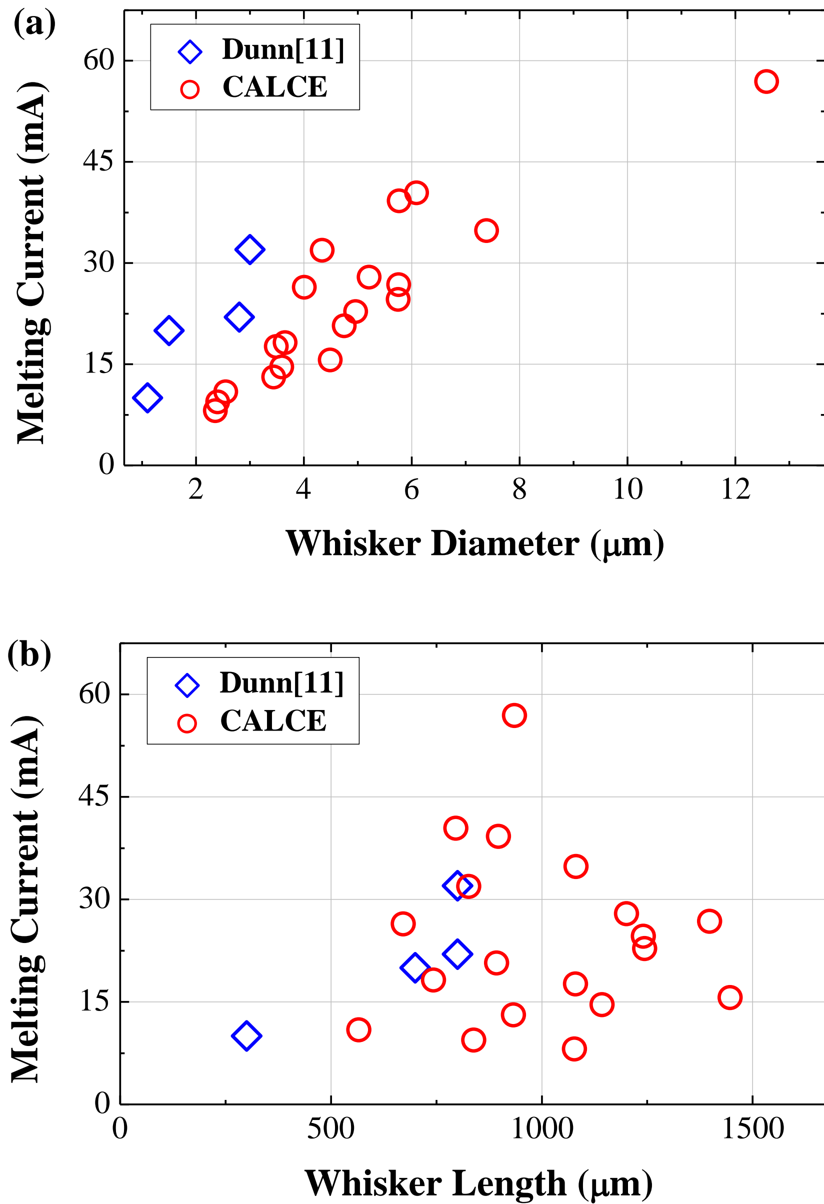

Figure 70 Measured melting current of tin whisker depending on whisker diameter and whisker length (CALCE versus Dunn [11])

Preece [75] and Onderdonk [76] developed the equation which can estimate the melting current of wires. Theoretically, the melting current of tin wire can be estimated as using following Preece's equation (12) [75]:

$$I = a \cdot d^{\frac{3}{2}} \qquad (12)$$

where I is the melting current (A), a is the constant (for tin: 0.406×10^6 $A/m^{3/2}$), and d is the diameter of wire.

The melting current of wire can be also estimated using the Onderdonk's equation as following (13) [76]:

$$I = A\sqrt{\frac{\log_{10}\left(\frac{T_m - T_a}{234 + T_a} + 1\right)}{33 \cdot S}} \qquad (13)$$

where, A is the cross-sectional area (mil), T_m is the melting temp of material in degree Celsius, T_a is the reference temperature (20 C°) and S is the fusing time in seconds.

Figure 71 presents the measured melting current and estimated melting current based on Preece's and Onderdonk's equation. The melting current of tin whiskers is 6 times higher than estimation by Preece's equation and 10 times higher than the estimated melting current by Onderdonk's equation. The larger difference between the measured melting current and estimated melting current by Preece's and Onderdonk's equation might be caused by the material and geometry difference between wire and tin whiskers. The Onderdonk developed the equation to estimate

the melting current of copper conductors and Preece used the wires between 0.01 to 0.036 inch (254 ~ 915 μm) [75, 76]. However, the average whisker diameter in test is 4.87 μm which is approximately 50 times smaller than the smallest wire used by Preece. Tin whisker also naturally has oxide layer on its surface and melting point of tin oxide layer is much higher (1630 C°) than tin (232 C°). When the tin whisker melted, the tin oxide layer may contain the melted tin until the oxide layer is disconnected. The remaining tin inside the tube of oxide layer was observed in whiskers after the melting current measurement as shown in figure 70(d) and 72. It may suggest that the melted tin was flowing inside the tube of oxide layer. Thus, the tin whisker may able to carry more current that the estimated current level from the Preece's and Onderdonk's equation.

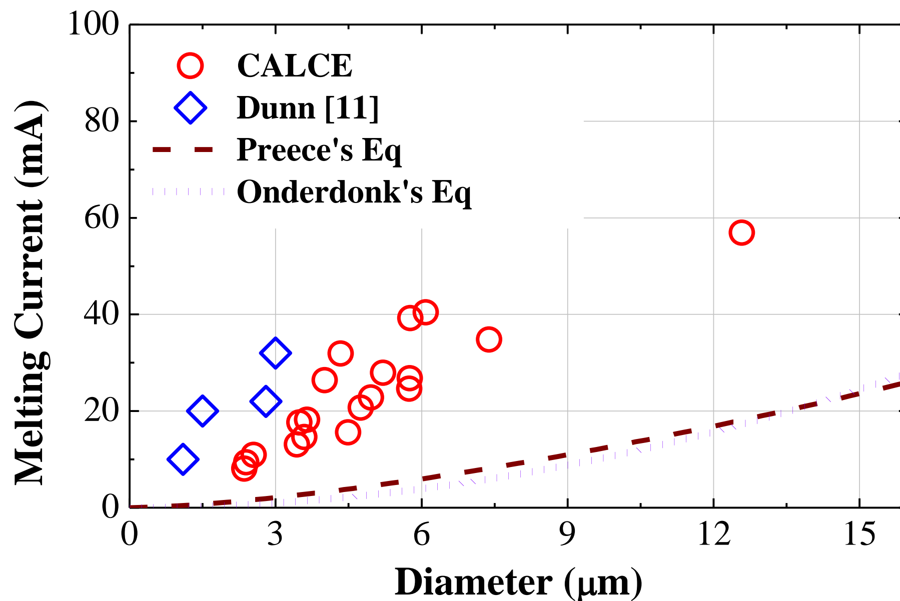

Figure 71 Measured melting current versus estimated melting current by Preece's and Onderdonk's equation

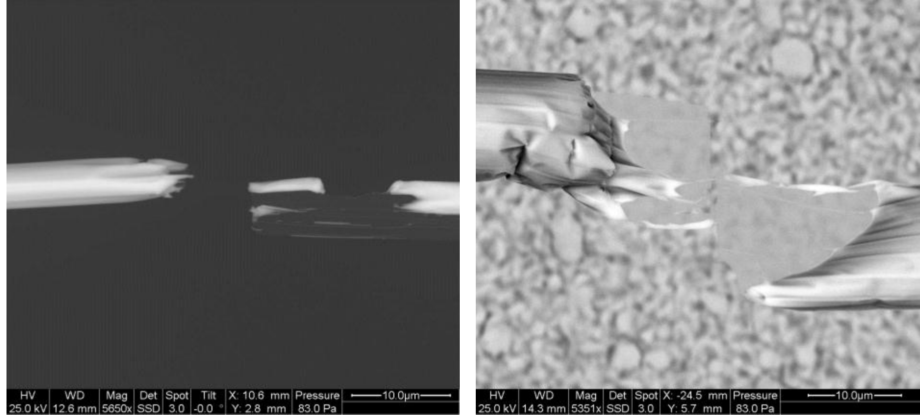

Figure 72 Remained melting tin with oxide layer after the melting current measurement

Stupian [77] derived the equation for melting current of tin whisker by assuming that the temperature distribution in a whisker internally heated by ohmic loss. The maximum current can whisker flow which is the melting current of whisker current can be expressed as following (14):

$$I_{melt} = 0.076 \frac{A}{L} mA \qquad (14)$$

where, A is the cross-sectional area (μm^2) and L is the length of whisker (cm), respectively. The measured melting current of whisker is much higher than the calculated melting current.

Leidecker [78] also derived the melting current of tin whisker in vacuum condition as following (15):

$$I_{melt,vac} = \frac{87.5mV}{R_0} \qquad (15)$$

where, $I_{melt,vac}$ is the melting current of tin whisker in vacuum condition, and R_0 is the resistance of whisker at ambient, respectively.

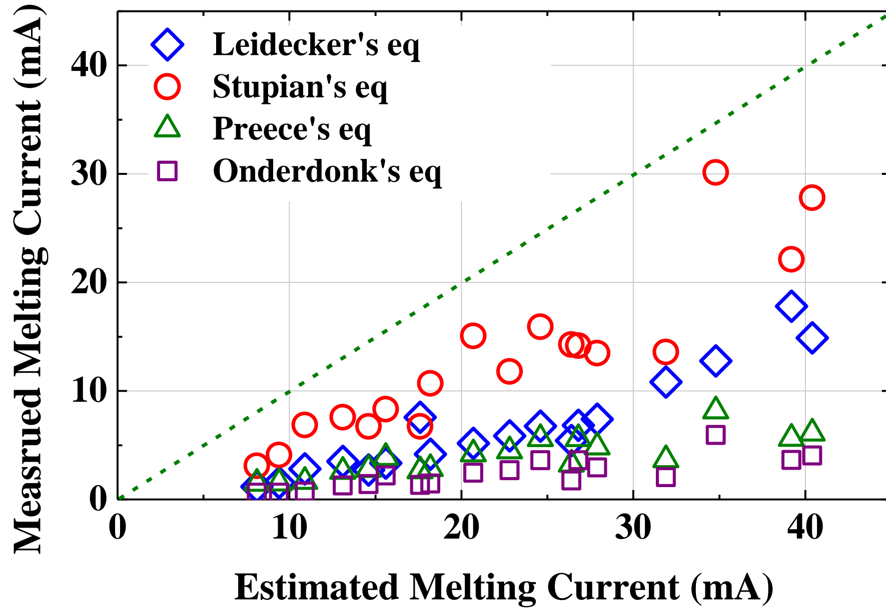

Figure 73 Measured melting current versus estimated melting current for tin whiskers

The measured melting current of whisker is at least 2 times higher than the estimated melting current using four equations. Among four equations, the Stupian's equation can estimate the melting current with smallest difference comparing to the measured melting current. The difference between measured melting current of whisker and estimated melting current decreased as the diameter increased, but the tin whiskers are able to carry at least two times higher current value than estimated current value.

3. Summary

The melting current of tin whiskers were measured in ambient condition and compared with calculated melting current by Preece's, Onderdonk's, Stupian's and Leidecker's equations. The melting current of tin whisker was increased as the whisker diameter increased and the range of melting current was 10 ~ 60 mA. The tin whisker can carry higher current value than the theoretically estimated current value.

Chapter 7: Contributions and Future work

1. Contribution

This dissertation has investigated the electrical characteristic of tin whisker induced electrical shorts and metal vapor arcs failure in order to assess their risk. The experimental investigation provided the effect of several factors which can determine the propensity of electrical shorts and vapor arcs failure. Finally, the distribution of the voltage that can induce the electrical shorts by whisker has been provided and the prediction model for assessing the tin whisker induced vapor arc failure has been developed.

The contributions from this dissertation are:

- Established contact force as a critical parameter in determination of breakdown voltage for tin whisker induced shorts.
- Determined that a bridging whisker that exhibits buckling will exceed the contact force and exhibit negligible breakdown voltage.
- Established a physical metric based on whisker geometry and electrical circuit characteristics for assessing the risk of tin whisker induced metal vapor arc formation.
- Developed a logistic regression model based on the physical metric to assess the likelihood of tin whisker induced metal vapor arc formation.

2. *Future work*

The effects of the contacted material and the contact force on likelihood of the electrical shorting caused by tin whiskers were investigated in this dissertation. The other factor may affect the level of the breakdown voltage is the oxide layer. Since the dielectric strength which may determine the breakdown voltage can be varied depending on the thickness of oxide layer and its crystalline structure (SnO vs SnO_2). It is reported in this thesis that the observed oxide layer on tin whisker surface was not uniform even on the surface of single whisker. In addition, the thickness of oxide layer on tin whisker will be varied depending on the environmental conditions. Therefore, the understanding regarding the effect of oxide layer on breakdown of tin whisker may improve the risk assessment in shorting failure by tin whiskers.

In this dissertation, it was observed that the breakdown can occur with constant level of the voltage, which was the time-dependent breakdown. It implies that the electrical failure can occur even the level of the voltage in electronic system is lower than the breakdown voltage. Thus, the measurement of time-dependent breakdown of tin whisker would be the one other future work in electrical shorting propensity of tin whiskers.

In terms of metal vapor arc by tin whiskers, it would be useful to investigate the required conditions for the sustained vapor arc (Type II arc event). The electric field strength or vapor arc density might be related with the sustained vapor arc. The characteristic of sustained vapor arc and its requirements would be used to specify the prediction model depending on the type of arc event.

It also would be valuable information that the effect of ramp time of the power source on likelihood of tin whisker-induced vapor arc. It is known that the whisker can’t form the vapor arc due to the relatively slow ramp time of power supply comparing to the lead-acid battery; however, the minimum required ramp time that can initiate the vapor arc by tin whiskers is still not investigated. It is recommended to use the power source which can control the ramp time to evaluate the likelihood of the arc formation by tin whiskers. This information would be quite useful to the designers for power supply or power converter to avoid the whisker-induced vapor ac failures.

As the part of mitigation strategy for preventing tin whisker induced metal vapor arcs, the evaluation of different types of conformal coating would be another topic for the future work. Since the thickness of conformal coating layer and types of conformal coating whether it can act as flammable retard or not can affect either the formation or quenching of the metal vapor arc by tin whiskers.

Appendices

- Journal publications

– S. Han, M. Osterman, and M. Pecht, "Electrical Shorting Propensity of Tin Whiskers," *IEEE Transitions on Electronics Packaging Manufacturing*, Vol. 33, No. 3, July 2010

– S. Han, S. Meschter, M. Osterman, and M. Pecht, "Evaluation of Effectiveness of Conformal Coating as Tin Whisker Mitigation," accepted to *Journal of Electronic Materials*, 6 July 2012

– S. Han, M. Osterman, and M. Pecht, "Tin Whisker-induce Metal Vapor Arcing," Plasma Sources Science and Technology, Paper under review

– S. Han, M. Osterman, and M. Pecht, "Effects of Arcing Parameters on Metal Vapor Arcing by Tin Whiskers," to be submitted to *IEEE Trans. on Reliability*

– S. Han, M. Osterman, and M. Pecht, "Prediction Model for Tin Whisker-induced Metal Vapor Arcing," to be submitted

– S. Han, M. Osterman, and M. Pecht, "Electrical Characteristic of Tin and Zinc Whiskers," to be submitted

- Publications in conference

– S. Han, K. Kim, C. Yu, M. Osterman, and M. Pecht, "Observations of the Spontaneous Growth of Tin Whiskers in Various Reliability Conditions," ECTC 2008 58th, May 2008

- S. Han, M. Osterman, and M. Pecht, “Tin Whisker Growth on Conformally Coated SnPb Assemblies,” 4th International Symposium on Tin Whiskers, College Park, MD, Jun 23-24, 2010
- S. Han, C. Johnson, M. Osterman, and M. Pecht, “Effectiveness of Conformal Coatings on Surface Mount Components as Tin Whisker Mitigation,” Reliability Microelectronics for Military Applications, Linthicum Heights, MD, May 17-19, 2011
- S. Han, M. Osterman, and M. Pecht, “Likelihood of Metal Vapor Arc by Tin Whiskers,” Reliability Microelectronics for Military Applications, Linthicum Heights, MD, May 17-19, 2011
- S. Han, M. Osterman, and M. Pecht, “Assessment of Tin Whisker Induced Metal Vapor Arcing,” 5th International Symposium on Tin Whiskers, College Park, MD, Sept 14-15, 2011

References

[1] S. Ganesan and M. Pecht, Lead-free electronics. Hoboken, N.J.: Wiley-Interscience, 2006.

[2] K. G. Compton, A. Mendizza, and S. M. Arnold, "Filamentary Growths on Metal Surfaces - Whiskers," Corrosion, vol. 7, pp. 327-334, 1951.

[3] S. C. Britton, "Spontaneous Growth of Whiskers on Tin Coatings: 20 Years of Observation," Transactions of the Institute of Metal Finishing, vol. 52, pp. 95-102, 1974.

[4] B. D. Dunn, "Whisker formation on Electronic Materials," Circuit World, vol. 2, pp. 32-40, 1976.

[5] G. Grossmann and C. Zardini. (2011). The ELFNET Book on Failure Mechanisms, Testing Methods, and Quality Issues of Lead-free Solder Interconnects.

[Online] Available: http://dx.doi.org/10.1007/978-0-85729-236-0, (last accessed 07/27/2012).

[6] S. E. Koonce and S. M. Arnold, "Growth of Metal Whiskers," Journal of Applied Physics (letters to the editor), vol. 24, pp. 365-366, 1954.

[7] J. W. Evans and W. Engelmaier. (2007). A guide to lead-free solders physical metallurgy and reliability. Available: http://dx.doi.org/10.1007/978-1-84628-310-9, (last accessed 07/27/2012).

[8] K. N. Tu. (2007). Solder joint technology materials, properties, and reliability.

[Online] Available: http://site.ebrary.com/id/10182543, (last accessed 07/27/2012).

[9] Environmental Acceptance Requirements for Tin Whisker Susceptibility of Tin and Tin Alloy Surface Finishes, J. S. S. T. Association JESD201, 2006.

[10] J. Cheng, P. T. Vianco, and J. C. M. Li, "Hollow Tin/chromium Whiskers," Applied Physics Letters, vol. 96, pp. 184102-3, 2010.

[11] B. D. Dunn, W. R. Burke, and B. Battrick, "A Laboratory Study of Tin Whisker Growth," European Space Agency. European Space Research and Technology Center, ESTEC, Noordwijk (Netherlands), 1987.

[12] H. Leidecker and J. Brusse. Tin Whiskers: A History of Documented Electrical System Failures- A briefing prepared for the Space Shuttle program office 2006.
[Online] Available: http://nepp.nasa.gov/whisker/reference/tech_papers/2006-Leidecker-Tin-Whisker-Failures.pdf, (last accessed 07/27/2012).

[13] H. P. Kehrer and H. G. Kadereit, "Tracer Experiments on the Growth of Tin Whiskers," Applied Physics Letters, vol. 16, pp. 411-12, 1970.

[14] K. Chen and G. D. Wilcox, "Observations of the Spontaneous Growth of Tin Whiskers on Tin-Manganese Alloy Electrodeposits," Physical Review Letters, vol. 94, p. 066104, 2005.

[15] J. D. Eshelby, "A Tentative Theory of Metallic Whisker Growth," Physical Review, vol. 91, p. 755, 1953.

[16] K. N. Tu, "Irreversible Processes of Spontaneous Whisker Growth in Bimetallic Cu-Sn Thin-film Reactions," Physical Review B (Condensed Matter), vol. 49, pp. 2030-4, 1994.

[17] K. W. Moon, C. E. Johnson, M. E. Williams, O. Kongstein, G. R. Stafford, C. A. Handwerker, and W. J. Boettinger, "Observed Correlation of Sn Oxide Film to Sn

Whisker Growth in Sn-Cu Electrodeposit for Pb-free Solders," Journal of Electronic Materials, vol. 34, pp. 31-3, 2005.

[18] J. Smetana, "Theory of Tin Whisker Growth: "The End Game"," IEEE Transactions on Electronics Packaging Manufacturing, vol. 30, pp. 11-22, 2007.

[19] X. Chen, Z. Yun, F. Chonglun, and J. A. Abys, "Understanding Whisker Phenomenon: The Driving Force for Whisker Formation," CircuiTree, pp. 10-21, 2002.

[20] B. Z. Lee and D. N. Lee, "Spontaneous Growth Mechanism of Tin Whiskers," Acta Materialia, vol. 46, pp. 3701-14, 1998.

[21] M. Dittes, P. Oberndorff, P. Crema, and V. Schroeder, "Tin Whisker Formation in Thermal Cycling Conditions," Singapore, 2003, pp. 183-8.

[22] C. H. Pitt and R. G. Henning, "Pressure-induced Growth of Metal Whiskers," Journal of Applied Physics, vol. 35, pp. 459-460, 1964.

[23] T. Shibutani, Q. Yu, M. Shiratori, and M. G. Pecht, "Pressure-induced Tin Whisker Formation," Microelectronics Reliability, vol. 48, pp. 1033-1039, 2008.

[24] M. Dittes, P. Oberndorff, P. Crema, and P. Su, "Tin Whisker Formation - A Stress Relieve Phenomenon," AIP Conference Proceedings, pp. 348-59, 2006.

[25] J. Brusse, G. Ewell, and J. Siplon, "Tin Whiskers: Attributes and Mitigation," in CART EUROPE 2002: 16th Passive Components Symposium, 2002, pp. 67-80.

[26] R. Schetty, "Minimization of Tin Whisker Formation for Lead-free Electronics Finishing," Circuit World, vol. 27, pp. 17-20, 2001.

[27] S. H. Liu, C. Chih, P. C. Liu, and T. Chou, "Tin whisker Growth Driven by Electrical Currents," Journal of Applied Physics, vol. 95, pp. 7742-7, 2004.

[28] P. Oberndorff, M. Dittes, P. Crema, P. Su, and E. Yu, "Humidity Effects on Sn Whisker Formation," Electronics Packaging Manufacturing, IEEE Transactions on, vol. 29, pp. 239-245, 2006.

[29] J. W. Osenbach, J. M. DeLucca, B. D. Potteiger, A. Amin, R. L. Shook, and F. A. Baiocchi, "Sn Corrosion and Its Influence on Whisker Growth," IEEE Transactions on Electronics Packaging Manufacturing, vol. 30, pp. 23-35, 2007.

[30] S. Arnold, "Repressing the Growth of Tin Whiskers," Plating, 53, pp. 96-99, 1966.

[31] R. D. Hilty, N. E. Corman, and H. Herrmann, "Electrostatic Fields and Current-flow Impact on Whisker Growth," IEEE Transactions on Electronics Packaging Manufacturing, vol. 28, pp. 75-84, 2005.

[32] NASA Goddard Space Flight Center, Tin Whisker (and Other Metal Whisker) Homepage, [Online] Available: http://nepp.nasa.gov/whisker, April 2005, (last accessed 07/27/2012).

[33] Nuclear Regulatory Commission www site, [Online] Available: http://www.nrc.gov/reading-rm/doc-collections/nuregs/staff/sr0933/sec3/200.html, (last accessed 07/27/2012).

[34] P. Daddona, "Reactor Shutdown: Dominion Learns Big Lesson from a Tiny Tin Whisker", The Day (New London, CT), July 4, 2005

[35] L. Corbid, "Constraints on the Use of Tin Plate in Miniature Electronic Circuits",Proceedings 3rd International SAMPE Electronics Conference, pp. 773-779, June 20-22, 1989.

[36] R. Dore, "Launches of Hughes HS 601 Satellites Ready to Resume", Hughes Press Release, Aug.1998

[37] Boeing www site, "Launches of Huges HS 601 Satellites Ready to Resume”, [Online] Available: http://www.boeing.com/defense-space/space/bss/hsc_pressreleases/98_08_11_601ok.html, (last accessed 07/27/2012).

[38] Food and Drug Administration, "ITG #42: Tin Whiskers- Problems, Causes and Solutions", [Online] Available: http://www.fda.gov/ICECI/Inspections/InspectionGuides/InspectionTechnicalGuides/ucm072921.htm, (last accessed 07/27/2012).

[39] Y. Zhang, C. Su, C. Fan, and J. Abys, "Tin Whisker Growth and Prevention", Journal of Surface Mount Technology, October, 2000

[40] Y. Fukuda, M. Osterman, and M. Pecht, "The Effect of Annealing on Tin Whisker Growth," IEEE Transactions on Electronics Packaging Manufacturing, vol. 29, pp. 252-8, 2006.

[41] J. W. Osenbach, R. L. Shook, B. T. Vaccaro, B. D. Potteiger, A. N. Amin, K. N. Hooghan, P. Suratkar, and P. Ruengsinsub, "Sn Whiskers: Material, Design, Processing, and Post-plate Reflow Effects and Development of an Overall Phenomenological Theory," IEEE Transactions on Electronics Packaging Manufacturing, vol. 28, pp. 36-62, 2005.

[42] M. Sobiech, U. Welzel, R. Schuster, E. J. Mittemeijer, W. Hugel, A. Seekamp, and V. Muller, "The Microstructure and State of Stress of Sn Thin Films after

Post-Plating Annealing: An Explanation for the Suppression of Whisker Formation?," 2007, pp. 192-197.

[43] Y. Wang, D. Ding, T. Liu, K.-P. Galuschki, Y. Hu, A. Gong, M. Shen, H. Sun, X. Wang, J. Sun, M. Li, and D. Mao, "Effect of Ni barrier on the Tin Whisker Formation of Electroplating Sn on Lead-frame Alloy," in 2010 11th International Conference on Electronic Packaging Technology and High Density Packaging, ICEPT-HDP 2010, August 16-19, 2010, Xi'an, China, 2010, pp. 980-983.

[44] M. N. Chen, S. J. Ding, Q. Q. Sun, D. W. Zhang, and L. K. Wang, "Effect of Pulse-plated Nickel Barriers on Tin Whisker Growth for Pure Tin Solder Joints," Journal of Electronic Materials, vol. 37, pp. 894-900, 2008.

[45] iNEMI (May 2005). “Recommendations on Lead-free Finishes for Components Used in High-Reliability Products,” Report of International Electronics Manufacturing Initiative,

[Online] Available:

http://thor.inemi.org/webdownload/projects/ese/tin_whiskers/User_Group_mitigation_May05.pdf, (last accessed 07/27/2012).

[46] J. Kadesch and H. Leidecker, "Effects of Uralane Conformal Coating on Tin Whisker Growth," in 37th Nordic annual conference, ed. Helsingor, Denmark, 2000.

[47] T. A. Woodrow and E. A. Ledbury, "Evaluation of Conformal Coatings as a Tin Whisker Mitigation Strategy," presented at the IPC/JEDEC 8th International Conference on Lead-Free Electronic Components and Assemblies, San Jose, CA, 2005.

[48] T. A. Woodrow and E. A. Ledbury, "Evaluation of Conformal Coatings as a Tin Whisker Mitigation Strategy, Part II," presented at the SMTA International Conference, Rosemont, IL, 2006.

[49] R. D. Hilty and N. E. Corman, "An Electrical Characterization of Tin Whiskers," San Francisco, CA, United States, 2007, pp. 0993-E02-02.

[50] K. J. Courey, S. S. Asfour, J. A. Bayliss, L. L. Ludwig, and M. C. Zapata, "Tin Whisker Electrical Short Circuit Characteristics Part I," Electronics Packaging Manufacturing, IEEE Transactions on, vol. 31, pp. 32-40, 2008.

[51] K. J. Courey, S. S. Asfour, A. Onar, J. A. Bayliss, L. L. Ludwig, and M. C. Wright, "Tin Whisker Electrical Short Circuit Characteristics Part II," Electronics Packaging Manufacturing, IEEE Transactions on, vol. 32, pp. 41-48, 2009.

[52] D. Van Westerhuyzen, Backes, P., Linder, J., Merrell, S., Poeschel, R, "Tin Whisker Induced Failure in Vacuum," in Proceedings of International Symposium for Testing and Failure Analysis, 1992, pp. 407-412.

[53] G. Davy, "Relay Failure Caused by Tin Whiskers," Northrop Grumman, Technical Article, October 2002.

[54] B. L. J. Richardson, "Tin Whisker Initiated Vacuum Metal Arcing in Spacecraft Electronics," in Proceedings 1992 Government Microcircuit Applications Conference, 1992, pp. 119-122.

[55] M. S. Mason and G. Eng, "Understanding Tin Plasmas in Vacuum: A New Approach to Tin Whisker Risk Assessment," Journal of Vacuum Science and Technology A: Vacuum, Surfaces and Films, vol. 25, pp. 1562-1566, 2007.

[56] M. Mason and G. Eng, "Understanding Tin Plasmas: A New Approach to Tin Whisker Risk Assessment," in Reliability physics symposium, 2007. proceedings. 45th annual. ieee international, 2007, pp. 150-155.

[57] R. D. Hilty and N. E. Corman, "Tin Whisker Reliability Assessment by Monte Carlo simulation," in Proc. IPC/JEDEC Lead-Free Symp., 2005.

[58] T. Fang, M. Osterman, S. Mathew, and M. Pecht, "Tin Whisker Risk Assessment," Circuit World, vol. 32, pp. 25-29, 2006.

[59] T. Fang, S. Mathew, M. Osterman, and M. Pecht, "Assessment of Risk Resulting from Unattached Tin Whisker Bridging," Circuit World, vol. 33, pp. 5-8, 2007.

[60] P. G. Slade, Electrical Contacts: Principles and Applications. New York: Dekker, 1999.

[61] J. Brusse, "Tin Whisker Observations on Pure Tin-plated Ceramic Chip Capacitors," in AESF SUR/FIN Proceedings, 2002, pp. 45-64.

[62] W. H. Kruskal and W. A. Wallis, "Use of Ranks in One-Criterion Variance Analysis," Journal of the American Statistical Association, vol. 47, pp. 583-621, 1952.

[63] N. J. Kasdin and D. A. Paley, Engineering Dynamics : A Comprehensive Introduction. Princeton, N.J.: Princeton University Press, 2010.

[64] L. Panashchenko, “Evaluation of Environmental Tests for Tin Whisker Assessment,” Univ. of Maryland thesis, December 2009.

[65] Smetana J. ‘‘NEMI Tin whisker user group—tin whisker acceptance test requirements’’, NEMI Tin Whisker Workshop, June 1–2, 2004, Las Vegas, NV.

[66] R. Holm and E. Holm, Electric Contacts : Theory and Application. Berlin; New York: Springer-Verlag, 1967.

[67] M. M. Atalla, "Arcing of Electrical Contacts in Telephone Switching Circuits: Part V - Mechanism of the Short Arc and Erosion of Contacts," Bell System Technical Journal, vol. 34, pp. 1081-1102, 1955.

[68] C. H. Corliss, "Temperature of Copper Arc," United States Bureau of Standards - Journal of Research - Physics and Chemistry vol. 66A, pp. 5-12, 1962

[69] M. F. Hoyaux, Arc Physics. New York: Springer-Verlag New York, 1968.

[70] P. Malkin, "The Vacuum Arc and Vacuum Interruption," Journal of Physics D: Applied Physics, vol. 22, p. 1005, 1989.

[71] C. Zhuan-Ke, H. Mizukoshi, and K. Sawa, "Contact Erosion Patterns of Pd Material in DC Breaking Arcs," Components, Packaging, and Manufacturing Technology, Part A, IEEE Transactions on, vol. 17, pp. 61-67, 1994.

[72] C. Y. Peng, and T. S. So, "Logistic Regression Analysis and Reporting: A Primer" Understanding Statistics, vol. 1(1), pp. 31-70, 2002.

[73] J. A. Swets, "Measuring the Accuracy of Diagnostic Systems," Science, vol. 240, pp. 1285-1293, 1988.

[74] T. Fawcett, "An Introduction to ROC Analysis," Pattern Recognition Letters, vol. 27, pp. 861-874, 2006.

[75] W. H. Preece, "On the Heating Effects of Electric Currents," Proceedings of the Royal Society of London, vol. 36, pp. 464-471, 1883.

[76] E, R. Stauffacher, "Short-time Current Carrying Capacity of Copper Wire", General Electric Review No., 6, vol. 31, pp. 326-327, June 1928.

[77] G. W. Stupian, "Tin Whiskers in Electronic Circuits," Aerospace Technical Report, Number 92(2925)-7, 1992.

[78] J. Brusse, H. Leidecker, and L. Panashchenko, "Metal Whiskers: Failure Modes & Mitigation Strategies", Microelectronics Reliability & Qualification Workshop (MRQW), Dec. 5, 2007.